UNIVERSITÀ
DEGLI STUDI
DI PADOVA

UNIVERSITA' DEGLI STUDI DI PADOVA

DIPARTIMENTO DI INGEGNERIA INDUSTRIALE

CORSO DI LAUREA MAGISTRALE IN CHEMICAL AND PROCESS ENGINEERING

Tesi di Laurea Magistrale in

Chemical and Process Engineering

Techno-economic analysis of sustainable bio-based lubricant production from lignin and waste cooking oil

Relatore: Prof.ssa Elena Barbera

Laureando: ANDREA GUARISE

ANNO ACCADEMICO 2023 - 2024

Abstract

The aim of this thesis is to evaluate the techno-economic feasibility of a high-value biolubricant production process, starting from lignin and waste cooking oil, as a side process in a generic biorefinery in the U.S. that uses corn stover as lignocellulosic feedstock for ethanol production.

In the proposed process, lignin is sourced from the unhydrolyzed solids (UHS), which represent the portion of the biomass feedstock that is not utilized for ethanol production. Typically, this lignin-rich residue is burned to generate steam and electrical energy for internal plant operations. In the proposed process, however, the lignin is converted into its aromatic monomers through hydrothermal liquefaction (HTL) using pressurized water at 320 °C, resulting in a mixture of phenolic compounds, mainly phenol.

These phenolic compounds undergo hydrodeoxygenation (HDO) to produce benzene, while fatty acid methyl esters (FAMEs) are obtained through transesterification of waste cooking oil (WCO). The final biolubricant product is produced through aromatic alkylation of FAMEs with benzene, forming phenyl-branched FAMEs (PBFAMEs). PBFAMEs exhibit improved lubricity and oxidative stability compared to standard FAMEs, making them a suitable lubricant improver for ultra-low sulfur diesel (ULSD) engines. This biolubricant can be sold as a by-product of the biorefinery.

Process simulations are performed using the Aspen Plus software, while the economic analysis uses as a benchmark the design and economics of a generic biorefinery in the U.S., as proposed by the National Renewable Energy Laboratory (NREL) of the U.S. Department of Energy (DOE).

The final goal of this study is to compare the minimum ethanol selling price (MESP) with and without the integration of the biolubricant production process, to determine its techno-economic feasibility. The results indicate an improvement in the economic performance of the biorefinery, with the MESP decreasing from $3.02 per gallon in the base case (ethanol production only) to $2.64 per gallon when the bio-lubricant process is included. This represents approximately a 13% reduction in the selling price of ethanol.

Table of Contents

List of Acronyms

CAPEX: Capital Expenditure

DCFROR: Discounted Cash Flow Rate of Return

DOE: Department of Energy

FAME: Fatty Acid Methyl Ester

FBR: Fixed Bed Reactor

FCI: Fixed Capital Investment

FFA: Free Fatty Acid

FzBR: Fluidized Bed Reactor

HDO: Hydrodeoxygenation

HTL: Hydrothermal Liquefaction

IEA: International Energy Agency

IHRS: Induction-Heating Reactor System

ISBL: Inside Battery Limits

MESP: Minimum Ethanol Selling Price

MPO: Methyl n-(Phenyl)Octadecanoate

NPV: Net Present Value

NREL: National Renewable Energy Laboratory

NRTL: Non-Random Two Liquids

OPEX: Operational Expenditure

OSBL: Outside Battery Limits

PBFAME: Phenyl-Branched Fatty Acid Methyl Ester

PEM: Proton Exchange Membrane

RHRS: Resistive-Heating Reactor System

TBR: Trickle Bed Reactor

TCI: Total Capital Investment

TDC: Total Direct Costs

TIC: Total Indirect Costs

UHS: Unhydrolyzed Solids

ULSD: Ultra-Low Sulfur Diesel

UNIFAC: Universal Quasi-Chemical Functional Group Activity Coefficients

USDA: United States Department of Agriculture

WCO: Waste Cooking Oil

WWT: Waste Water Treatment

Introduction

The global population's growth continues to drive an increasing demand for energy and industrial commodities. Despite improvements in renewable energy technologies, fossil fuels and petroleum-derived chemicals remain dominant in energy production and industrial applications, contributing significantly to greenhouse gas emissions, environmental degradation, and global warming. While renewable energy sources like solar and wind offer alternatives for power generation, biomass stands as the only viable renewable resource for producing chemicals. Biomass contains organic molecules that can potentially replace petroleum-based compounds; however, developing economically competitive biomass-based chemical production processes remains a critical challenge.

This thesis evaluates the techno-economic feasibility of producing biolubricants from waste biomass, specifically lignin and waste cooking oil (WCO). Biolubricants represent a promising alternative for replacing petroleum-derived lubricants, offering improved sustainability while addressing the growing demand for renewable industrial chemicals. The study focuses on integrating biolubricant production within a biorefinery that produces ethanol from corn stover, utilizing by-products and waste streams to improve economic performance while promoting environmental sustainability.

The first chapter of the thesis reviews the key processes and materials involved in biolubricant production. These include hydrothermal liquefaction (HTL) for converting lignin into phenolic compounds, hydrodeoxygenation (HDO) for further transforming these compounds into aromatics, transesterification for producing FAMEs from WCO, and aromatic alkylation for synthesizing the final biolubricant product from FAMEs and aromatic compounds. Additionally, the chapter highlights the importance of lignocellulosic biomass as a renewable resource and biolubricants as high-value, sustainable alternatives to traditional lubricants.

The second chapter details the integration of biolubricant production within the biorefinery context. Lignin, a waste product from the ethanol production process, is converted into a phenol-rich biocrude through HTL, which is subsequently processed through HDO to produce aromatic compounds such as benzene. Concurrently, WCO undergoes transesterification to yield FAMEs. The final alkylation process combines benzene with FAMEs to produce the biolubricant, characterized by improved lubricity and oxidative stability compared to standard FAMEs. This chapter also outlines the experimental data, assumptions, and methodologies employed to scale laboratory batch processes to industrial-scale continuous operations, with all processes modeled and simulated using Aspen Plus software.

The third chapter describes the methodology applied in this work for conducting a comprehensive techno-economic analysis of the integrated biolubricant production process. Equipment sizing forms the basis for estimating capital costs using Capcost (2017) software and the NREL (2011) guidelines for total capital investment (TCI) calculation. Operational costs are assessed using pricing data for raw materials and utilities, combined with material and energy balances derived from the Aspen simulations. Parameters and assumptions used to perform a discounted cash flow analysis on the overall process with and without the integration of the biolubricant production process are also included.

Finally, the fourth chapter presents the results of the techno-economic analysis, starting from material and energy balances obtained from the Aspen simulations, and the economic performance metrics for the biorefinery, both with and without the integrated biolubricant production process. The comparative analysis is performed through the calculation of the minimum ethanol selling price (MESP) as the main economic indicator. Sensitivity analyses on key cost drivers, such as WCO price and biolubricant selling price, further explore the financial viability of the process under varying market conditions.

I would like to express my sincerest gratitude to Dr. Randy L. Maglinao (Montana State University-Northern) and Prof. Sandeep Kumar (Old Dominion University) for their precious collaboration and for sharing essential information that significantly contributed to this work. Additionally, I would like to thank Prof. Alberto Bertucco for his contribution to this research.

Chapter 1: Background

In this chapter, a comprehensive literature review, covering lignocellulosic biomass and main processes to transform it, is presented, focusing on novel processes to convert lignin into valuable products.

1.1 Lignocellulosic Biomass

Biomass is the general definition of a heterogeneous group of materials derived from plants, animals, and humans, including agricultural and forestry residues, animal waste, liquid and solid municipal wastes, algae and aquatic crops, etc (Tursi, 2019).

The current approach to biomass emphasizes its use as a valuable energy source rather than as landfill material. Through several processes such as direct combustion, thermochemical treatments (e.g., pyrolysis, liquefaction, gasification), and biochemical methods (e.g., enzymatic hydrolysis and microbial conversion), biomass can be converted into fuels and energy (Nanda et al., 2015) (Tursi, 2019).

Among these processes, thermochemical and biochemical treatments are the most promising, with increasing technological developments in biomass conversion to fuels and chemicals that will decrease production costs, thereby enhancing the competitiveness of the biomass industry against the petroleum one.

This work focuses on lignocellulosic biomass, which originates from plant materials and consists mostly of cellulose, hemicellulose, and lignin, with only a small fraction of inorganic compounds (Tursi, 2019) (Cai et al., 2017). Table 1.1 shows the average compositions by weight (wt%) of typical lignocellulosic biomasses.

Table 1.1: Average mass composition of different lignocellulosic biomasses (Cai et al., 2017)

Biomass	**Cellulose (wt%)**	**Hemicellulose (wt%)**	**Lignin (wt%)**
Hardwood (Poplar)	50.8-53.3	26.2-28.7	15.5-16.3
Softwood (Pine)	45.0-50.0	25.0-35.0	25.0-35.0
Wheat Straw	35.0-39.0	23.0-30.0	12.0-16.0
Corn Cob	33.7-41.2	31.9-36.0	6.1-15.9
Corn Stalk	35.0-39.6	16.8-35.0	7.0-18.4
Rice Straw	29.2-34.7	23.0-25.9	17.0-19.0
Sugarcane Bagasse	25.0-45.0	28.0-32.0	15.0-25.0
Sorghum Straw	32.0-35.0	24.0-27.0	15.0-21.0
Grasses	25.0-40.0	25.0-50.0	10.0-30.0
Switchgrass	35.0-40.0	25.0-30.0	15.0-20.0

1.1.1 Cellulose

Cellulose is a complex carbohydrate made of long chains of monomeric units of D-glucose, linked by glycosidic bonds, with molecular formula $(C_6H_{12}O_6)_n$, where *n* represents the degree of polymerization.

Among the three macromolecules in plants biomasses, cellulose is the most abundant. Its utilization in pulp and paper industries, and more recently in biorefineries, improved the studies about its structure and methods to break it down.

The reactivity and morphology of the cellulose chain are affected by strong inter- and intra-molecular hydrogen bonds, as illustrated in figure 1.1. This structural stability is an important characteristic that affects how cellulose can be processed (Tursi, 2019).

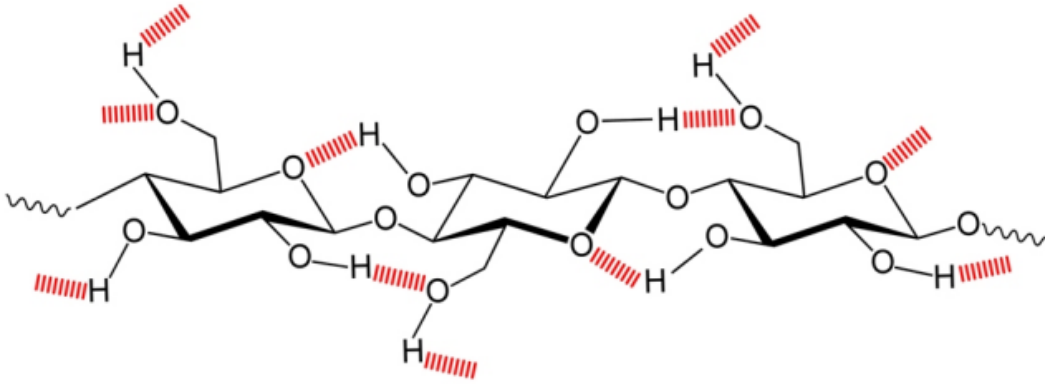

Figure 1.1: Cellulose molecular structure, with hydrogen bonds marked in red (Tursi, 2019)

At a larger scale, cellulose is divided into crystalline and amorphous regions. The amorphous regions are more exposed, making them more accessible to hydrolysis by cellulase enzymes, which break down cellulose into D-glucose monomers (Tursi, 2019).

1.1.2 Hemicellulose

Hemicellulose is a major constituent of plant cell walls, consisting of heterogeneous polysaccharides, depending on the plant species.

Unlike cellulose, hemicellulose is mostly amorphous and consists of chains of both pentose sugars (e.g., xylose, arabinose) and hexose sugars (e.g., glucose, mannose, galactose). This structure makes hemicellulose an important source of glucose and other organic compounds used in the paper industry and in biorefineries (Tursi, 2019).

1.1.3 Lignin

Lignin is a complex amorphous aromatic polymer found in plant cell walls, where it improves the plant's structural integrity by binding fibers together, thus increasing compactness and resistance (Tursi, 2019).

Lignin constitutes between 15% and 30% of biomass by weight, but it composes up to 40% of its total energy content (Riyang et al., 2020). Structurally, lignin is made up of phenylpropane units linked by ether and carbon-carbon (C-C) bonds, along with intermolecular hydrogen bonds, giving it a complex and rigid structure. This composition makes lignin insoluble in most solvents, except for alkaline solutions (Tursi, 2019).

Figure 1.2 illustrates the chemical structure of lignin.

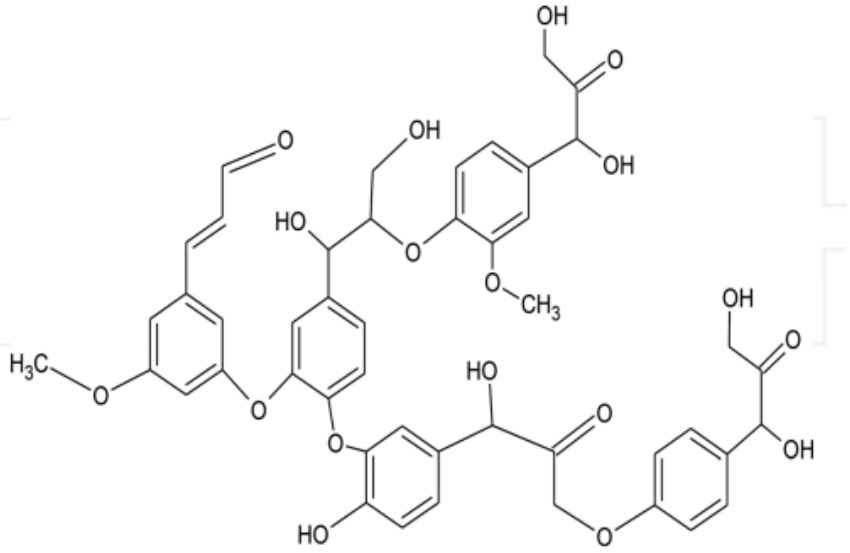

Figure 1.2: Molecular structure of lignin (Mahmood et al., 2018)

To access the cellulose within plant fibers, lignin must be broken down. Currently, lignin is often a low-value by-product in industries that process lignocellulosic biomass, such as paper production. These industries typically use alkaline or acidic pretreatments to isolate cellulose and hemicellulose for further processing, while the lignin by-product is almost entirely burned for energy. For example, the paper industry produces large amounts of Kraft lignin during hardwood and softwood delignification, but only around 2% of this lignin is further processed to produce fuels or chemicals; most of it is burned to generate energy (Mahmood et al., 2018).

Similarly, biorefineries and sugar mills separate cellulose and hemicellulose from agricultural residues and sugarcane, respectively, and then burn the residual lignin (Tursi, 2019) (Mahmood et al., 2018).

The quality and chemical composition of lignin vary based on the extraction method used. Numerous depolymerization processes have been investigated to break down lignin into valuable aromatic compounds suitable for fuel and chemical production.

These processes can be divided into two main categories: chemical and biological processes. Chemical processes include oxidation, pyrolysis, gasification, and liquefaction. Biological processes include enzymatic oxidation and microbial conversion (Tursi, 2019).

1.1.4 Role of Biomass as a Renewable Resource

Direct and indirect effects of the use of fossil fuels are greenhouse gases (GHG) emissions, air and water pollution, global warming, and climate change (Nanda et al., 2015).

Biomass can be defined as a renewable resource because the carbon dioxide (CO_2) released by its combustion is used by living plants in their metabolic processes, thereby keeping a balanced carbon cycle (Tursi, 2019).

In the “World Energy Outlook 2023”, the International Energy Agency (IEA) reports an increasing global energy consumption, and fossil fuels utilization will reach its peak in 2030. Notably, projections indicate that around 30% of the global energy supply will be given by renewable resources (e.g., solar energy, wind energy, hydro energy, bioenergy, etc.), up from around 15% in recent years. In the U.S., this figure is even lower, with renewable energy accounting for 12% of the total energy consumption in 2021, according to the U.S. Energy Information Administration (EIA), as shown in Figure 1.3.

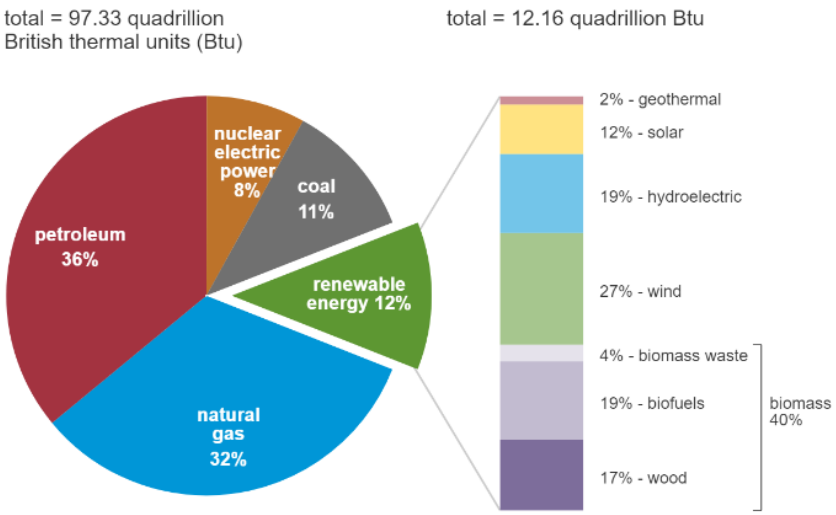

Figure 1.3: U.S. total energy consumption per source, 2021 (EIA)

While most renewable resources can produce electricity only, biomass can be converted into liquid fuels, which represent almost 40% of global energy consumption (Nanda et al., 2015).

Bioethanol, primarily derived from agricultural residues, is the most widely produced biofuel globally and is commonly blended with gasoline at 5% (E5) and 10% (E10) by volume. However, some countries, such as U.S., Canada, and Sweden, are implementing ethanol-gasoline blending programs including fuels composed of 85% ethanol and 15% gasoline (E85) by volume, with the possibility of reducing global gasoline consumption of 32% (Nanda et al., 2015).

1.2 Conversion of Corn Stover to Ethanol

The U.S. Department of Energy (DOE) supports the research and development of cost-competitive technologies to convert renewable biomass resources into bio-based fuels and chemicals. These efforts aim to reduce GHG emissions and decrease dependence on oil, as outlined in the DOE's Biomass Multi-Year Program Plans (MYPP) (MYPP, 2011) (MYPP, 2023).

The National Renewable Energy Laboratory (NREL, 2011), in its report titled “Process Design and Economics for Biochemical Conversion of Lignocellulosic Biomass to Ethanol (2011)”, developed a detailed techno-economic analysis on the ethanol production from corn stover, a lignocellulosic feedstock, for use as a gasoline additive.

Corn stover, which refers to the remaining plant material above-ground after the corn harvest (leaves, stalks, husks, cobs), is chosen as biomass feedstock for large-scale biorefineries because it is the most abundant agriculture residue in the U.S., with a composition of 32% glucan, 19% xylan, and 13% lignin by weight (NREL, 2011), consistent with the corn stover average composition of 35% cellulose, 20% hemicellulose and 12% lignin by weight (Phiri et al., 2024).

1.2.1 Process Description

In the biorefinery, the primary focus is on carbohydrates, such as glucan and xylan, which are broken down through a pretreatment process involving hydrolysis catalyzed by diluted sulfuric acid and heat at 158 °C for 5 minutes. This process produces glucose and xylose monomers and oligomers, while reducing cellulose crystallinity and chain length, facilitating subsequent enzymatic hydrolysis to yield additional glucose. During this process, 5% of lignin is converted into soluble lignin, while most of it remains inert.

After conditioning, where the slurry is treated with ammonia to reach a pH suitable for enzyme activity, the mixture of water, cellulose, sugars and lignin, the so-called hydrolysate, is sent to the enzymatic hydrolysis (or enzymatic saccharification) process. Here, cellulose is converted to glucose at 48 °C for 84 hours using cellulase enzymes. After hydrolysis, the slurry is cooled with water and sent to the fermentation process, where recombinant bacterium *Zymomonas mobilis*, fed with corn steep liquor and diammonium phosphate as nutrients, serves as the ethanologen. This bacterium carries out simultaneous fermentation of both glucose and xylose into ethanol at 32 °C over 180 hours.

The overall process, starting from corn stover, has a theoretical ethanol yield, based on feedstock carbohydrates, of 76% (79 gal/dry ton of feedstock).

After the batch fermentation process, a critical step for this study takes place: distillation and solid recovery. Distillation separates ethanol from water, which is sent to wastewater treatment (WWT), producing a near-azeotropic ethanol-water mixture. A vapor-phase molecular sieve adsorption column is then used to further dehydrate the ethanol to 99.5% purity. Prior to this, a liquid-solid separation process removes unconverted insoluble and dissolved solids, referred to as unhydrolyzed solids (UHS), from water and solubles. The UHS are dewatered using a pressure filter and sent to a combustor/turbogenerator, where unconverted biomass and anaerobic biogas from WWT are combusted to generate electricity and steam for plant operations, making the plant energy self-sufficient, while generating extra-electricity that is sold to the grid.

A simplified flow diagram of the overall process, including *in-situ* enzyme production, is shown in Figure 1.4.

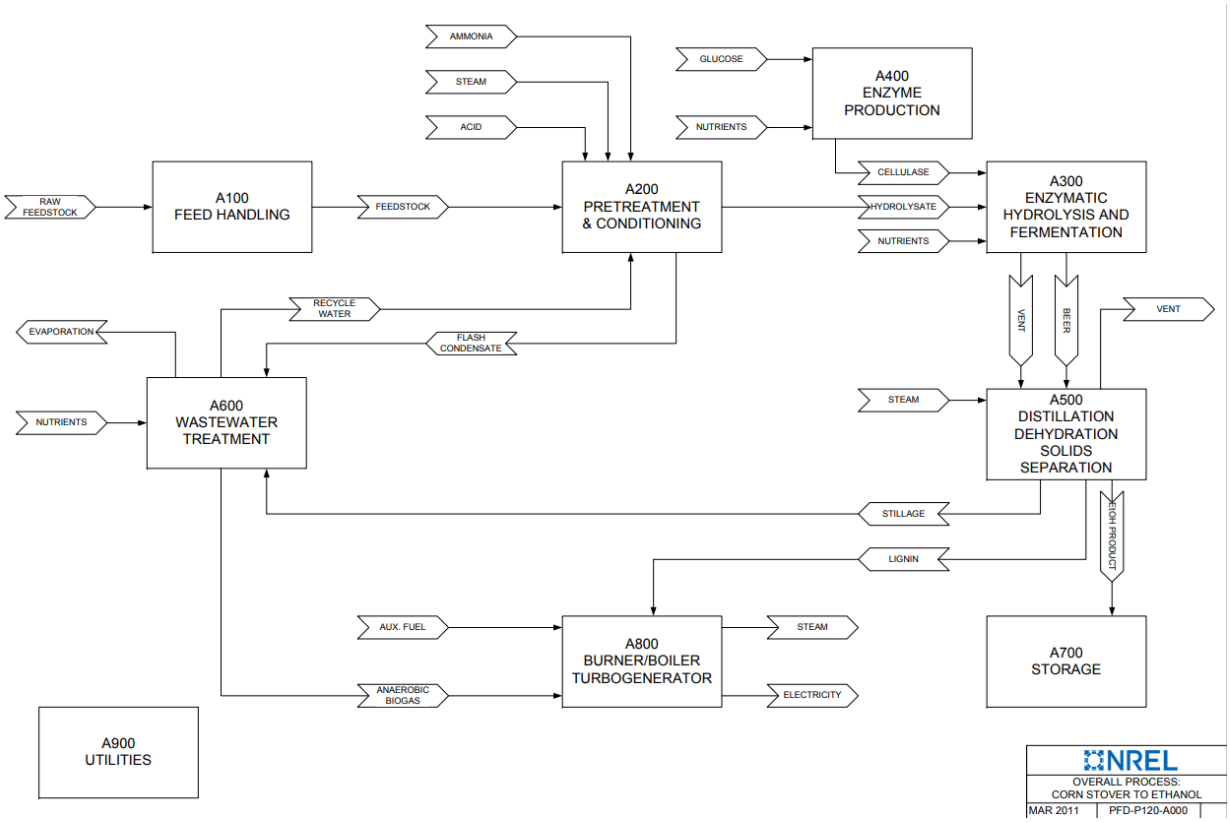

Figure 1.4: Simplified flow diagram of corn stover conversion to ethanol (NREL). UHS stream is denoted as "LIGNIN"

UHS consist of 64% insoluble solids, mainly lignin, and they represent a valuable biomass feedstock for the production of bio-based chemicals, particularly aromatic compounds. Several studies aim to maximize biomass utilization for the substitution of oil-based chemicals, rather than simply burning the UHS for energy production.

1.3 Hydrothermal Liquefaction (HTL) of Lignin

Hydrothermal liquefaction (HTL) of biomass is a thermochemical process that converts solid biomass into a liquid fuel (biocrude) in the presence of water, operating within a temperature range of 250–450 °C and pressures of 10–35 MPa (Castello et al., 2018).

Under these conditions, water can be either a sub-critical liquid, or a relatively dense supercritical fluid, considering its critical point is around 374 °C and 22 MPa. Near its critical point, water exhibits advantageous solvent properties, such as lower viscosity and dielectric constant, which facilitate the dissolution of organic compounds, as well as a higher ionic product, enhancing catalytic activity for acid–base reactions (Shah et al., 2022).

HTL can be applied to a wide range of biomass types such as wood, sewage sludge, kraft lignin, algae, agricultural and urban wastes, either dry or wet (IEA).

The standard approach to processing these biomass types is to convert them via thermochemical methods into energy (e.g., direct combustion) or into fuels and chemicals through processes such as gasification, pyrolysis, and HTL. Among these, HTL is the most suitable for wet biomass because it does not require pre-drying of the feedstock, reducing energy requirements (Shah et al., 2022).

1.3.1 Mechanism

Biomass from various sources has different chemical compositions, characterized by varying relative amounts of cellulose, hemicellulose, and lignin, and the mechanism involved in the conversion of biomass into biocrude has not been completely elucidated in the literature.

However, the pathway of HTL of lignocellulosic biomass generally comprises three main steps: depolymerization, decomposition and recombination (Gollakota et al., 2018).

Depolymerization of lignocellulose produces a wide variety of monomers, which are then broken into smaller fragments through decomposition reactions such as cleavage, decarboxylation and dehydration; these fragments are then further transformed into biocrude, gas phase and aqueous phase products, and solid residues, through recombination reactions such as repolymerization, condensation and cyclization (Xu et al., 2021).

The main products of lignocellulosic biomass HTL, categorized according to each biopolymer that composes the lignocellulose, are listed in Table 1.2.

Table 1.2: Main products of HTL of lignocellulosic biomass (Xu et al., 2021) (Hirayama et al., 2024)

Biopolymer	HTL products
CELLULOSE	Glucose, fructose, aldehydes, ketones, hydroxymethylfurfural, oligosaccharides
HEMICELLULOSE	Furfural, lactic acid, formic acid, glyceraldehyde, acetone aldehyde
LIGNIN	Phenol, anisole, guaiacol, catechol, vanillic acid, diphenyl ether, xanthene

1.3.2 Catalysis

Catalysis is important in HTL to improve both the yield of biocrude and selectivity toward desired biocrude composition, thereby achieving specific properties.

Catalysts in HTL are generally categorized as homogeneous catalysts, such as alkaline salts and organic acids, and heterogeneous catalysts, including transition metals, metal oxides, and activated carbon (Shah et al., 2022).

Homogeneous catalysts, which are soluble in the aqueous phase, are typically classified into carbonates and hydroxides of alkali and alkaline earth metals (e.g., Na, Ca, K) and organic acids (e.g., formic acid, acetic acid, sulfuric acid) and their solutions. These catalysts are advantageous due to their low cost and ability to partially suppress char formation. However, their high solubility in water makes recovery challenging, and they may contribute to reactor system corrosion (Shah et al., 2022).

In contrast, heterogeneous catalysts commonly used in HTL include metal oxides (e.g. CeO_2, ZrO_2), noble metals, such as Pd and Pt based catalysts, and other transition metals. Although they are more expensive, and some precipitates or salts of carboxylic or phenolic groups can accumulate on the catalyst surface, they are easily regenerated (Shah et al., 2022).

Among the above-mentioned catalysts, alkali catalysts are the most effective for HTL of lignocellulosic biomass in improving biocrude yield and suppressing char formation, with best performances achieved by K_2CO_3, compared to the other carbonates and hydroxides of potassium and sodium, with studies indicating it can increase biocrude yield by a factor of 2 or 3 compared to the non-catalytic process (Zhou, 2014) (Bi et al., 2017).

1.3.3 HTL of Lignin

Lignin is one of the most diffused bio-based macromolecules in the world, and it is the only one containing aromatic structures. This feature makes lignin a promising source for aromatic platform chemicals, which are currently mostly derived from crude oil (Schuler et al., 2017).

However, due to the challenges in obtaining aromatic compounds from lignin in a cost-effective manner, most of the lignin is burned for energy production. As described in Section 1.2.1, this is common in biorefineries, where cellulose and hemicellulose are mainly utilized for ethanol production, while lignin is burned to produce steam and electrical energy.

HTL offers a pathway to produce aromatic compounds from lignin, mostly phenolic compounds, but without further processing of these products, HTL is not profitable due to the limited yields (Schuler et al., 2017).

Several studies aimed to evaluate the best conditions, in terms of operating temperature, lignin-to-water ratio, residence time, and catalyst type, in order to maximize biocrude yield through the HTL of different types of lignin (Yiin et al., 2022).

An important challenge in these experimental approaches is the limited scalability of the process for industrial applications. Excessive water and catalyst consumption, along with large residence times, contribute to increase reactors size and operational costs in continuous processes.

Rana et al. performed two different experiments for HTL of kraft lignin. The first one, using heterogeneous catalyst MoO_3/SBA-15 (10 wt%), achieved a maximum biocrude yield of 56.4%, with

a lignin-to-water ratio of 1:30. While effective, the high water demand at this ratio is impractical for industrial scale-up. Additionally, heating the feed to 350°C leads to large energy consumptions, and the required residence time of 60 minutes would necessitate very large reactor volumes for continuous operation (Rana et al., 2018).

The second experiment used K_2CO_3 (10 wt%) as homogeneous catalyst, leading to a maximum biocrude yield of 48.5%, at a slightly lower temperature, and with a lignin-to-water ratio of 1:10. Although these conditions are better than those of the first experiment, a 40-minute residence time remains excessive for developing a continuous industrial process with contained reactor volumes (Rana et al., 2019).

Similarly, Zhou (2014) conducted HTL using K_2CO_3 (1.6 wt%) as homogeneous catalyst, at 130 °C and with a lignin-to-water ratio of 1:6, achieving a biocrude yield of 45.6%. However, a 60-minute residence time was still required to reach this yield, leading to issues for scalability.

To summarize, the main challenges in converting lignin to phenolic compounds through continuous HTL processes are high water consumption and large residence times. Water usage could be decreased by implementing a water recycling loop, while residence times might be reduced by employing higher heating rates within the reactor. Additionally, to enhance arene yields in subsequent processes, the biocrude produced should be rich in monomeric phenols.

The work of Hirayama et al. (2024) investigated the influence of reaction temperature, residence time and heating rate on the yield of carbon recovery in biocrude for the HTL of alkali lignin, catalyzed by K_2CO_3 (1.6 wt%).

The results indicated that the highest carbon recovery in biocrude (52.2 wt% of the total carbon present in the lignin) was achieved at 320 °C, with a residence time of 1 minute and a heating rate of approximately 100 °C/min. This rapid heating is made possible using an induction-heating reactor system (IHRS), which is a contactless heating method that generates a magnetic field to heat any ferromagnetic material within the confines of the induction coils. This innovative reactor system contrasts with the more commonly used resistive-heating reactor system (RHRS), which typically provides a heating rate of 5–10 °C/min and requires longer preheating of the slurry, negatively impacting the biocrude yield.

The advantages of utilizing the induction-heating reactor system (IHRS) are mainly related to the shorter residence time. A brief residence time (1 minute) minimizes further depolymerization and decomposition reactions, which would otherwise decrease the yield of biocrude in favor of gas and solid products. Indeed, the highest biocrude yield (49.3 wt%) was obtained with a residence time of 1 minute, whereas the yield decreased to 37.3 wt% with a residence time of 15 minutes. Additionally, shorter residence times are cost-effective in an industrial-scale plant, as they reduce the reactor volume.

Furthermore, the experiments demonstrated the efficacy of adding phenol (4 wt% of the feed) as a capping agent, which reduces repolymerization reactions and enhances the liquid product (biocrude) yield.

The differences in carbon recovery (wt%) among the various phases of the products using IHRS and RHRS are illustrated in Figure 1.5.

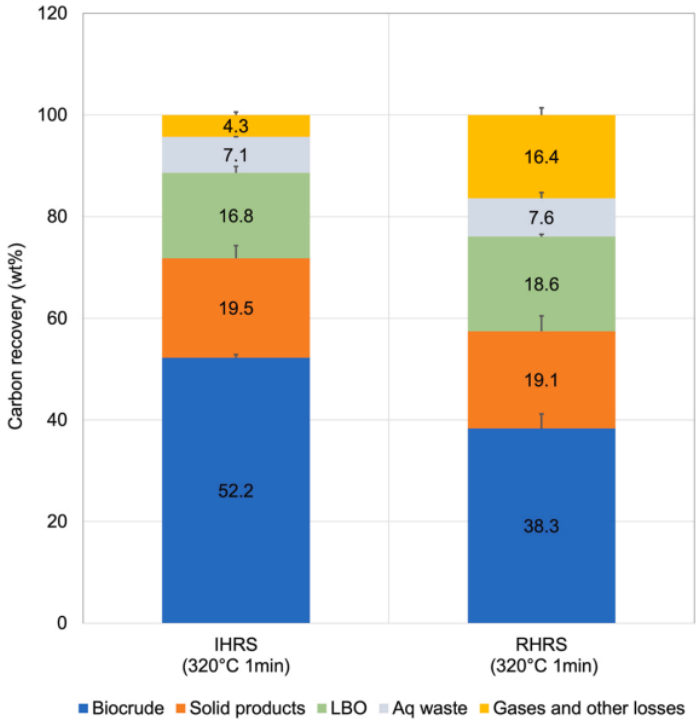

Figure 1.5: Carbon recovery in different phases of the HTL products (Hirayama et al., 2024)

Utilizing the IHRS instead of the RHRS under optimal conditions for biocrude yield, specifically at 320 °C and a residence time of 1 minute, results in an additional carbon recovery of 13.9 wt%. This increase signifies an improvement in recovery of valuable organic compounds in the biocrude (Hirayama et al., 2024).

1.4 Hydrodeoxygenation (HDO) of Biocrude

Lignin-derived biocrude requires further processing to produce high-quality fuels and chemicals. For this purpose, several processes are possible, including catalytic cracking, hydrodeoxygenation (HDO), steam reforming, and esterification.

Among these processes, catalytic HDO is particularly promising due to its economic feasibility, high deoxygenation yields (which increases the heating value and stability of the products), and relatively moderate operating temperatures (Prabhudesai et al., 2021).

The HDO process for lignin-derived biocrude involves the chemical removal of oxygen in the form of water and small oxygenates (e.g., CO_x) from the phenolic compounds present in the bio-oil. This

reaction occurs in a hydrogen-rich atmosphere in the presence of a catalyst, at temperatures between 200°C and 500°C and pressures up to 20 MPa (Riyang et al., 2020) (Zhang et al., 2020) (Prabhudesai et al., 2021).

The main products of HDO are either cycloalkanes or arenes, depending on operating conditions and type of catalyst used. Cycloalkanes formation proceeds via aromatic ring saturation, with larger hydrogen consumption but relatively low temperature, while the formation of arenes preserves the aromatic ring structure, which reduces hydrogen demand, but typically necessitates higher temperatures (Riyang et al., 2020).

1.4.1 Mechanism

Given the wide variety of compounds present in biocrude, studies on the mechanisms, kinetics, and catalytic performances in HDO reactions are typically conducted using model compounds, such as phenol, guaiacol, eugenol, anisole, cresol, and vanillin (Riyang et al., 2020) (Zhang et al., 2020) (Prabhudesai et al., 2021) (Maki et al., 2017).

Molecular structures of the above-cited compounds are presented in Figure 1.6.

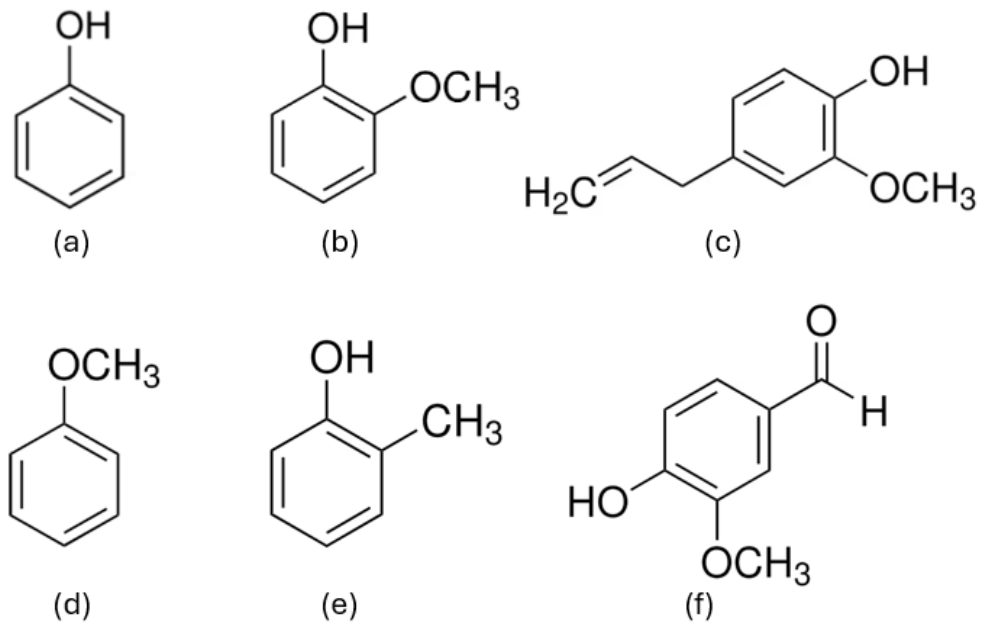

Figure 1.6: Molecular structure of biocrude model compounds. Phenol (a), guaiacol (b), eugenol (c), anisole (d), cresol (e), vanillin (f)

There are generally three main pathways for the HDO reaction of phenolic compounds, each leading to one of two possible products: cycloalkanes (e.g., cyclohexane) or arenes (e.g., benzene). The key step is the C-O bond cleavage, which can occur through different mechanisms. In the formation of cycloalkanes, the initial step involves hydrogenation of the aromatic ring, followed by dehydration of

the hydroxyl group. On the other hand, the formation of arenes proceeds through direct deoxygenation of the hydroxyl group, without any aromatic ring saturation (Prabhudesai et al., 2021) (Riyang et al., 2020).

A third, less common pathway has also been identified: the tautomerization-deoxygenation mechanism. In this pathway, the phenolic compound first undergoes isomerization to an unstable ketonic intermediate, followed by hydrogenation of the carbonyl group. After that, saturation of the aromatic ring may or may not occur, followed by deoxygenation, eventually leading to the formation of either cycloalkanes or arenes, depending on catalyst selectivity and hydrogen pressure (Prabhudesai et al., 2021) (Maglinao et al., 2019) (Maglinao et al., 2024) (Zhang et al., 2020).

Figure 1.7 represents the three possible pathways of HDO of p-cresol, a biocrude model compound.

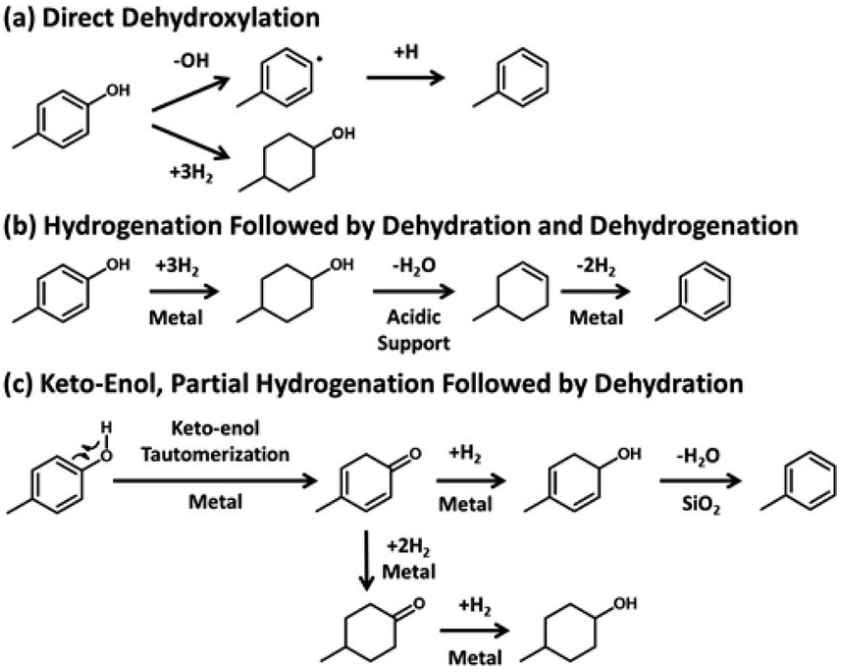

Figure 1.7: Possible pathways of p-cresol's HDO (Gu et al., 2016)

1.4.2 Catalysis

The HDO of biocrude involves different mechanisms and product formations, with pathway selectivity influenced by temperature, hydrogen pressure, and catalyst choice.

Studies on the stability and activity of various catalysts for biocrude HDO have explored noble, non-noble, and transition metal catalysts, such as Pt, Pd, Ru, Ni, Mo, etc., in the form of oxides, carbides, sulfides and phosphides. Moreover, different support materials have been utilized, such as Al_2O_3, ZrO_2 and activated carbon (Prabhudesai et al., 2021) (Bu et al., 2012).

Hydrogenation takes place on the metallic site, while deoxygenation, dehydration and hydrogenolysis require acidic sites, generally provided by the catalyst support material (Prabhudesai et al., 2021).
Originally, catalysis of biocrude HDO was studied using sulfide catalysts such as CoMo and NiMo, commonly used in the hydrodesulfurization processes in petroleum refineries (Riyang et al., 2020). However, maintaining the activity of these catalysts requires a sulfur atmosphere, which bio-based feedstocks cannot supply, and the introduction of a sulfur source would lead to H_2S emissions and the necessity to separate contaminants from the final products (Prabhudesai et al., 2021).
Currently, noble metal catalysts such as Pd, Pt and Ru are studied for their activity toward hydrogenation reactions, using different supports, such as Al_2O_3, which provides acidic sites for the deoxygenation process but tends to deactivate due to coking, and activated carbon, which is less acidic, but retains longer activity (Prabhudesai et al., 2021) (Maglinao et al., 2019) (Zhang et al., 2020) (Riyang et al., 2020).

1.4.3 Lignin-Derived Biocrude Conversion to Arenes through HDO Process

Production of aromatic hydrocarbons, or arenes, is a valuable alternative as fuel additives due to their high octane numbers (Riyang et al., 2020). More importantly, they serve as important platform chemicals that are currently derived almost exclusively from crude oil (Schuler et al., 2017) (Maglinao et al., 2024).
The selective production of arenes from biocrude through HDO can be achieved using different catalysts, such as noble metals over specific supports, high temperature, and moderate hydrogen pressure, to avoid complete saturation of the aromatic ring (Riyang et al., 2020).
Aromatic hydrocarbons are the main products of catalyzed HDO of phenol, anisole and guaiacol, using Mo- and Ni-based catalysts at high temperatures, while cycloalkanes formation takes place below 340 °C (Maki et al., 2017).
Ni and Fe catalysts on zeolite supports (HBeta) also demonstrate selectivity toward direct deoxygenation rather than the hydrogenation/dehydration pathway, which indicates weak adsorption of aromatic compounds on the catalyst surface. The main arenes generated from the HDO of biocrude model compounds include benzene, toluene, and xylene (Qu et al., 2021) (Shafaghat et al., 2016).
In large-scale HDO of lignin-derived biocrude, another important aspect is the choice of solvent, used for reducing the viscosity of biocrude, which is higher than that of pure model compounds, with different solvents showing selectivity toward either cycloalkanes or arenes formation (Maglinao et al., 2024) (Maglinao et al., 2019).
Water as a solvent in biocrude HDO has been found to increase hydrogenation rates compared to alkane solvents, promoting aromatic ring saturation and therefore decreasing arenes yields. Conversely, a

reduced hydrogenation rate was found using alkane solvents, such as hexadecane and cyclohexane, in HDO of phenols catalyzed by Pd/C and Ru/TiO_2 (He et al., 2014) (Maglinao et al., 2019) (Nelson et al., 2015). Moreover, solubility of phenolic compounds in water is very low, leading to severe problems at industrial scale, while miscibility ranges of phenols and alkane solvents are much larger (Maglinao et al., 2019).

Maglinao et al. (2024) investigated the selective production of arenes from phenolic compounds typically found in lignin-derived biocrude, using p-cresol as a representative model compound. HDO of p-cresol was conducted at 250°C and 4.2 MPa hydrogen pressure with Pd/C as a catalyst, comparing hexadecane and water as solvents. The main aromatic product was toluene. The experiment has been performed in a batch reactor with a 4-hour residence time and without agitation, yielding over 13% of toluene by mass when using hexadecane as a solvent, compared to a reduced yield of less than 1% when using water.

Additional experiments by Maglinao et al. included semi-batch processes, in which hydrogen was gradually introduced into the reactor until reaching the desired pressure, as well as different model compounds and solvent compositions. Moreover, a multi-step approach has been implemented, where hydrogenation and dehydration/dehydrogenation reactions occur in two different reactors, each one with a different solvent. More details about the results of these experiments will be presented in Section 2.3.

Unlike previous HDO studies (Maki et al., 2017) (Qu et al., 2021) (Shafaghat et al., 2016), which assumed direct deoxygenation as the primary mechanism for arene production, this process of toluene production is hypothesized to proceed via the tautomerization/deoxygenation pathway, as evidenced by the detection of ketones in the products mixture (Maglinao et al., 2024).

The tautomerization/deoxygenation pathway for converting monomeric phenol to benzene on a Pd/C catalyst is illustrated in Figure 1.8. The mechanism involves initial hydrogenation of the carbonyl group of the keto-tautomer intermediate, followed by deoxygenation of the hydroxyl group through dehydration (Maglinao et al., 2024).

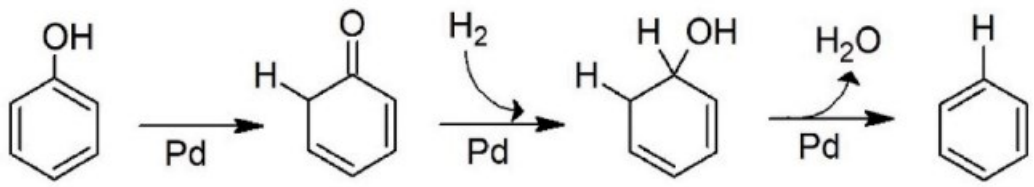

Figure 1.8: Mechanism of benzene production through HDO of phenol over Pd/C catalyst

1.5 Biolubricants

Lubricants are substances used to reduce the friction and wear between two moving surfaces. Typically, they also provide other functions such as heat generation reduction, heat dissipation, and prevention from corrosion and contamination of parts (Totten, 2006).

Although most lubricants are petroleum-based, researchers estimate that up to 90% of them could be substituted with biolubricants, renewable, bio-based compounds derived from vegetable oils or animal fats (Hussein et al., 2021). This transition is critical, as industrial demand for lubricants continues to increase, and over 50% of lubricants are released into the environment through spills, evaporation, or improper disposal, with 95% of these being petroleum-based, causing significant environmental damage (Reeves et al., 2017).

For these reasons, current environmental regulations are putting more restrictive rules on lubricants to minimize the environmental impact, particularly replacing petroleum-based lubricants with biodegradable and non-toxic biolubricants. For these purposes, an increase of research and development in more cost-competitive biolubricant production processes is taking place, mostly using non-food-competitive raw materials (Cecilia et al., 2020).

1.5.1 Properties

The key properties of lubricants include viscosity, lubricity, pour point, and foam resistance.

Viscosity of a lubricant is defined as its resistance to flow, and high viscosity is desirable when thicker lubricant films are necessary, as in diesel engine oils. Moreover, viscosity is highly dependent on temperature, and small changes in viscosity in large ranges of temperatures are desirable for lubricating purposes. This property is defined as viscosity index: normally, biolubricants have higher viscosity index compared to petroleum-based lubricants, indicating lower viscosity changes when varying temperature (Barbera et al., 2022) (Reeves et al., 2017).

Lubricity of a lubricant is defined as its ability to reduce friction and wear when creating a lubricant film between two moving surfaces, thereby reducing energy losses and heat generation. In general, biolubricants have better lubricity than petroleum-based lubricants. There are three types of lubrication regimes: boundary, mixed, and hydrodynamic, in order of increasing lubricant film thickness. This film may vary in thickness relative to the surface roughness of the lubricated components, affecting the extent of friction and wear. A thicker film ensures no sliding contact between the surfaces (Chan et al., 2018) (Barbera et al., 2022).

Figure 1.9 illustrates the three lubrication regimes.

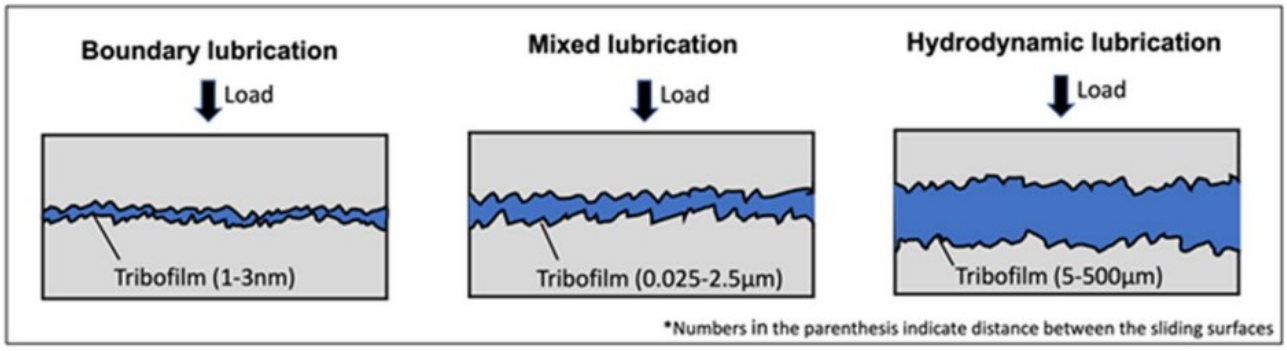

Figure 1.9: Lubrication regimes (Barbera et al., 2022)

The pour point of a liquid fuel or a lubricant is the lowest temperature at which it remains in the liquid phase, without creating wax crystals which could clog filters and pipes of the engine. This is a key characteristic for low temperature applications, as in engines that have to work at ambient temperatures below 0 °C. Generally, bio-based oils have higher pour point compared to petroleum-based oils, thus they have poorer cold flow properties (Barbera et al., 2022).

The foam resistance measures the lubricant's tendency to avoid foam formation, which can reduce lubricity and heat dissipation due to air bubbles. Generally, biolubricants have lower foam resistance because of their reduced oxidative stability (Barbera et al., 2022).

Vegetable oils, mostly triglycerides, and the products of their transesterification, the so-called fatty acid methyl esters (FAMEs), have a molecular structure made of a polar head (glycerol or ester group) and a non-polar tail (fatty acids carbon chain), with properties influenced by this molecular structure, as illustrated in Figure 1.10.

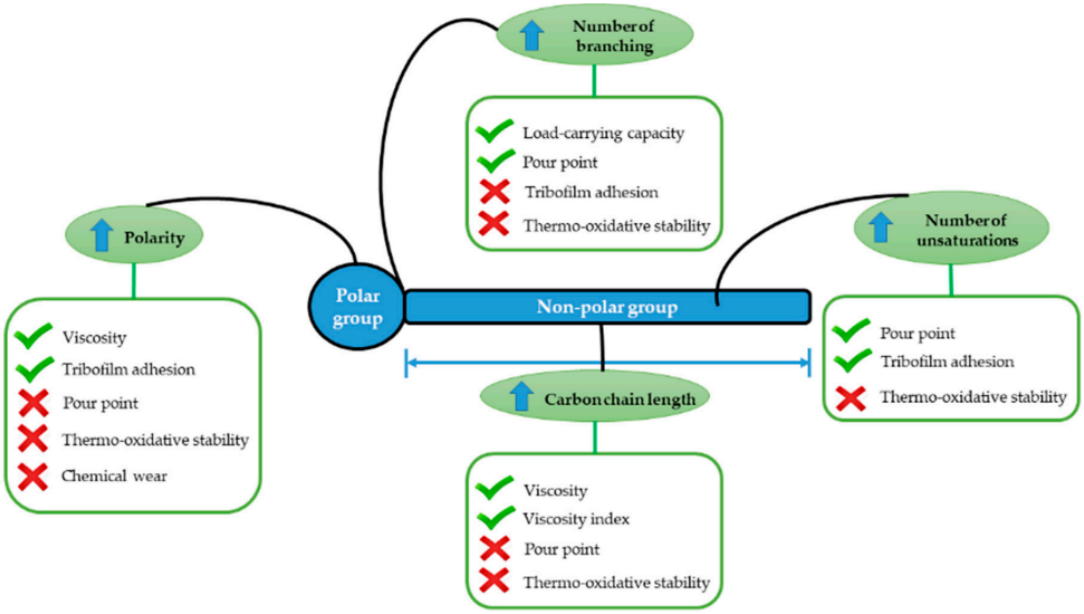

Figure 1.10: Relation between properties and molecular structure of FAMEs (Cecilia et al., 2020)

1.5.2 Biolubricants' Production Processes

As described in the previous section, the main disadvantages of natural oils compared to petroleum-based oils are higher pour point and lower foam resistance, related to lower oxidative stability. When producing biolubricants from triglycerides, the best strategy is molecular modification to balance cold-flow properties and oxidative stability, which can sometimes conflict, as elucidated in figure 1.10. Moreover, the use of additives in small amounts (up to 7%) is a common method to obtain the desired properties, mostly oxidative stability (Chan et al., 2018).

Biolubricants production methods focus on modifying ester groups, reducing unsaturations, and adding branches to fatty acid chains. These processes include epoxidation, estolide synthesis, esterification and transesterification (Cecilia et al., 2020) (Barbera et al., 2022).

Epoxidation of the C-C double bond improves oxidative stability, and the subsequent oxirane ring opening reaction generates a saturated and branched fatty acid chain, enhancing both cold flow properties and oxidative stability (Barbera et al., 2022).

Estolide synthesis process links fatty acids through ester bonds, forming oligomeric esters with improved oxidative stability, viscosity index, and cold-flow properties (Cecilia et al., 2020).

Esterification of fatty acids or transesterification of triglycerides are employed to produce FAME, also called biodiesel, esters that are usually added to the diesel fuel to improve lubricating performances. Other processes, such as alkylation or additional transesterification, can further improve lubrication properties of FAME, producing high value biolubricants (Barbera et al., 2022) (Hussein et al., 2021) (Maglinao et al., 2019). This topic will be further covered in the next sections.

1.6 Transesterification of Triglycerides

Transesterification is a substitution reaction in which an ester and an alcohol react in the presence of a catalyst to produce a different ester and a different alcohol (Norjannah et al., 2016). At an industrial scale, transesterification is utilized in polymer production processes (Kricheldorf et al., 2022), and in conversion of vegetable oils and animal fats into biodiesel (Mandari et al., 2022) (Borges et al., 2012) (Leung et al., 2010).

Biodiesel, a mixture of fatty acid esters, can be used either as a pure fuel or blended with petroleum-based diesel in compression ignition engines without requiring engine modifications (Borges et al., 2012) (Leung et al., 2010). Among the several biodiesel production methods, transesterification of natural triglycerides is the most common industrially (Leung et al., 2010).

Typical biodiesel feedstocks include edible vegetable oils, such as canola, palm, and sunflower oils; animal fats; and non-edible oils, such as waste cooking oil (WCO). However, edible oils and animal fats present challenges due to high costs and competition with the food industry. Additionally, animal

fats are solid at room temperature, complicating processing (Singh and Singh, 2010). In contrast, WCO offers a cost-effective and non-food-competitive alternative, especially considering that raw materials account for 60-80% of biodiesel production costs (Mandari et al., 2022), but it may contain impurities, such as free fatty acids (FFAs) and water, requiring pretreatment processes (Leung et al., 2010).

1.6.1 Mechanism

The most common transesterification process involves the reaction between vegetable oil and methanol in a 1:6 molar ratio to ensure complete conversion of the triglycerides, at 50-60 °C, and using a homogeneous alkali catalyst, such as KOH or NaOH, to produce fatty acid methyl esters (FAME) and glycerol as a by-product (Leung et al., 2010) (Mandari et al., 2022).
The simplified form of the transesterification reaction is illustrated in Figure 1.11.

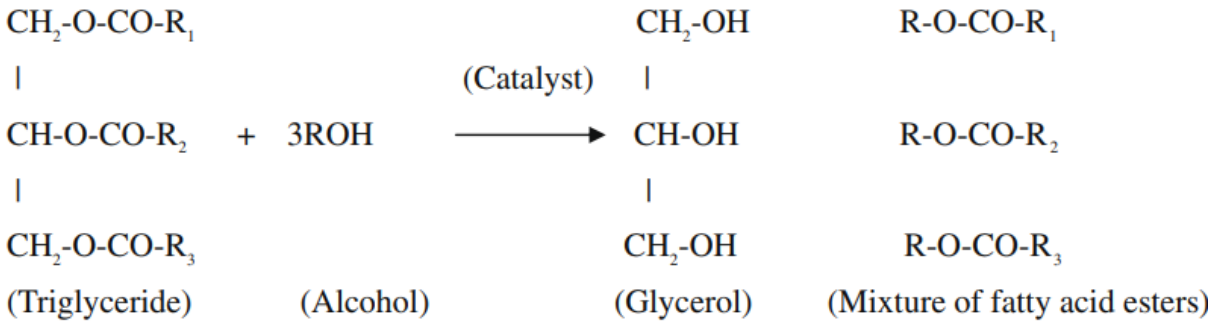

Figure 1.11: Transesterification of triglycerides (Leung et al., 2010)

Methanol and ethanol are the preferred alcohols due to their high reactivity and relatively low cost compared to longer-chain alcohols (Borges et al., 2012).
Impurities in the feedstock, such as water and FFAs, can lead to side reactions that reduce biodiesel yield. Water promotes the formation of diglycerides and FFAs through triglyceride hydrolysis, while FFAs react with the alkali catalyst, producing soap and water in a saponification reaction (Leung et al., 2010). These two side reactions are illustrated in Figure 1.12 and Figure 1.13.

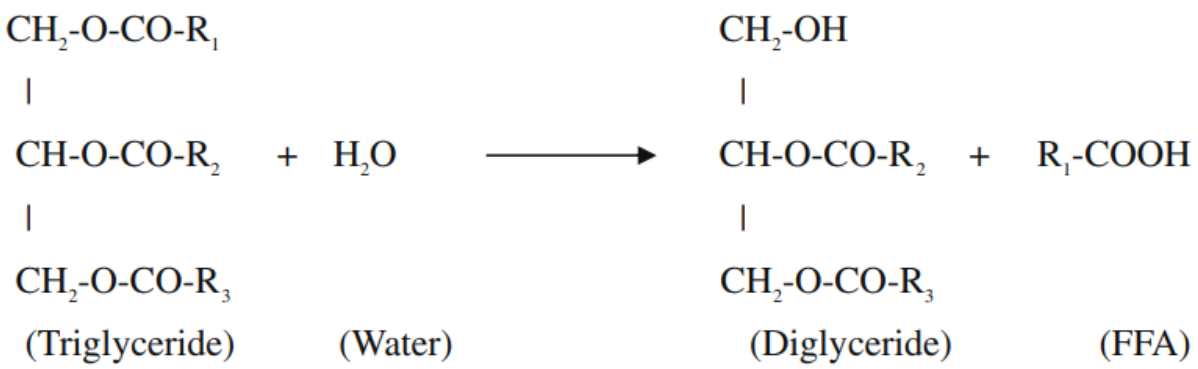

Figure 1.12: Hydrolysis of triglycerides (Leung et al., 2010)

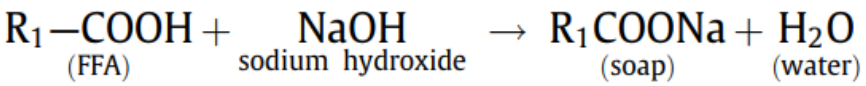

Figure 1.13: Saponification of free fatty acids (FFAs) (Leung et al., 2010)

To minimize these side reactions, feedstock must be anhydrous, and FFAs should be converted to FAMEs through acid-catalyzed esterification with methanol when using an alkali catalyst. Additionally, high temperatures should be avoided as they accelerate hydrolysis, further affecting yield (Borges et al., 2012) (Leung et al., 2010) (Mandari et al., 2022).

1.6.2 Catalysis

Triglycerides and alcohols typically do not form a single liquid phase due to immiscibility. Consequently, the effective contact area for the transesterification reaction is limited, necessitating the use of a catalyst to improve reaction kinetics. Heterogeneous catalysts enhance reaction rates by increasing the contact area between the two reactants, while homogeneous catalysts, usually dissolved in the alcohol, improve both the reactivity of alcohol molecules and mass transfer (Mandari et al., 2022).

Homogeneous catalysts are categorized into alkali and acid types. Alkali catalysts, such as NaOH and KOH, are the most used due to their high activity toward transesterification reactions, resulting in high oil conversion and biodiesel yield, and because of their low cost. However, alkali catalysts require separation from the alcohol after the reaction and need low levels of FFAs to avoid saponification (Leung et al., 2010) (Mandari et al., 2022).

Acid catalysts, such as concentrated sulfuric acid (H_2SO_4), can tolerate higher FFA concentrations in the oil feed, as they catalyze both esterification and transesterification reactions without causing saponification. However, they are less commonly used than alkali catalysts due to issues with corrosion, higher operating temperatures, and lower catalytic activity (Leung et al., 2010) (Gebremariam et al., 2018).

Currently, several studies focus on heterogeneous and enzymatic catalysis. Heterogeneous catalysts, such as CaO, offer advantages including a long catalyst lifetime, prevention of saponification, and reduced water consumption for purification processes. However, these catalysts require higher alcohol-to-oil molar ratios and reaction temperatures and pressures (Borges et al., 2012).

Enzymatic catalysts, such as lipase, could be a non-toxic option that avoids soap formation during transesterification. However, enzymes are expensive and sensitive to denaturation, limiting their industrial applicability (Leung et al., 2010) (Norjannah et al., 2016).

1.6.3 Transesterification Process

Depending on the feedstock and catalyst, the process configuration may vary, but the general catalyzed transesterification process follows similar main steps. In this process, oil is introduced into a stirred tank reactor together with an alcohol in stoichiometric excess to ensure complete conversion of triglycerides, and a pre-mixed catalyst. The transesterification reaction then produces biodiesel and glycerol. Afterward, the resulting two-phase mixture is directed to a decanter: the lighter biodiesel phase exits from the top and is sent to a purification column, while the alcohol and glycerol, containing dissolved catalyst, exit from the bottom and proceed to a distillation column. Here, the alcohol is separated and recycled back to the reactor, while glycerol and the catalyst are sent to a neutralization process, except in enzymatic catalysis (Perez et al., 2014). This general process is illustrated by the simplified process flow diagram (PFD) in Figure 1.14.

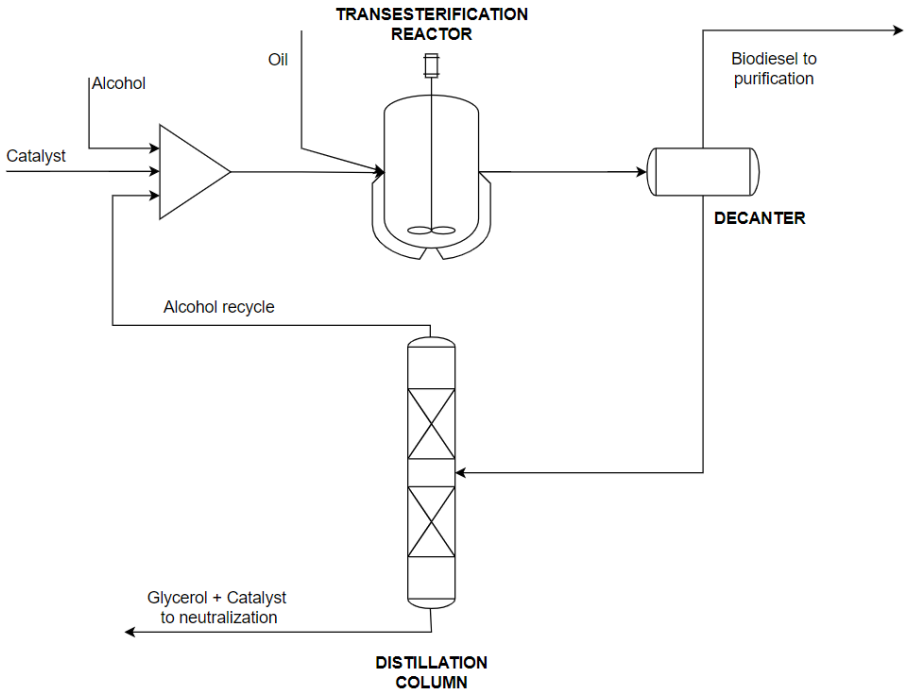

Figure 1.1412: Simplified PFD of a generic transesterification process

The work of Karmee et al. (2015) summarizes the differences of three possible layouts for converting WCO and methanol into biodiesel and glycerol using three different homogeneous catalysts: alkali, acid and enzymatic.

When using an alkali catalyst such as KOH, WCO requires pretreatment through an acid-catalyzed esterification with methanol to convert FFAs into FAMEs, thereby preventing soap formation. Only after pretreatment, the oil is fed into the reactor together with the mixture of methanol and KOH (Karmee et al., 2015).

For a process using an acid catalyst like H_2SO_4, pretreatment of WCO is unnecessary, as the acid catalyst not only prevents soap formation, but also catalyzes the esterification of FFAs present in the WCO. The other main unit operations are the same as the alkali catalyzed process (Gebremariam et al., 2018) (Karmee et al., 2015).

In the case of an enzymatic catalyst such as lipase, the WCO does not require pretreatment. The enzyme is recovered after the reactor through centrifugation, avoiding the need for neutralization (Norjannah et al., 2016) (Karmee et al., 2015).

After biodiesel production, it can either be sold as a finite product or employed for further processing. For example, Hussein et al. (2021) proposed a transesterification process of FAME with ethylene glycol, using CaO as heterogeneous catalyst, to produce dioleoyl ethylene glycol ester, a biolubricant. In another approach, Maglinao et al. (2019) proposed an aromatic alkylation of biodiesel with toluene,

catalyzed by K30 montmorillonite, to produce a phenyl-branched FAME (PBFAME) with improved lubrication properties, methyl n-(i-methylphenyl)octadecanoate (n-MMPO).

1.7 Alkylation of Arenes

Alkylation is a chemical reaction involving the addition of an alkyl group to an organic molecule, typically to alter its physical and chemical properties (Lin and March, 2001).

In the chemical industry, the alkylation of aromatic compounds is of particular interest, as in the alkylation of benzene with ethylene or propylene to produce ethylbenzene and cumene, respectively (Busca, 2007). These reactions are known as Friedel-Crafts alkylations, named after the chemists who developed them in 1877. This type of reaction is an electrophilic aromatic substitution, enabling the formation of a C-C bond between an aromatic ring and an electrophilic group while preserving the ring's aromaticity (Ohata, 2024) (Oliveira et al., 2017).

1.7.1 Mechanism

Currently, the generally accepted Friedel-Crafts alkylation mechanism involves different steps, illustrated in Figure 1.15.

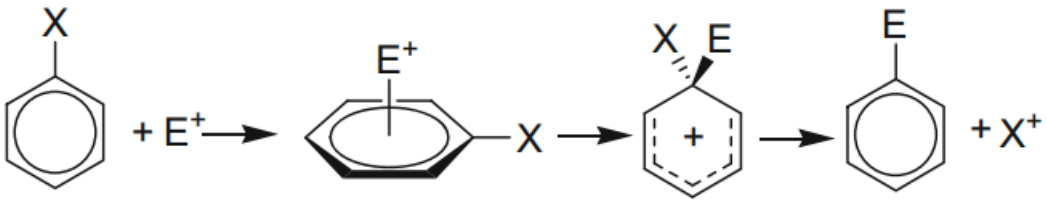

Figure 1.15: Friedel-Crafts reaction mechanism (Oliveira et al., 2017)

The first step is the formation of a π-complex, an intermediate created through electrostatic interactions between the electrophile and the aromatic ring. Following this, the electrophile attacks the aromatic ring, temporarily breaking the aromatic ring. The reaction concludes with the deprotonation of the resulting cation, which restores the ring's aromaticity and completes the alkylation process (Oliveira et al., 2017).

In industrial applications, the electrophile is often an unsaturated hydrocarbon activated by an acid catalyst. Reaction yields and selectivities depend significantly on the catalyst employed (Busca, 2007).

1.7.2 Catalysis

Catalysis in Friedel-Crafts alkylation can be achieved using either liquid or solid acid catalysts, involving both Lewis and Brønsted acid sites (Busca, 2007).

Traditional catalysts include Lewis acids like aluminum chloride ($AlCl_3$) and Brønsted acids such as sulfuric acid (H_2SO_4), which have high activity toward alkylation reactions at relatively low

temperatures. However, their environmental toxicity and the requirement for separation from the final product limit their suitability for sustainable and environmentally friendly processes (Busca, 2007) (Rueping et al., 2020).

On the other hand, solid acid catalysts, including zeolites, Amberlyst resins, and montmorillonite clays, provide heterogeneous catalysis that do not require separation steps and generally have longer lifetimes. Despite these advantages, their activity in alkylation reactions is typically lower than that of liquid acids, necessitating higher operating temperatures (Busca, 2007) (Maglinao et al., 2019).

1.7.3 Aromatic Alkylation of FAMEs

Some studies have explored the aromatic alkylation of unsaturated fatty acids to improve properties such as oxidative stability (by saturating C-C double bonds) and cold-flow properties (by introducing branching). This reaction holds potential for producing bio-based materials, including paints, lubricants, and polymers (Ngo et al., 2013) (Bian et al., 2017) (Maglinao et al., 2019).

Maglinao et al. (2019) investigated the alkylation of toluene with canola biodiesel, a mixture rich in unsaturated FAMEs (e.g., methyl oleate and methyl linoleate), to produce phenyl-branched fatty acid methyl esters (PBFAMEs) with enhanced lubrication properties. The reaction was conducted in a packed-bed reactor at 250 °C using K30 montmorillonite clay as a catalyst, with a 1:12 molar ratio of biodiesel to toluene maintained in the liquid phase under a pressurized nitrogen atmosphere. After separating excess toluene, the product mixture included both saturated and unsaturated FAMEs, as well as a newly formed compound, n-MMPO, a PBFAME derived from the alkylation of the C-C double bond in methyl oleate, with high methyl oleate conversion due to the additional formation of methyl oleate isomers, and a n-MMPO yield of more than 30%. The molecular structure of n-MMPO is illustrated in Figure 1.16.

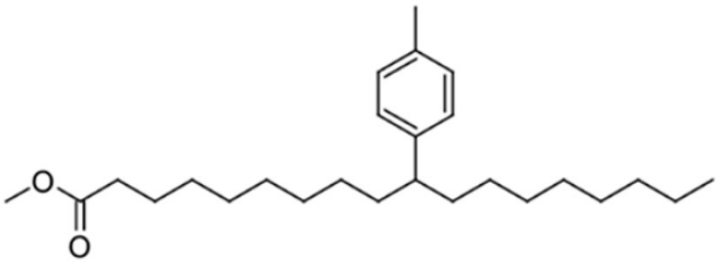

Figure 1.16: Molecular structure of n-MMPO (Maglinao et al., 2019)

The presence of n-MMPO in the FAME mixture improves both oxidative stability and cold-flow properties. This novel biodiesel formulation is a promising lubricant improver for ultra-low sulfur

diesel (ULSD), a cleaner diesel fuel with less than 15 ppm sulfur content but reduced lubrication properties compared to standard diesel (Maglinao et al., 2019).

1.8 Aim of the Thesis

The aim of this thesis is to perform process simulations and a techno-economic analysis for the production of phenyl-branched fatty acid methyl esters (PBFAMEs), to be used as biolubricant improvers. The proposed production process uses lignin and WCO as feedstocks, functioning as an auxiliary process to improve economics and environmental sustainability of a biorefinery that converts corn stover into ethanol.

Specifically, lignin derived from the UHS of the biorefinery undergoes HTL to yield phenolic compounds, which are then subjected to HDO to produce aromatic hydrocarbons, namely benzene. Concurrently, WCO is converted into FAMEs through transesterification. The benzene and FAMEs are then reacted in an alkylation process to produce a mixture of FAMEs and PBFAMEs, which are sold as by-products of the biorefinery.

Process simulations are performed using the Aspen Plus software. The economic analysis follows Turton's guidelines for estimating capital and operational expenditures (CAPEX and OPEX), while the cash flow analysis is based on assumptions used by NREL in its biorefinery's techno-economic analysis to evaluate the minimum ethanol selling price (MESP). The final goal of this study is to compare the MESP ($/gal) with and without the integration of the biolubricant production process, to determine its techno-economic feasibility.

Chapter 2: Process Description and Simulation

In this thesis, the investigated and simulated processes are the hydrothermal liquefaction (HTL) of lignin to produce biocrude, the hydrodeoxygenation (HDO) of biocrude to produce benzene, and the alkylation of benzene with fatty acid methyl esters (FAMEs) to produce phenyl-branched FAMEs (PBFAMEs). The lignin originates from the unhydrolyzed solids (UHS) of the biorefinery simulated by the National Renewable Energy Laboratory (NREL, 2011), which produces approximately 61 MMgal/yr of ethanol, starting from a feedstock of 2,200 dry ton/day of corn stover. On the other hand, FAMEs are derived from the process simulation by Hussein et al. (2021). Consequently, the ethanol production and transesterification processes are not detailed in this chapter, and further information on these can be found in the respective references.

A simplified block flow diagram (BFD) of the overall process is presented in this chapter, followed by a detailed description of each process (i.e., HTL, HDO, and alkylation) that includes process flow diagrams (PFDs), assumptions on the processes, and simulations specifics. In the absence of detailed kinetic studies for these specific processes, the reactions are modeled based only on experimental data on product yields. Catalyst properties are considered only for the sizing of the reactors and during economic evaluations; however, catalysts are not simulated in Aspen Plus to maintain simplicity in the process modeling at such an early design stage, focusing more on material and energy balances. Stream tables of the Aspen Plus simulations can be found in Appendix A.

2.1 Overall Process Description

The overall process is illustrated in the simplified BFD in Figure 2.1, highlighting only main streams and unit operations.

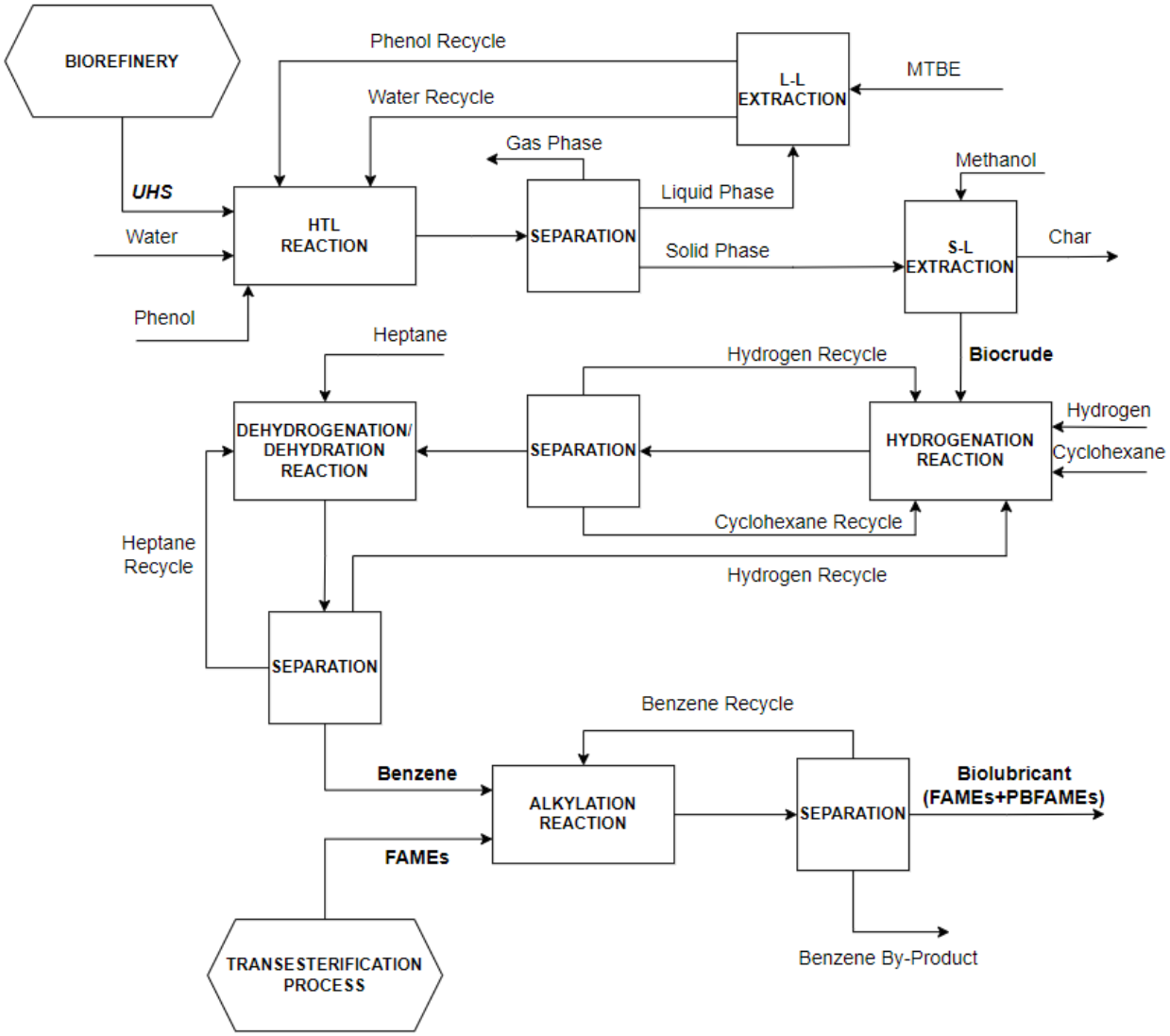

Figure 2.1: BFD of the overall process

UHS (i.e., lignin and water) from the biorefinery are combined with additional water and phenol (serving as a capping agent) and introduced into the HTL reactor. This reaction yields several products, including biocrude, gaseous products (mainly CO_2), and solid products. After removing the gaseous products through flashing, the liquid and solid phases are separated. Phenol is extracted from the liquid phase using methyl tert-butyl ether (MTBE), then both phenol and water are recycled back to the HTL reactor. The biocrude is retained in the solid phase and it is extracted with methanol, while the remaining solid products, called "char," are sent to the biorefinery's combustor.

The HDO process is implemented in two stages: an initial hydrogenation step followed by a dehydrogenation/dehydration step, each conducted in different reactors with distinct solvents. Biocrude is mixed with cyclohexane and introduced to the hydrogenation reactor together with

hydrogen gas. This reaction produces a mixture whose main products are fully saturated aromatic rings derived from the phenolic compounds in the biocrude. This product stream then enters a separation unit, where hydrogen and cyclohexane are recovered and recycled back to the hydrogenation reactor. The remaining organic compounds are mixed with heptane and sent to the dehydrogenation/dehydration reactor, yielding benzene as the main product.

After separation and recycling of the heptane, benzene is mixed with FAMEs from the transesterification process and sent to the alkylation reactor. Here, a portion of the unsaturated FAMEs reacts with benzene to produce PBFAMEs. The alkylation product is then processed in a separation unit to recover unreacted benzene, which is recycled back to the reactor, yielding the final biolubricant product, i.e., a mixture of FAMEs and PBFAMEs.

2.2 HTL Process

The HTL process converts the solid lignin present in the UHS into a liquid product called biocrude, which is rich in phenolic compounds. The assumptions and calculations required for the process simulation are based on personal communication and experimental data reported by Hirayama et al. (2024).

2.2.1 Process Description

A simplified PFD of the HTL process is presented in Figure 2.2. To avoid overlapping streamlines, heat exchangers shared between two different process streams (i.e., those that do not use external utilities) are highlighted in red. Additionally, streams that flow on the opposite side relative to the main process streams are also marked in red. These auxiliary streams move upwards when heated by the main streams and downwards when cooled.

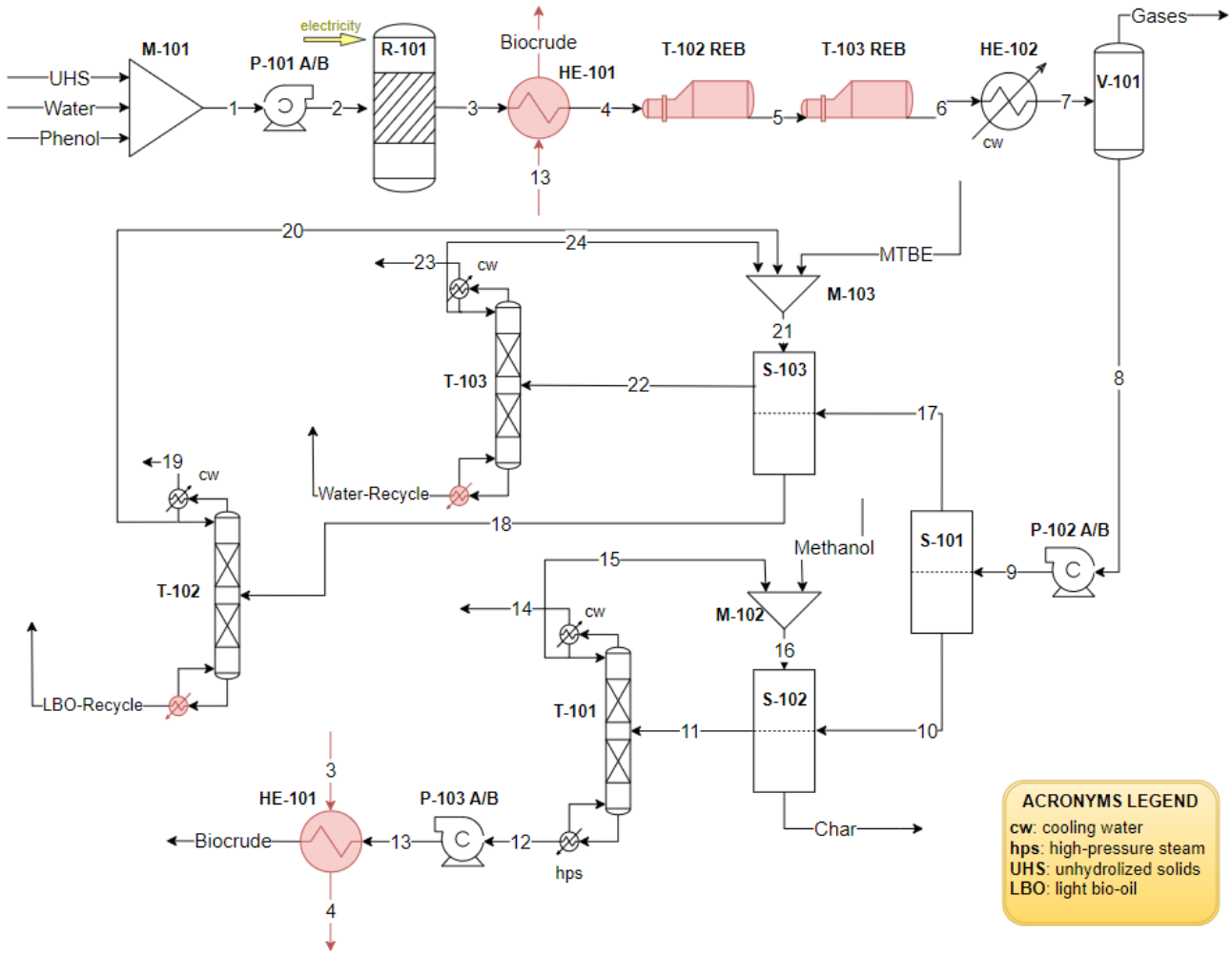

Figure 2.2: Simplified PFD of the HTL process

The UHS stream, originating from solids separation in the biorefinery (see Section 1.2), is a slurry composed primarily of water and insoluble solids, mainly lignin. This stream is mixed with additional water and phenol (4 wt%), reaching a solid concentration of 10 wt%, and is then pumped into the reactor at 117 bar. The HTL reaction occurs at 320 °C and 117 bar, near the critical point of water, with a residence time of 1 minute. The rapid heating of the slurry (approximately 100 °C/min) is permitted by the induction-heating system of reactor R-101. This system uses electrical power to generate a strong magnetic field, allowing the coils to heat more quickly than conventional resistive-heating reactor systems (RHRS), increasing biocrude yield (Hirayama et al., 2024).

The reactor outlet (stream 3) is a heterogeneous mixture consisting of solid, liquid, and vapor phases. During the reaction, the lignin structure is broken down, producing light gases such as CO_2 and CH_4, liquid biocrude (with phenol as the main component), and solid char. The addition of phenol as a capping agent reduces char formation (Hirayama et al., 2024). This hot stream at 320 °C undergoes heat recovery through several heat exchangers. It preheats the final biocrude up to 250 °C in HE-101

before sending it to the HDO process. Additionally, it serves as the hot stream in the reboilers of distillation columns T-102 and T-103, reducing overall steam consumption, and is finally cooled to 32 °C using cooling water in HE-102.

After cooling, the pressurized stream is sent to an atmospheric flash vessel (V-101). Here, light gases produced during HTL exit from the top, while the remaining slurry is directed to separation units. These gases should be further treated before being vented to the atmosphere, but the potential gas treatments were not considered in this work. Composition and flowrate of gases stream is shown in Table 2.1.

Table 2.1: Gases stream composition and flowrate

Component	**Wt%**
Water	2.2%
Phenol	0.1%
Anisole	3.5%
CH_4	3.9%
CO	14.3%
CO_2	75.9%
Methanol	0.2%
Total mass flowrate	61 tonne/day

The slurry from stream 8 is pressurized to 7 bar by pump P-102 and sent to a solid-liquid separator (S-101), where the organic phase and char are separated from the aqueous phase. The organic phase, which includes solid char and some water, is directed to a liquid-solid extraction unit (S-102) using methanol as the extraction solvent for biocrude. The char is removed from the bottom and sent to the biorefinery's combustor (approximately 145 tonne/day, with a LHV of 22.2 MJ/kg), while the mixture of biocrude, methanol, and water is directed to an atmospheric distillation column (T-101). In T-101, methanol and some water exit at 66 °C from the top and are recycled back to S-102, after mixing with fresh methanol. The biocrude is collected from the bottom at 111 °C, then pumped by P-103 and heated in HE-101 to the required conditions for the hydrogenation process (250 °C, 40 bar). Biocrude stream composition and flowrate are shown in Table 2.2.

Table 2.2: Biocrude stream composition and flowrate

Component	Wt%
Water	3.9%
Phenol	49.4%
Anisole	20.4%
Catechol	12.7%
Guaiacol	7.7%
Lactic Acid	0.1%
Acetic Acid	0.1%
Glycolic Acid	0.2%
Methanol	1.4%
Xanthene	4.1%
Total mass flowrate	397 tonne/day

The aqueous phase exiting S-101 (4,588 tonne/day) contains 3.7 wt% of phenol. A light bio-oil (LBO) stream, containing mostly phenol (93 wt%), is recovered in S-103 through liquid-liquid extraction using MTBE. Both outlet streams from this process contain MTBE, which is subsequently recovered from the tops of distillation columns T-102 and T-103 and recycled back to S-103. Meanwhile, water (4,429 tonne/day) and LBO (167 tonne/day) streams are recycled to the feed of reactor R-101.

2.2.2 Assumptions on the Process

The process described in the previous subsection involves simulating a continuous industrial-scale process derived from a laboratory-scale batch process. To perform this scale-up and simplify the simulation, several assumptions were made.

The UHS from the biorefinery are composed of water, soluble solids, and insoluble solids, with lignin as the main insoluble component. For simplification, it is assumed that UHS consists only of water (36 wt%) and lignin (64 wt%), with a mass flow rate of 35,554 kg/h, as indicated in the report by NREL. The flow rates of all other inlet streams are derived based on this reference.

According to the experiments conducted by Hirayama et al. (2024), lignin is mixed with water, phenol, and K_2CO_3 as a catalyst. However, the simulation neglects the presence of the catalyst, assuming that it is fully dissolved in water due to its high solubility (Shah et al., 2022). Assumptions regarding catalyst recovery and deactivation are outlined in Section 3.2. The feed compositions for the HTL reactor in both the experiment and the simulation are provided in Table 2.3.

Table 2.3: Composition of HTL reactor feed in the experiment and in the simulation

Component	Wt% in the Experiment	Wt% in the Simulation
Water	84.4%	86.0%
Lignin	10.0%	10.0%
Phenol	4.0%	4.0%
K_2CO_3	1.6%	-

In the absence of kinetic data for this specific HTL process, the overall yields of the main classes of products (i.e., biocrude, solid and gaseous products, and LBO) were calculated according to the study proposed by Hirayama et al. (2024). The calculations are based on the carbon recoveries (CR) measured for the experiment using IHRS at 320 °C for 1 minute residence time, and the carbon content in each reactant and product. With the following procedure, the yield of each product with respect to the inlet lignin is calculated.

The carbon that enters the reactor comes mainly from lignin and phenol, thus the inlet mass of carbon is based on the amount of lignin and phenol fed to the reactor. An example with an inlet of 1 kg of lignin (and thus 0.4 kg of phenol) is shown in Table 2.4.

Table 2.4: Mass of carbon entering the process

Component	Component mass inlet (kg)	Wt% of C in the component	Mass of C inlet (kg)
Lignin	1.0	52.3%	0.52
Phenol	0.4	76.6%	0.31
TOTAL	1.4	-	0.83

Once the total mass of C ($m_{C,TOT}$) is known, together with the CR and the wt% of elemental C for each class of products ($wt\%_C$ in i), given by the measurements performed by Hirayama et al. (2024), the two following equations can be used to calculate the mass outlet of each class of products (m_i).

$$m_{C,i} = CR \times m_{C,TOT} \tag{2.1}$$

$$m_i = \frac{m_{C,i}}{wt\%_C \; in \; i} \tag{2.2}$$

Table 2.5 summarizes the mass of each product class for this feed scenario, corresponding to a total inlet mass of 10 kg (including water and catalyst), with a total carbon mass of 0.83 kg. Solid products are categorized as "char," and LBO is assumed to be pure phenol. Experimental data were used to determine the carbon content of gaseous products.

Table 2.5: HTL products yields for 1 kg of lignin inlet

Class of products (i)	**CR (wt%)**	$m_{C,i}$ **(kg)**	$wt\%_C$ **in i**	m_i **(kg)**
Biocrude	52.2%	0.43	62.9%	0.68
Char	19.5%	0.16	60.7%	0.26
Gaseous Products	4.3%	0.04	29.2%	0.14
LBO	16.8%	0.14	76.6%	0.18
TOTAL	92.8%	0.77	-	1.26

The missing class of products is the aqueous waste, which contains carbon in the form of lactic, acetic, and glycolic acid, and methanol. The composition of each product class (excluding char) was obtained from further experimental measurements. Water amount was adjusted to ensure the total mass composition of HTL products sums to 100%, as shown in Table 2.6.

Table 2.6: Composition of HTL reaction products for each class of products

Class of Products	Component	Wt%
AQUEOUS WASTE	Water	84.5%
	Lactic Acid	0.2%
	Acetic Acid	0.1%
	Glycolic Acid	0.3%
	Methanol	1.0%
BIOCRUDE	Phenol	6.7%
	Anisole	1.5%
	Catechol	0.9%
	Guaiacol	0.6%
	Xanthene	0.3%
GASEOUS PRODUCTS	CH_4	<0.1%
	CO	0.2%
	CO_2	1.0%
SOLID PRODUCTS	Char	2.7%

This composition is used to simulate the outlet of the HTL reactor (R-101), according to the principle of mass conservation. It is assumed that some of the water reacted, and that unreacted lignin is contained in the char. Phenol is the most abundant product, partly because of its significant input (4 wt% of the feed), followed by anisole and catechol as major phenolic products.

In the experimental setup from Hirayama et al. (2024), the gaseous products are released after the reaction, while the liquid and solid phases are separated through vacuum filtration, modeled by separator S-101 in the simulation. The liquid phase consists of aqueous waste and LBO, while biocrude is trapped in the solid phase. The simulation assumes that char, along with anisole, guaiacol, catechol, and xanthene, are completely separated into the solid phase, with a solid fraction in stream 10 of 18 wt%, similar to the experimental one (i.e., between 15 wt% and 20 wt%). Phenol is split almost in half to ensure that 78% of the inlet phenol is recovered as LBO (Hirayama et al., 2024).

Subsequent steps involve extracting biocrude and LBO from their respective phases. In the experiment, acetone is used to extract biocrude from the solid products, while in the simulation methanol is chosen due to its similar behavior but lower cost. Methanol is fed in excess to S-102, ensuring complete extraction of biocrude components from the char. The residual char, containing some water and

dissolved organic acids, is sent to the biorefinery's combustor. After distillation to recycle methanol, the extracted biocrude is directed to the HDO process.

For the liquid phase extraction, diethyl ether (DEE) was used in the experiment to separate LBO from the aqueous phase. In the simulation, MTBE is selected as a cost-effective alternative, effectively extracting most of the phenol. However, MTBE accounts for 93 wt% of the extract (stream 18), and during separation in distillation column T-102, some phenol is recycled with MTBE, reducing the amount of LBO available for recycling to the HTL reactor feed.

2.2.3 Simulation Specifics

The process simulation of the hydrothermal liquefaction (HTL) process in the Aspen Plus software presents several challenges. Firstly, components such as lignin and char are considered non-conventional components due to their complex biomass-derived structure. To estimate their properties in the simulation, it is necessary to input specific parameters that Aspen Plus can use to develop property models for enthalpy and density. The parameter used in the simulation is the ultimate analysis (i.e., the elemental composition), retrieved from the experimental measurements. Table 2.7 provides the specific input parameters and property models used for these non-conventional components, based on models typically used for coal and char.

Table 2.7: Input parameters for non-conventional components on Aspen Plus

	Lignin	**Char**
Enthalpy Model	HCOALGEN	HCJ1BOIE
Density Model	DCHARIGT	DCHARIGT
Ultimate Analysis	C (52.3%), H (4.7%), N (0.3%), O (42.7%)	C (60.7%), H (4.5%), N (0.3%), O (34.5%)

After defining both conventional and non-conventional components, the next step is selecting an appropriate thermodynamic model. Given that the process involves several polar liquid-phase components without dissolved salts, the Non-Random Two-Liquids (NRTL) model is chosen. For most components, binary interaction parameters are retrieved from Aspen Plus databases. However, some phenolic compounds and organic acids do not have experimental binary parameters. In these cases, the missing parameters are estimated using the UNIFAC (Universal Quasi-Chemical Functional Group Activity Coefficients) method, a group-contribution model that predicts binary parameters when experimental data are missing. Aspen Plus employs the R-PCES (Reliable Prediction of Chemical Equilibria and Separation) framework for these estimations.

For the simulation of the HTL process, the main blocks are modeled as:

- R-101: yield reactor (*RYield*), which requires input only for the product yield distribution based on the HTL reaction yields (see Table 2.6). Product flow rates are adjusted to maintain mass conservation.
- T-200 REB and T-300 REB: coolers (*Heater*) with specified heat duties derived from the results of the reboiler duties of the respective distillation columns.
- S-101 and S-102: separators (*Sep*) with user-defined split fractions for each component, simulating phase separations based on experimental data.
- S-103: extraction vessel (*Extract*), where phenol and water are considered the key components for defining the two liquid outlet phases.
- Distillation Columns: rigorous distillation columns (*RadFrac*).

This setup allows for a realistic simulation of the HTL process, accounting for both the non-conventional nature of biomass components and the complex interactions between polar liquid-phase components.

The recycles of the solvents (i.e., methanol and MTBE) are modeled through design specifications on the total flowrates of circulating solvents, adjusting the make-ups to reach the desired values.

2.3 HDO Process

The HDO process converts the phenolic compounds of the biocrude into arenes, such as benzene. The assumptions and calculations required for the process simulation are based on experimental data in the form of personal communications by Maglinao et al. (unpublished data).

2.3.1 Process Description

A simplified PFD of the HDO process is presented in Figure 2.3. To avoid overlapping streamlines, heat exchangers shared between two different process streams (i.e., those that do not use external utilities) are highlighted in red. Additionally, streams that flow on the opposite side relative to the main process streams are also marked in red. These auxiliary streams move upwards when heated by the main streams and downwards when cooled.

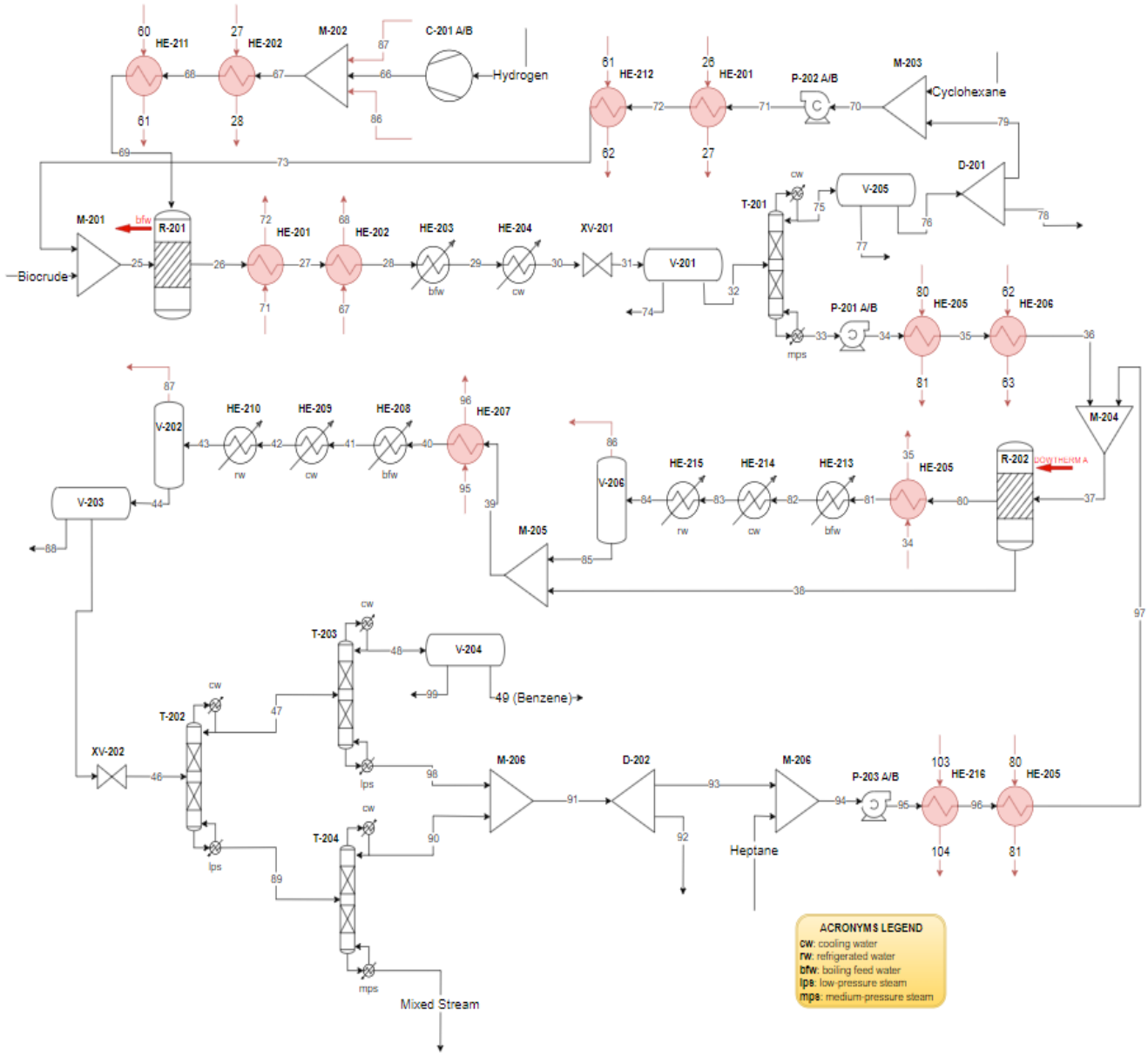

Figure 2.313: Simplified PFD of the HDO process

The biocrude produced from the HTL process is mixed with cyclohexane as a solvent in a 1:1 mass ratio and sent to the hydrogenation reactor (R-201). Hydrogen is fed from the top, reacting with biocrude at 250 °C and 40 bar. This reaction saturates the aromatic rings of phenolic compounds, producing cyclic compounds, mainly cyclohexanol. The exothermic reaction is cooled by boiling feed water (bfw), producing medium-pressure steam (mps). After the reactor, the hot effluent is cooled through heat exchangers, recovering energy by heating other streams and generating low-pressure steam (lps) in HE-203. It is then cooled to 50 °C in HE-204 and depressurized to 1 bar through valve XV-201.

At these conditions, the mixture separates into two phases: an organic phase and an aqueous phase. The water, together with some xanthene and methanol, is removed in the decanter V-201. The remaining stream is fed to a distillation column (T-201) to recover and recycle cyclohexane. Cyclohexane is separated from water in V-205, partially purged to prevent accumulation of impurities, and mixed with fresh cyclohexane. It is then pressurized to 40 bar in P-202 and heated to 269 °C across two heat exchangers using other process streams as heating sources. Preheating at 269 °C ensures that the feed to the hydrogenation reactor reaches 250 °C, as the mixing with biocrude reduces its temperature.

The bottoms product from T-201, containing hydrogenated biocrude, is pumped to 40 bar and heated to 250 °C for the subsequent dehydration/dehydrogenation step. This stream is mixed with heptane (1:1.7 mass ratio) as a solvent and fed into the dehydration/dehydrogenation reactor (R-202) at 250 °C and 40 bar. The reaction is endothermic, and heating is provided by condensing Dowtherm A vapor at 355 °C. The main product is benzene, but also hydrogen is released during the reaction.

The R-202 reactor outlet comprises both liquid and gas phases. The gas stream is utilized to heat another process stream, to generate lps, and is then partially condensed in HE-215 using 5 °C refrigerated water (rw). It enters flash vessel V-206, where hydrogen is separated for recycling back to the hydrogenation reactor, while the liquid stream is mixed with the R-202 outlet liquid phase, forming stream 39 at 223 °C. This stream heats another process stream and generates lps before being cooled to 25 °C and flashed in V-202 to recover additional dissolved hydrogen. After separating residual water in V-203, the organic mixture is sent to a separation unit consisting of three distillation columns.

The most volatile component is benzene, which exits from the top of T-203 together with some heptane and water, and is sent to a decanter (V-204) for water separation. After that, stream 49 (mostly benzene) is sent to the alkylation process. Composition and mass flowrate of this stream, as well as the benzene yield relative to inlet lignin, are summarized in Table 2.8.

Table 2.8: Stream 49 composition and benzene flowrate and yield

Component	**Wt%**
Benzene	95.2%
Heptane	4.2%
Cyclohexane	0.3%
Water	0.3%
Benzene mass flowrate	106 tonne/day
Lignin to benzene yield ($\frac{\text{kg of benzene outlet}}{\text{kg of lignin inlet}}$)	0.19

Heptane exits from the "middle" sections (bottoms of T-203 and top of T-204) and is partially purged. The remaining heptane is mixed with fresh heptane, pressurized, heated to the dehydration/dehydrogenation conditions, and recycled to R-202. The bottoms of T-204 contain a mixture of several organic compounds requiring further processing not simulated in this work. Possible transformations and applications of these compounds are discussed in Section 4.1. The composition and flowrate of the mixed stream are presented in Table 2.9.

Table 2.9: Composition and mass flowrate of the mixed stream

Component	**Wt%**
Heptane	20.3%
Phenol	5.5%
Anisole	15.9%
Guaiacol	3.1%
Cyclohexanol	10.8%
Methoxycyclohexane	19.0%
Dicyclohexyl Ether	20.6%
Hydrogen	0.2%
Xanthene	4.1%
Total mass flowrate	283 tonne/day

A key aspect of the process is the hydrogen feed to R-201, shown in the upper part of Figure 2.3. Fresh hydrogen is combined with recycled hydrogen streams recovered from flash vessels V-202 and V-206. The total hydrogen feed is preheated to 250 °C by process streams before entering R-201. In the

simulation, the hydrogen feed is set to match the stoichiometric requirements of the hydrogenation reaction, thus no excess hydrogen remains in the hydrogenation reactor outlet. Further details on assumptions and simplifications are discussed in the next subsection.

2.3.2 Assumptions on the Process

As with the HTL process simulation, the HDO process also involves several assumptions and simplifications to scale up from laboratory-scale batch experiments to an industrial continuous process. Without experimental kinetic data specific to this process, reaction modeling is based on yield distributions, requiring assumptions to estimate the HDO product composition.

First of all, the experimental reactions are performed in the presence of catalysts. In the simulation, catalyst presence is neglected for sake of simplicity.

Studies on the HDO of lignin-derived biocrude, summarized in Section 1.4.3, cannot be applied to this process because they use specific model compounds and combine hydrogenation and dehydration/dehydrogenation in a single reactor. Maglinao et al. (unpublished data) conducted relevant experiments with biocrude similar to that obtained from HTL of lignin by Hirayama et al. (2024), using a multi-step approach where hydrogenation and dehydration/dehydrogenation occur in separated reactors. Hydrogenation occurs first, in the presence of Pd/C catalyst and cyclohexane as a solvent, while dehydration/dehydrogenation follows in a separate reactor using Al_2O_3 and Pd/C catalysts, with heptane as the solvent. This experimental setup is replicated in the HDO process simulation, even though some product yield assumptions are necessary due to a lack of detailed data.

The procedure involves proposing a set of reactions based on observed products and personal communications, followed by iterative adjustments of yields and conversions to match the product composition observed in experiments. A set of six reactions for the hydrogenation process is illustrated in Figure 2.4.

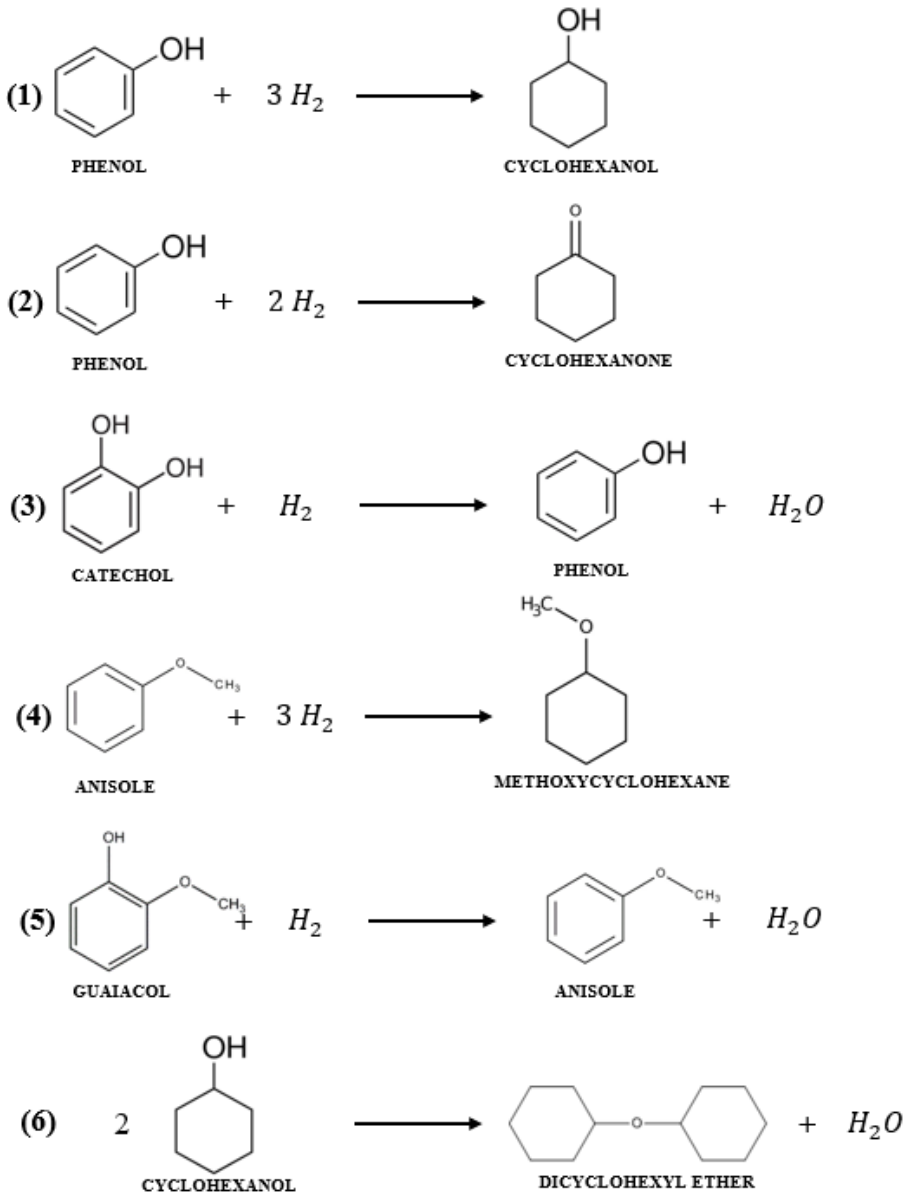

Figure 2.4: Proposed reactions for the hydrogenation process of lignin-derived biocrude

The following assumptions are the result of the iterative yield and conversion calculations:

- Cyclohexane does not react.
- Guaiacol conversion is set at 23%.
- Catechol conversion is set at 100%.
- The only oligomer formed is dicyclohexyl ether through cyclohexanol esterification.
- No side reactions or additional compound reactions occur.

After validating this procedure (i.e., matching simulated and detected product compositions), the same yields and conversions are applied to the biocrude from the simulated HTL process mixed

with cyclohexane, which has a slightly different composition compared to the one of the experiments, as highlighted in Table 2.10.

Table 2.10: Hydrogenation reactor feed composition in the experiment and in the simulation

Component	Wt% from experiment	Wt% from simulation
Phenol	26.0%	24.2%
Anisole	11.0%	10.1%
Catechol	5.0%	6.2%
Guaiacol	4.0%	3.8%
Cyclohexane	50.0%	49.9%
Others	4.0%	5.8%

It is noted that hydrogen reacts, so the mass of hydrogenated biocrude equals the sum of the liquid feed mass and the reacted hydrogen. For simplification, the hydrogen feed rate is set to match the stoichiometric reacted hydrogen, assuming no hydrogen remains in the reactor outlet. In reality, excess hydrogen is necessary, but assuming that no pressure drops occur along R-201, the unreacted hydrogen can be directly recycled back to the reactor, and thus it is neglected in the simulation. Excess hydrogen flowrate will be considered during the sizing of R-201 in Section 3.1.1. For a biocrude feed of 397 tonnes/day, hydrogen consumption is 19 tonnes/day (approximately 0.05 kg of hydrogen per kg of biocrude fed).

The final calculated composition of R-201 outlet is used to simulate the reaction in Aspen Plus. Compositions of detected compounds during the experiment and overall composition of the simulated hydrogenation products are presented in Table 2.11. Differences in some products wt% are attributed to the varying inlet compositions.

Table 2.11: partial composition of hydrogenated biocrude from the experiment and overall composition of hydrogenation products from simulation

Component	Wt% from experiment	Wt% from simulation
Phenol	0.3%	0.3%
Anisole	N/A	4.1%
Guaiacol	3.0%	2.9%
Cyclohexane	N/A	48.9%
Cyclohexanol	19.4%	19.3%
Methoxycyclohexane	7.6%	7.1%
Cyclohexanone	3.8%	3.8%
Water	N/A	3.6%
Dicyclohexyl Ether	N/A	7.1%
Xanthene	N/A	2.0%
Methanol	N/A	0.7%
Others	N/A	0.2%
TOTAL	**34.1%**	**100.0%**

Following solvent separation, the hydrogenated biocrude is directed to the dehydration/dehydrogenation reactor. In experiments, heptane is mixed with the hydrogenated biocrude at a mass ratio of 1.77:1, which is also used in the simulation. The reaction occurs at 250 °C and an autogenous pressure of 42 bar, simulated at 40 bar with preheated feeds.

Some undetected compounds are present in both inlet and outlet streams. The same approach as in the hydrogenation reaction is applied, with four proposed reactions depicted in Figure 2.5, including two hydrogenation reactions due to hydrogen release during dehydrogenation.

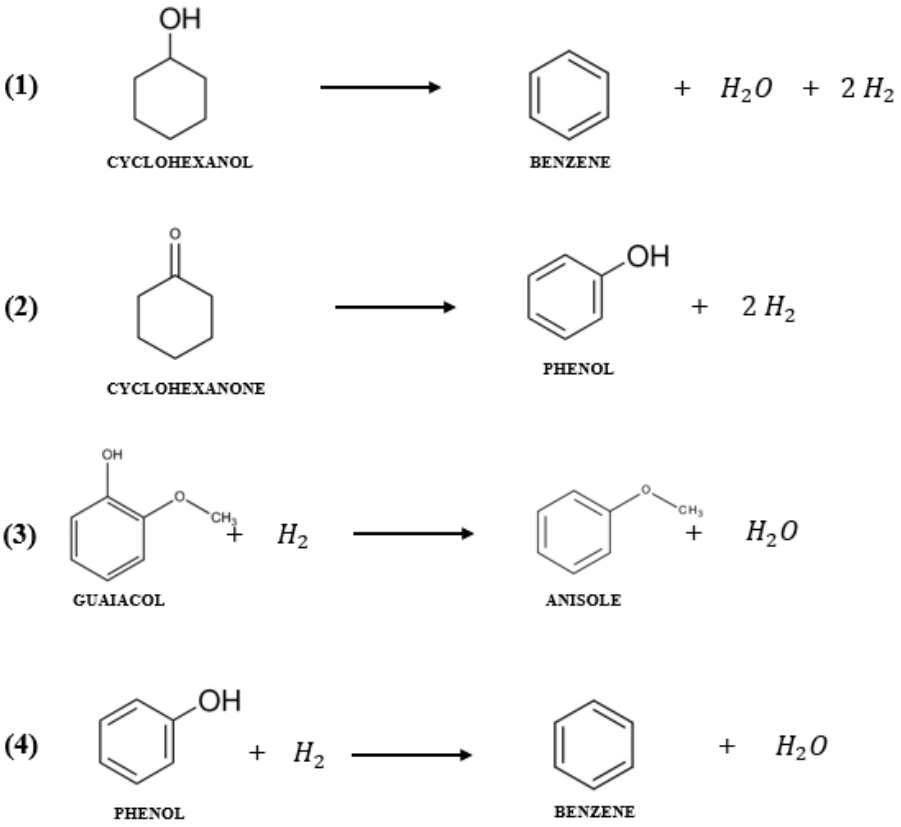

Figure 2.5: Proposed reactions for the dehydration/dehydrogenation process

The following assumptions are made during iterative yields and conversions calculations:

- Cyclohexanol conversion is equal to 80%.
- Cyclohexanone conversion is equal to 100%.
- Guaiacol conversion is equal to 60%.
- Anisole does not react.
- Methoxycyclohexane does not react.
- Heptane does not react.
- There are no side reactions, and other compounds do not react during the process

After verification (i.e., matching detected and simulated product compositions), the conversions and yields are applied to the dehydration/dehydrogenation feed, accounting for differences in the composition after cyclohexane separation and before heptane mixing, as shown in Table 2.12.

Table 2.12: composition of hydrogenated biocrude after cyclohexane separation in both the experiment and the simulation

Component	Wt% from experiment	Wt% from simulation
Phenol	0.9%	0.7%
Guaiacol	7.1%	6.3%
Cyclohexane	0.6%	0.4%
Cyclohexanol	37.3%	41.6%
Methoxycyclohexane	11.7%	14.6%
Cyclohexanone	8.2%	8.0%
Others	34.2%	28.4%

An important factor influencing product composition is cyclohexanol content in the reactor feed, a primary reactant for benzene production. In the experiment, cyclohexane separation via evaporation caused losses of other compounds. The simulation, using a rigorous distillation column, minimizes cyclohexanol losses in the distillate.

The final calculated composition of the R-202 outlet is applied to the simulated reactor in Aspen Plus. Uncertainty is higher than in hydrogenation reaction due to the limited number of detected products. Water and hydrogen, formed during the reaction, were not measured experimentally, but are estimated since the simulation's yield reactor requires total outlet composition, including both liquid and vapor phases. The measured liquid product and the simulated feed composition comparison is shown in Table 2.13, while the overall R-202 outlet composition is presented in Table 2.14.

Table 2.13: partial liquid product composition after dehydration/dehydrogenation reaction from experiment and from calculations with simulated feed

Component	Wt% from experiment	Wt% calculated
Phenol	1.4%	1.6%
Guaiacol	1.2%	0.9%
Methoxycyclohexane	4.1%	5.5%
Benzene	10.3%	11.0%
Others	83.0%	81.0%

Table 2.14: Overall outlet composition of the dehydration/dehydrogenation reactor in the simulation

Component	Wt%
Phenol	1.5%
Anisole	4.4%
Guaiacol	0.9%
Cyclohexane	0.1%
Cyclohexanol	3.0%
Methoxycyclohexane	5.3%
Water	2.7%
Dicyclohexyl Ether	5.6%
Xanthene	1.3%
Hydrogen	0.5%
Heptane	64.0%
Benzene	10.6%

Aspen Plus identifies liquid and vapor phases at the R-202 outlet. Subsequent processing aims to recover hydrogen while minimizing benzene loss, which is purified and sent to the alkylation process. During hydrogen recovery in flash vessels V-202 and V-206, traces of benzene and heptane appear in the recycled hydrogen stream; however, these are neglected in the simulation, assuming pure hydrogen is recycled to R-201, and neither benzene nor heptane are present in the reactor outlet.

2.3.3 Simulation Specifics

The process simulations for the HDO and the alkylation processes are integrated into a single Aspen Plus file to enable efficient heat recovery between streams from both processes. This integration is evident in the HDO PFD (Figure 2.3), where several heat exchangers serve both sections of the plant (Section 200 and Section 300), leading to shared property methods across the simulations.

In Aspen Plus, all components except dicyclohexyl ether are available in the standard databases as conventional components. Dicyclohexyl ether, a product of cyclohexanol esterification (Reaction 6, Figure 2.4), is rare, with limited studies on its properties. Given the lack of experimental data, the component's 2D molecular structure is imported from the *NIST Chemistry WebBook*, and Aspen Plus's "NIST TDE" tool is used to estimate its thermodynamic properties.

Consistent with the HTL process simulation, the presence of liquid mixtures containing several polar components without dissolved salts leads to the selection of the NRTL model as the primary

thermodynamic framework. However, for blocks involving pressurized hydrogen gas, the Soave-Redlich-Kwong (SRK) equation of state (EOS) is employed, as it more accurately predicts the thermodynamic properties of non-ideal gases. Missing binary interaction parameters in the NRTL model are estimated using the UNIFAC method.

The main process simulation blocks are modeled as:

- R-201 and R-202: yield reactors (*RYield*), which require input only for the product yield distribution based on the hydrogenation and the dehydration/dehydrogenation reactions yields. Product flow rates are adjusted to maintain mass conservation.
- V-201, V-203, V-204, V-205: decanters (*Decanter*), where water is selected as the key component of the second liquid phase.
- V-202, V-206, C-201: the two flash vessels and the compressor deal with pressurized hydrogen gas, thus they are modeled using SRK as the property method, which better estimates degree of vaporization of hydrogen during flash processes and work required for the compression.
- Distillation Columns: rigorous distillation columns (*RadFrac*).

As with the HTL process simulation, the recycles of solvents (i.e., cyclohexane and heptane) and hydrogen are modeled through design specifications on the required flowrates, adjusting the make-ups to reach the desired values.

2.4 Alkylation Process

The alkylation process involves the addition of a phenyl group (i.e., benzene) to the carbon chain of unsaturated FAMEs to produce PBFAMEs, utilized as biolubricant improvers in diesel fuels. The assumptions and calculations required for the process simulation are based on experimental data in the form of personal communications by Maglinao et al., while FAMEs composition is retrieved from process simulation results in Hussein et al. (2021).

2.4.1 Process Description

A simplified PFD of the alkylation process is presented in Figure 2.6. To avoid overlapping streamlines, heat exchangers shared between two different process streams (i.e., those that do not use external utilities) are highlighted in red. Additionally, streams that flow on the opposite side relative to the main process streams are also marked in red. These auxiliary streams move upwards when heated by the main streams and downwards when cooled.

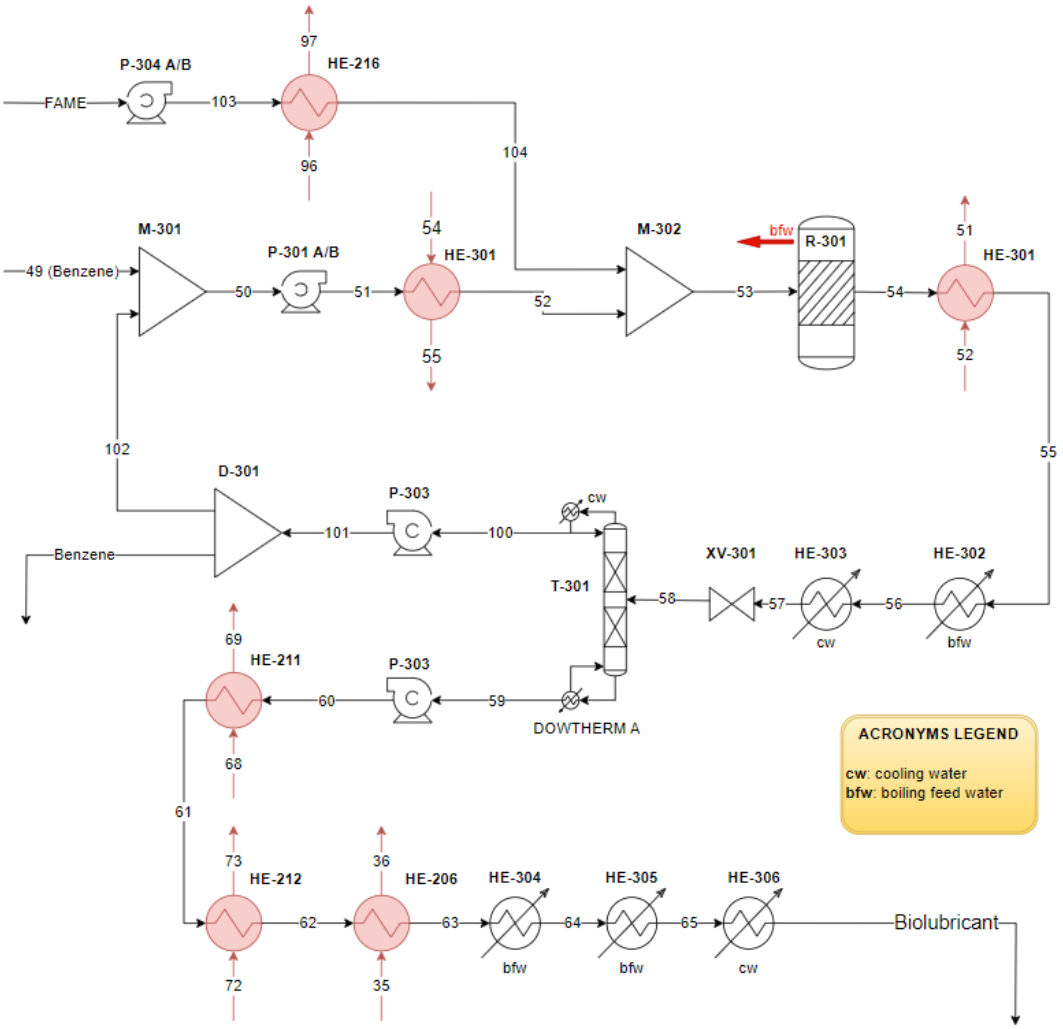

Figure 2.6: Simplified PFD of the alkylation process

Stream 49 (95 wt% benzene) is mixed with the recycle of unreacted benzene (stream 102), pumped to 40 bar and preheated to 175 °C by the alkylation reactor outlet through HE-301. Concurrently, FAMEs at 320 °C from the transesterification of WCO (Hussein et al., 2021) are pumped to 40 bar and serve as hot fluid to heat up another process fluid, before being mixed with benzene at 227 °C. Composition of FAMEs (or biodiesel) is shown in Table 2.15, where methyl palmitate and methyl stearate are saturated FAMEs, while methyl oleate, methyl linoleate, and methyl linolenate have one, two, and three C-C double bonds, respectively.

Table 2.15: FAMEs composition from transesterification of WCO (Hussein et al., 2021)

	Component	Wt%
Saturated FAMEs	Methyl Palmitate	29.9%
(37.4 wt%)	Methyl Stearate	7.5%
Unsaturated FAMES	Methyl Oleate	23.6%
(62.6 wt%)	Methyl Linoleate	35.7%
	Methyl Linolenate	3.3%

After mixing, the resulting liquid-phase feed (Stream 53) enters the alkylation reactor (R-301) at the target conditions of 210 °C and 40 bar. The exothermic alkylation reaction, which is kept isothermal by bfw to produce mps, occurs in R-301.

During the reaction, unsaturated FAMEs, specifically methyl oleate and methyl linoleate, react with benzene to form PBFAMEs. The reactor output is a mixture of FAMEs and PBFAMEs (the final biolubricant product), along with unreacted benzene and other compounds, mainly heptane. Post-energy recovery, where the stream is used to preheat the benzene feed and produce lps in HE-302, it is cooled to 40 °C before entering the vacuum distillation column (T-301) for biolubricant purification.

The distillation column operates under vacuum at 0.58 bar to lower the boiling point of the oils, minimizing degradation (Hussein et al., 2021). In the Aspen Plus simulation, the feed is depressurized to 0.58 bar through valve XV-301, then both the distillate and bottoms are repumped to 1 bar. In a real plant, a steam jet ejector could be employed for moderate vacuum distillation, as suggested by Turton et al. (2018). The reboiler in T-301 operates at 327 °C using condensing DOWTHERM A vapor at 355 °C instead of steam.

Given the higher volatility of benzene and heptane compared to the biolubricant, separation is efficient, and recovered benzene is recycled back to the reactor without further processing. However, due to excess benzene compared to the FAMEs feed, 54% of the benzene recycle is separated in the splitter D-301 and sold as a by-product.

Concurrently, the biolubricant product, exiting T-301 at 327 °C, serves as a hot fluid to heat three other process streams and generate mps in HE-304 and lps in HE-305 before being cooled to 30 °C with cooling water. The final biolubricant improver for diesel fuels consists of both saturated and unsaturated FAMEs and PBFAMEs, with composition and flowrate outlined in Table 2.16. Detailed molecular structures of PBFAMEs are discussed in the subsequent sub-section.

Table 2.16: Composition and flowrate of the biolubricant product

Component	Wt%
Methyl Palmitate	28.4%
Methyl Stearate	7.2%
Methyl Oleate	13.9%
Methyl Linoleate	21.1%
Methyl Linolenate	3.1%
PBFAMEs	26.3%
Total mass flowrate	324 tonne/day

2.4.2 Assumptions on the Process

Similar to previous process simulations, the lack of detailed kinetic studies and the scale-up from laboratory-scale batch experiments to industrial-scale continuous processes necessitate several assumptions and simplifications in modeling the alkylation reaction and yield distributions.

The main assumptions for the alkylation reaction are based on experiments conducted by Maglinao et al. (unpublished data). One key simplification in the simulation is the omission of the catalyst (K30 montmorillonite clays), which is essential in real processes, as no conversion of methyl oleate occurs without it (Maglinao et al., 2019).

In the actual experiments, methyl oleate was reacted with toluene instead of benzene due to the handling risks of benzene in laboratory settings. However, it is assumed that the simpler molecular structure of benzene, with its uniform reactive sites, would result in similar or even improved yields and conversions compared to toluene during the primary alkylation of unsaturated FAMEs (Smirniotis and Ruckenstein, 1995). Thus, the experimental yields and conversions of the alkylation reaction using toluene are assumed to be applicable to benzene when reacting with both methyl oleate and methyl linoleate.

The experiments were performed at 210 °C and 40 bar to avoid partial vaporization of the reactants. Considering the heterogeneous composition of the simulated FAMEs (as shown in Table 2.15), the mass of benzene fed is equal to the combined mass of methyl oleate and methyl linoleate, the two FAMEs undergoing alkylation. Consequently, 54% of the benzene recycle is separated in the splitter D-301 and sold as a by-product.

It is further assumed that methyl oleate and methyl linoleate exhibit similar behavior in terms of alkylation reactivity and adsorption on the catalyst. The main assumptions made for calculating the final product composition are as follows:

- The average yield of PBFAME (36.70%) relative to the methyl oleate feed in the experiments is applied to both methyl oleate and methyl linoleate.
- The average weight percentage of methyl oleate adsorbed on the spent catalyst (1.5 wt% of the inlet) is similarly applied to both methyl oleate and methyl linoleate.
- Only two reactions are considered: the aromatic alkylations of methyl oleate and methyl linoleate.

The aromatic alkylation reactions occur on the C-C double bonds in the FAMEs. Methyl oleate, with a single unsaturation at the C9 position, produces a saturated PBFAME. Methyl linoleate, which has two unsaturations at C9 and C12, mainly reacts at C9 due to its higher reactivity. Thus, the aromatic alkylation of methyl linoleate produces an unsaturated PBFAME, as a second alkylation at C12 is unlikely to occur based on personal communications. The resulting products are methyl 9-(phenyl)octadecanoate (saturated MPO) and methyl 9-(phenyl)octadec-12-enoate (unsaturated MPO), whose molecular structures are illustrated in Figure 2.7.

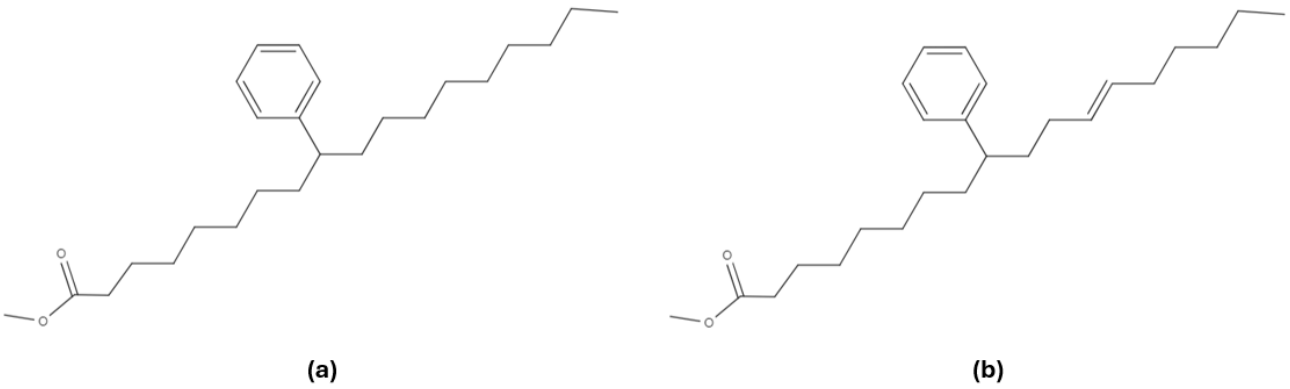

Figure 2.7: molecular structures of saturated MPO (a) and unsaturated MPO (b)

These PBFAME compounds are not available in standard databases. Therefore, for simulation purposes, both saturated and unsaturated MPO are represented by an aromatic ester with the same molecular formula as saturated MPO (i.e., $C_{25}H_{42}O_2$), referred to as benzyl stearate, or octadecanoic acid, phenylmethyl ester. It is assumed that benzyl stearate possesses similar properties to both PBFAMEs. Further details about this surrogated compound and its application in the simulation are discussed in the subsequent sub-section.

Following these assumptions, the yield distribution of alkylation products is determined and applied to the yield reactor (R-301). Reactor outlet composition is shown in Table 2.17, where PBFAMEs are defined as MPO.

Table 2.17: Alkylation reactor outlet composition

Component	Wt%
Methyl Palmitate	18.5%
Methyl Stearate	4.7%
Methyl Oleate	9.0%
Methyl Linoleate	13.7%
Methyl Linolenate	2.0%
MPO	17.1%
Benzene	33.2%
Heptane	1.6%
Others (water and cyclohexane)	0.2%

Additionally, isomers of methyl oleate were detected in the experimental products. It is assumed that the relative amounts of isomers produced are the same for both methyl oleate and methyl linoleate. The final detailed composition of the biolubricant product, compared to the simplified estimate from the simulation (Table 2.16), is presented in Table 2.18.

Table 2.18: Overall composition of biolubricant product

Component	Wt%
Methyl Palmitate	28.4%
Methyl Stearate	7.2%
Methyl Oleate	5.7%
Methyl Oleate Isomers	8.2%
Methyl Linoleate	8.7%
Methyl Linoleate Isomers	12.4%
Methyl Linolenate	3.1%
Saturated MPO	10.4%
Unsaturated MPO	15.9%
TOTAL	**100.0%**

2.4.3 Simulation Specifics

As outlined in sub-section 2.3.3, HDO and alkylation processes are simulated within a single Aspen Plus file, sharing the same specifications on property methods and main blocks (e.g., R-301 is a yield reactor, T-301 is a rigorous distillation column, etc.).

The simulation includes additional components: FAMEs derived from the transesterification process, as listed in Table 2.15, and an aromatic ester compound representing the produced PBFAMEs. All five FAMEs are available in the Aspen Plus databases. However, for the aromatic ester, benzyl stearate, its properties were estimated following the procedure described in sub-section 2.3.3 for dicyclohexyl ether. The component's 2D molecular structure was imported from the NIST Chemistry WebBook, and the Aspen Plus "NIST TDE" tool was used to estimate its thermodynamic properties.

Although benzyl stearate is not identical to the actual PBFAMEs produced, it was selected as a surrogate because it shares the same molecular formula and molecular weight (374.6 g/mol) as the saturated MPO, with the phenyl group attached at a different position relative to the ester group. This similarity ensures minimal impact on atomic balances. Aspen Plus estimated the boiling point of benzyl stearate to be 382 °C, which is slightly higher than the average boiling point of FAMEs (approximately 350 °C). This difference is relevant for the accurate simulation of the distillation column T-301. The molecular structure of benzyl stearate is depicted in Figure 2.8.

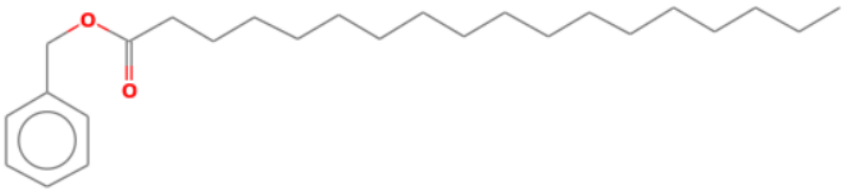

Figure 2.8: Molecular structure of benzyl stearate

The NRTL model was selected as the thermodynamic method for all components and process units. The UNIFAC method was employed to estimate any missing binary interaction parameters, including those for the simulated MPO, as it relies on the functional groups of the molecules.

Chapter 3: Techno-Economic Analysis

This chapter presents the methodologies and assumptions applied in the evaluation of capital expenditures (CAPEX) and operational expenditures (OPEX) for the integrated ethanol and biolubricant production process. Additionally, it details the cash flow analysis procedure conducted to compare the minimum ethanol selling price (MESP) with and without the integration of biolubricant production. Equipment and raw material costs are referred to year 2022, the most recent year with reliable pricing data.

The first section summarizes the specifics and assumptions involved in the CAPEX evaluation for the entire process. Equipment costs for the biorefinery, originally sourced from the NREL report, were updated from 2007 to 2022 values using the Chemical Engineering Plant Cost Index (CEPCI). For the additional novel processes, equipment sizing is performed initially to allow the estimation of both purchase and installation costs, followed by a comprehensive CAPEX evaluation procedure that aims at determining the overall direct and indirect costs associated with plant construction.

The second section provides a summary of the data required for OPEX evaluation. Variable OPEX (i.e., raw materials and utilities) are updated using the most recent reliable data available (typically from 2018 to 2022). Fixed OPEX, such as salaries and maintenance, are assumed to scale proportionally with CAPEX. This section also presents the pricing of by-products.

The third and final section describes the cash flow analysis procedure. Using the specifications proposed by the NREL report, the analysis calculates the MESP with and without the inclusion of the biolubricant production process.

3.1 CAPEX

The capital cost evaluation for the overall integrated process follows a standardized approach. However, different methodologies are employed for estimating the installation costs of various equipment components. For the reference biorefinery, the installation costs proposed by NREL are dated back to 2007, hence in this thesis they have been updated to 2022. For integrated processes, equipment sizing is conducted before the installation cost assessment. The size of the transesterification process equipment are obtained from the techno-economic analysis by Hussein et al. (2023), while the sizing of equipment for the simulated processes is determined using different methods. After estimating installation costs, the overall capital cost evaluation utilizes the procedure outlined in the NREL report as a benchmark.

3.1.1 Equipment Sizing and choice of Materials

Accurate sizing and material selection are fundamental to estimate purchase and installation costs, which are derived using cost correlations or specialized software. This study employs the "Capcost (2017)" Microsoft Excel tool, developed for use with the textbook “Analysis, Synthesis and Design of Chemical Processes, fifth edition” by Turton et al. (2018).

Capcost uses Turton et al.'s (2018) correlations and requires data on materials of construction (MOC), operating pressures (to determine wall thickness), reference dimensions (e.g., heat transfer area for heat exchangers, diameter and length for vessels, etc.), and power requirements for moving equipment such as pumps and compressors. Input data for each equipment type used in the overall process are summarized in Table 3.1. Low-cost components such as mixers, splitters, and valves are excluded from the purchase and installation cost estimates.

Table 3.1: Input data required by Capcost for each piece of equipment

PIECE OF EQUIPMENT	INPUT DATA
Heat Exchangers (S/T Fixed Tube Sheet, S/T Floating Head, Kettle Reboiler)	Tube side MOC and operating pressure (barg), shell side MOC and operating pressure (barg), heat transfer area (m^2)
Towers	Vessel MOC, tray or packing specifications (MOC and number of trays or height of packing), vessel diameter and height (m), operating pressure (barg)
Centrifugal Pumps	MOC, shaft power (kW), pressure at discharge (barg), number of spares
Reciprocating Compressors	MOC, fluid power (kW), number of spares
Vessels	Orientation (horizontal or vertical), vessel diameter and length (m), operating pressure (barg)
Jacketed Agitated Reactors	Reactor volume (m^3)
Centrifugal Centrifuges	Centrifuge diameter (m), number of spares
Leaf Filters	Filter area (m^2)

The input parameters required by Capcost are determined through various methods depending on the equipment type. The dimensions for most equipment in the simulated processes are generated using the Aspen Plus "Economics" tool, which maps and sizes all simulation blocks. However, specific pieces of equipment require alternative sizing approaches due to particular circumstances:

- Reboilers of T-102 and T-103 of the HTL process: they are simulated as standard coolers (*Heaters*) with specified heat duties derived from the results of the reboiler duties of the respective distillation columns. In practice, they are kettle reboilers where the hot fluid is the

effluent of the HTL reactor, and their heat transfer areas are not accurately predicted by Aspen Plus.

- Heat exchangers of the transesterification process: sizes are not provided by Hussein et al. (2023), necessitating independent evaluation.
- HTL reactor (R-301): its installation cost is estimated through a scale-up from pilot reactor costs using a capacity-based approach, without detailed sizing.
- Other reactors: reactors of HDO (R-201 and R-202) and alkylation (R-301) processes are sized according to fluid dynamic considerations to obtain number and dimensions of the vessels and possible intermediate heat exchangers. Transesterification and catalyst neutralization reactors of the transesterification process are modeled as jacketed agitated reactors whose volumes are retrieved from Hussein et al. (2023).

Detailed sizing procedures for the above-mentioned pieces of equipment are discussed in the subsequent sub-sections. After that, specifications used for the choice of the MOC are summarized.

3.1.1.1 Heat Exchangers

For shell-and-tube heat exchangers, including all condensers, and for kettle reboilers, the heat transfer area (A) required for cost estimation is calculated using a simplified formula:

$$A = \frac{Q}{U * \Delta T_{ml}} \tag{3.1}$$

where Q (W) is the heat duty (obtained from Aspen Plus); U (W/m^{2}K) is the overall heat transfer coefficient, estimated using the values proposed by Perry et al. (2018) for tubular heat exchangers (for shell-and-tube heat exchangers) and for coils immersed in liquids (for kettle reboilers), according to the type of fluids (e.g., water, alcohols, steam, vegetable oils, etc.) in tube side and shell side, respectively; ΔT_{ml} (K) is the logarithmic mean temperature difference in the heat exchanger, calculated from inlet and outlet temperatures of both the fluids.

An important design consideration for shell and tube heat exchangers is the choice between fixed-sheet and floating-head types. Floating-head heat exchangers, while more expensive, are easier to clean and are preferred for applications involving oils such as WCO and FAMEs. In contrast, fixed-sheet types are used for other fluids.

3.1.1.2 Hydrogenation Reactor (R-201)

The selected model for the hydrogenation reactor is a three-phase Trickle Bed Reactor (TBR), handling a liquid mixture of biocrude and cyclohexane, hydrogen gas, and a solid Pd/C catalyst. The TBR is a

vertical vessel with a packed catalyst bed, where both the liquid feed and hydrogen gas enter from the top (Ranade et al., 2011).

In the simulation, the hydrogen feed matches the stoichiometric requirement, with a flow rate of 777 kg/h. However, real hydrogenation processes require excess hydrogen. Bagnato and Sanna (2019) recommend hydrogen-to-biocrude molar ratios between 2 and 4, while Mailaram (2015) suggests using twice the hydrogen consumed. In this study, a ratio of 4 is adopted, leading to a total hydrogen feed of 1,576 kg/h.

With known liquid and gas flow rates, an overall residence time (θ) of 4 hours is targeted to complete the hydrogenation process. Given a liquid hourly space velocity (LHSV) of 2 h^{-1} (Bagnato and Sanna, 2019), the process requires 8 TBRs in series, each providing a 0.5-hour residence time. Intermediate cooling is provided by 8 heat exchangers using bfw to produce mps. The flow rates are assumed constant across reactors, with each heat exchanger managing 1/8 of the total heat duty of R-201.

Assuming a bed porosity (ϵ) of 0.4 for each reactor, the overall reacting system volume is 520 m^3 (65 m^3 per reactor). The diameters of the reactors are determined based on maintaining a trickle flow regime, which improves gas-liquid-solid contact (Ranade et al., 2011). After defining the flow regime, the design of the reactor is based on the transition curves diagram proposed by Ranade et al. (2011), shown in Figure 3.1.

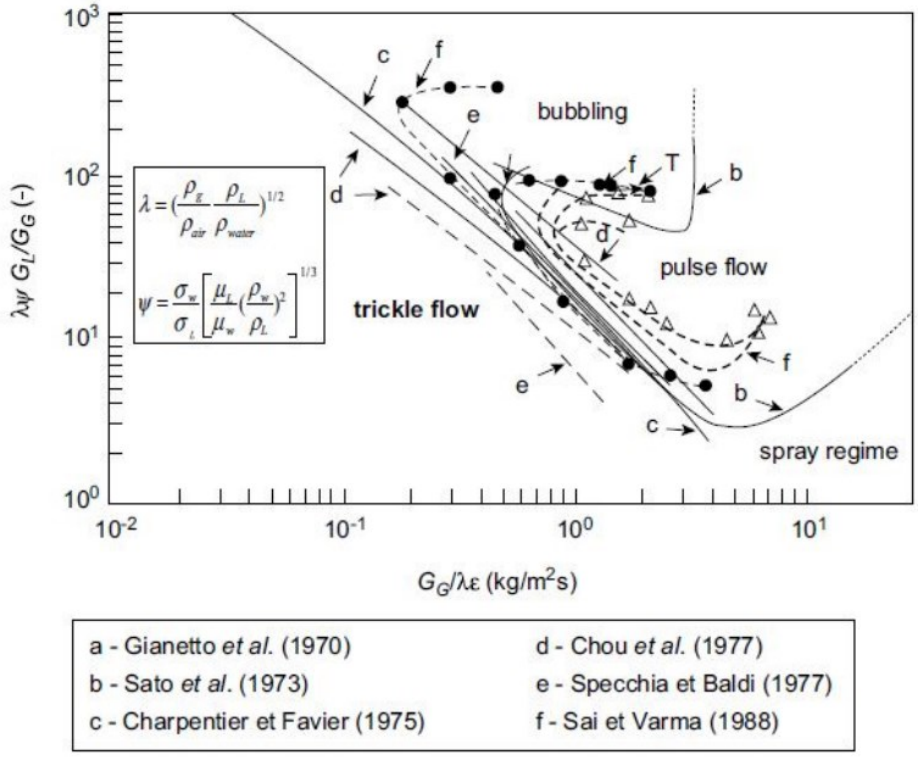

Figure 3.1: Transition curves diagram for different flow regimes in a TBR (Ranade et al., 2011)

This diagram utilizes dimensionless numbers λ and ψ, which normalize physical properties relative to water and air. It is used to graphically evaluate the value of $G_G/\lambda\epsilon$, where G_G is the mass flux of the gas inside the reactor, utilized to evaluate the actual cross-sectional area.

Table 3.2 summarizes the necessary properties of water and air, as well as the ones of liquid (biocrude and cyclohexane) and gas (hydrogen) feeds of the simulated process (retrieved by Aspen simulation), while Table 3.3 outlines main parameters and calculation results, including final reactor diameter.

Table 3.2: Physical properties of water, air, liquid and gas used in transition curves correlations

Physical Property	**Value**	**Unit of Measure**
Water density (ρ_w)	1,000	kg/m^3
Air density (ρ_a)	1.225	kg/m^3
Liquid density (ρ_L)	644.3	kg/m^3
Gas density (ρ_g)	1.890	kg/m^3
Water viscosity (μ_w)	1.14	mPa·s
Liquid viscosity (μ_L)	0.131	mPa·s
Water-air surface tension (σ_w)	73.0	mN/m
Liquid-gas surface tension (σ_w)	9.26	mN/m

Table 3.3: Parameters and results from transition curves diagram

Parameter or Result	**Value**	**Unit of Measure**
Liquid flowrate (G_L)	9.67	kg/s
Gas flowrate (G_G)	0.435	kg/s
Bed porosity (ϵ)	0.4	-
λ	1.00	-
Ψ	5.14	-
$\frac{\lambda\Psi G_L}{G_G}$	114	-
$\frac{G_G}{\lambda\epsilon}$	0.19	kg/m^{2}s
Reactor Diameter	2.7	m

The reactor length is calculated based on the fixed volume of 65 m^3 per reactor, and is equal to 11.4 m, resulting in an aspect ratio (ratio between length and diameter) of 4.2. The solid catalyst (Pd/C) is considered an operating cost due to its annual replacement (Azarpour et al., 2015), while the inert packing (Al_2O_3) is included in the purchase cost, assuming a bulk density of 1,400 kg/m^3. The heat transfer area for each intermediate heat exchanger is calculated using Eq. 3.1. Table 3.4 summarizes the main design parameters used in the evaluation of the purchase cost of the hydrogenation reactor system.

Table 3.4: Design parameters for hydrogenation reactor system purchase cost evaluation

Design Parameter	Value	Unit of Measure
Diameter of each vessel	2.7	m
Length of each vessel	11.4	m
Overall inert packing mass	435	tonne
Heat transfer area of each intermediate heat exchanger	30	m^2

The simplified configuration of the overall hydrogenation reactor system, made of 8 TBRs in series, with 8 intermediate heat exchangers, is illustrated in Figure 3.2.

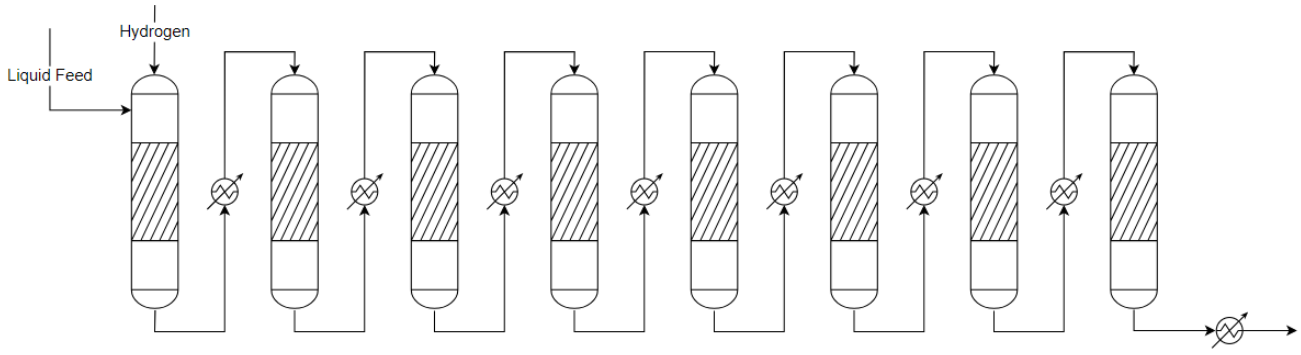

Figure 3.2: Simplified configuration of the hydrogenation reactor system (R-201)

3.1.1.3 Dehydration/Dehydrogenation Reactor (R-202)

The dehydration/dehydrogenation process is a liquid-phase reaction catalyzed by solid catalysts Pd/C and Al_2O_3. A fixed-bed reactor (FBR) is selected as a realistic commercial reactor for this process. As for the hydrogenation reactor, the design of the dehydration/dehydrogenation reactor is based on fluid dynamic considerations.

The FBR design focuses on minimizing pressure drops, a common challenge in packed bed reactors. An iterative procedure based on Perry et al. (2018) is applied, using fluid dynamic calculations for incompressible flows through packed beds of spherical particles. The Reynolds number (Re_P) is set, and the cross-sectional velocity (v_s) of the fluid is calculated using:

$$v_S = \frac{Re_P \cdot (1-\epsilon) \cdot \mu}{D_P \cdot \rho} \tag{3.2}$$

where ϵ (-) is the bed porosity; μ (Pa·s) is the fluid viscosity; ρ (kg/m^3) is the fluid density; D_P (m) is the nominal particles diameter.

The cross-sectional velocity is then used to calculate the diameter of the reactor based on the volumetric flowrate of the fluid, which is assumed to be constant along the reactor. The pressure drops per unit length ($\Delta p/L$) are then assessed with:

$$\frac{\Delta p}{L} = \frac{f_P \cdot \rho \cdot v_s^2 \cdot (1-\epsilon)}{D_P \cdot \varepsilon^3} \tag{3.3}$$

where f_P (-) is the friction factor derived from the Reynolds number, according to the flow regime. Table 3.5 summarizes parameters and calculation results of the proposed procedure.

Table 3.5: Parameters and calculation results for the design of the dehydration/dehydrogenation reactor system

Parameter or Result	Value	Unit of Measure
Volumetric liquid flowrate	0.0239	m^3/s
Liquid density (ρ)	506	kg/m^3
Liquid viscosity (μ)	0.0690	mPa·s
Bed porosity (ϵ)	0.4	-
Nominal particles diameter (D_P)	7.2	mm
Reynolds number (Re_P)	300	-
Cross-sectional velocity (v_s)	0.34	cm/s
Friction factor (f_P)	2.25	-
Pressure drops (Δp/L)	0.343	kPa/m

A slightly turbulent flow regime is selected, resulting in low liquid velocity and negligible pressure drops. The required residence time for the reaction is 2 hours. With a bed porosity of 0.4, the total reactor volume is 429 m^3, distributed across 3 FBRs in series (0.67-hour residence time each). Intermediate heating is provided by 3 heat exchangers, using condensing DOWTHERM A vapor as

the hot fluid. The heat transfer area for each exchanger is calculated similarly to the hydrogenation system, and only the inert packing mass is included in the purchase cost evaluation, with annual catalyst replacement considered an operating expense. The main design parameters used in the evaluation of the purchase cost of the dehydration/dehydrogenation reactor system are summarized in Table 3.6.

Table 3.6: Design parameters for dehydration/dehydrogenation reactor system purchase cost evaluation

Design Parameter	Value	Unit of Measure
Diameter of each vessel	3.0	m
Length of each vessel	20.3	m
Overall inert packing mass	360	tonne
Heat transfer area of each intermediate heat exchanger	15	m^2

Given the substantial length of each vessel (with an aspect ratio of 6.8), the FBRs are horizontally oriented. Although the final heat exchanger may be redundant in practice, it is included for consistency with the simulation, where the reactor outlet remains at 250 °C. Figure 3.3 illustrates the simplified configuration of the dehydration/dehydrogenation reactor system, including 3 FBRs in series with 3 intermediate heat exchangers.

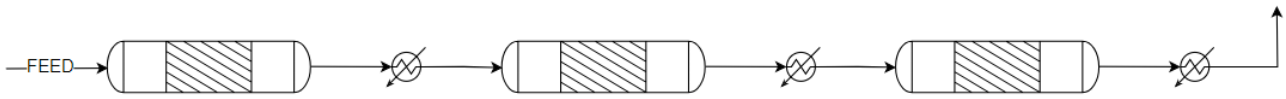

Figure 3.3: Simplified configuration of the dehydration/dehydrogenation reactor system (R-202)

3.1.1.4 Alkylation Reactor (R-301)

The alkylation process is a liquid-phase reaction catalyzed by a solid acid catalyst (K30 montmorillonite clays). The reactor is modeled as a fluidized bed reactor (FzBR), a vertical vessel where the liquid flows upward, fluidizing the solid powder composed of catalyst and inert sand. This configuration is chosen to simplify catalyst substitution, which occurs every 6 hours, according to experimental data.

The reactor design is based on fluid dynamic considerations, following the procedure proposed by Turton et al. (2018) for fluidized beds. After defining properties of both liquid feed and solid powder, Archimedes number (*Ar*, which is the ratio of gravitational forces over viscous forces) and minimum

fluidization Reynolds number (Re_{mf}) are calculated through Eq. 3.4 and Eq. 3.5, respectively, to subsequently evaluate the minimum fluidization velocity (u_{mf}) through Eq. 3.6:

$$Ar = \frac{D_P \cdot \rho_l (\rho_s - \rho_l) g}{\mu_l^2} \tag{3.4}$$

$$Re_{mf} = [(33.7)^2 + 0.0408 Ar]^{1/2} \text{-} 33.7 \tag{3.5}$$

$$u_{mf} = \frac{Re_{mf} \cdot \mu_l}{D_P \cdot \rho_l} \tag{3.6}$$

where D_P (m) is the nominal particles diameter in the bed; ρ_l and ρ_s (kg/m^3) are the densities of the liquid feed and the solid particles, respectively; g (m/s^2) is the acceleration of gravity; μ_l (Pa·s) is the liquid feed viscosity. Table 3.7 summarizes the main parameters and results, where liquid feed properties are obtained from Aspen simulation, and particle properties are sourced from Turton et al. (2018).

Table 3.7: Parameters and calculation results for the design of the alkylation reactor system

Parameter or Result	**Value**	**Unit of Measure**
Liquid density (ρ_l)	629	kg/m^3
Solid particles density (ρ_s)	2,650	kg/m^3
Liquid viscosity (μ_l)	0.153	mPa·s
Solid particles diameter (D_P)	150	µm
Archimedes number (Ar)	1,789	-
Reynolds number (Re_{mf})	1.07	-
Minimum fluidization velocity (u_{mf})	0.174	cm/s

The minimum fluidization velocity represents the lower limit required to achieve fluidization of the solid particles bed, which mainly consists of inert sand. A bubbling bed regime is selected to improve heat transfer, using an actual fluid velocity set at twice the minimum fluidization velocity. The exothermic reaction is maintained isothermal through internal cooling coils where bfw flows.

The selected fluid velocity, together with the volumetric flow rate of the feed (assumed constant), is used to evaluate the void cross-sectional area of the reactor. This area is further increased by considering that 25% of the actual reactor cross-sectional area is occupied by the cooling coils (Turton et al., 2018). Assuming a bed porosity of 0.5, the total reactor volume, including the volume occupied

by the internal coils, is 173 m^3. This volume is distributed across 4 FzBRs in series, with each reactor providing a residence time of 0.5 hours, to achieve a total residence time of 2 hours.
After the final reactor, a rotary drum filter is used to separate the solid particles, which are then recycled to the first reactor (after partial catalyst replacement). As in the previous reactor systems, the catalyst is considered an operating cost due to its substitution required every 6 hours, while the inert sand is accounted for in the reactor purchase cost. The main design parameters used in the evaluation of the purchase cost of the alkylation reactor system are summarized in Table 3.8.

Table 3.8: Design parameters for alkylation reactor system purchase cost evaluation

Design Parameter	Value	Unit of Measure
Diameter of each vessel	2.1	m
Length of each vessel	12.5	m
Overall inert sand mass	175	tonne
Rotary drum filter area	25	m^2

As a standard lay-out for FzBRs, the reactors are vertically oriented and the liquid flows upward. Figure 3.4 illustrates the simplified configuration of the alkylation reactor system, made of 4 FzBRs in series with internal coils, followed by a rotary drum filter.

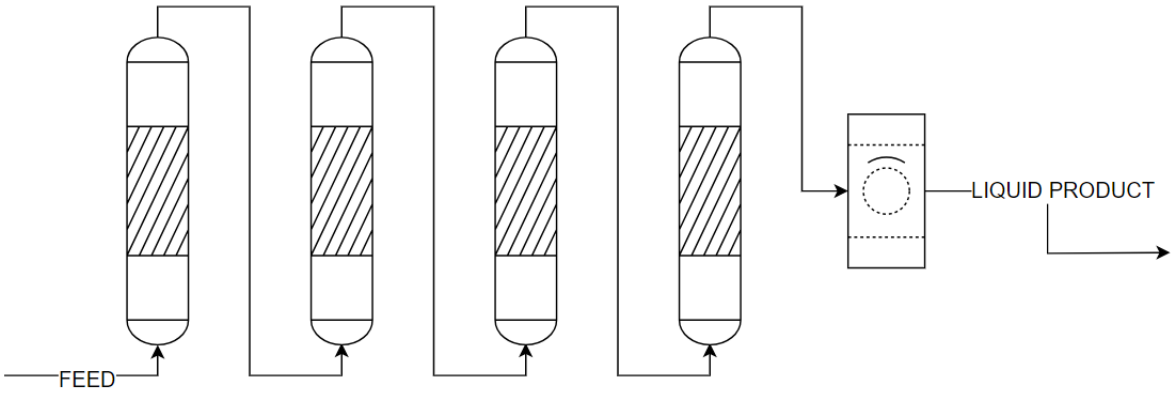

Figure 3.4: Simplified configuration of the alkylation reactor system (R-301)

3.1.1.5 Materials of Construction (MOC)

Selecting suitable materials for the equipment is crucial to ensure a long operational life of the plant, but it significantly impacts the final purchase costs. Carbon steel is the most cost-effective construction material, commonly used for moderate operating temperatures and non-corrosive environments.

However, its tensile strength decreases when temperatures approach 400 °C, and it exhibits poor chemical compatibility with FAMEs and pressurized hydrogen (due to hydrogen embrittlement) (Turton et al., 2018).

Given these limitations, while carbon steel is used in most of equipment, stainless steel is selected as the MOC for all components that handle FAMEs, pressurized hydrogen, and condensing DOWTHERM A vapor at 355 °C. Additionally, to ensure long operational lifetime and minimize maintenance, stainless steel is employed for all reactors, regardless of operating conditions.

3.1.2 Purchase and Installation Costs

The simplified approach applied in this study for updating the installation costs of biorefinery equipment is based on the Chemical Engineering Plant Cost Index (CEPCI) for the year of plant construction. The CEPCI is commonly used to update chemical plant construction costs to a desired time period. In this case, a straightforward calculation involving the CEPCI values for 2022 (reference year for this work) and 2007 (reference year for the 2011 NREL report) is performed to estimate the biorefinery equipment installation costs, as shown in Eq. 3.7:

$$Installation\ Cost_{2022} = Installation\ Cost_{2007} \frac{CEPCI_{2022}}{CEPCI_{2007}} \tag{3.7}$$

where $\mathrm{CEPCI}_{2022} = 813.0$ and $\mathrm{CEPCI}_{2007} = 525.4$, according to data from *Chemical Engineering Magazine* [1]. Based on these values, construction costs in 2022 show an increase of approximately 35% compared to 2007, resulting in significant rises in capital expenditures for new plants. The historical trend of the CEPCI values is illustrated in Figure 3.5.

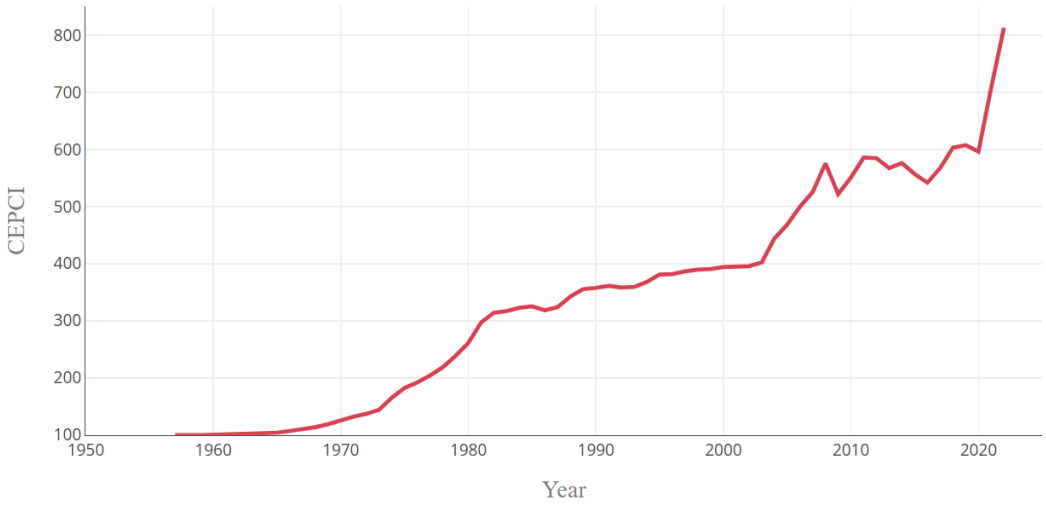

Figure 3.5: trend of CEPCI value from 1957 to 2022 (Chemical Engineering magazine)

As discussed in Section 3.1.1, Capcost is used to estimate the purchase and installation costs of equipment for the integrated biolubricant production process. These estimations use reference

dimensions and the CEPCI value for the specified year, following cost correlations proposed by Turton et al. (2018).

However, input data for cost estimation, summarized in Table 3.1, are characterized by specific applicability ranges. For instance, the costs of shell-and-tube heat exchangers can be evaluated for heat transfer areas between 10 and 1,000 m^2, while the maximum dimensions for towers are a diameter of 4 m and a height of 40 m. When a required value falls outside these ranges, the purchase cost estimation is performed using the scale-up correlation proposed by Turton et al. (2018):

$$\frac{Cost_{required}\ (\$)}{Cost_{base}\ (\$)} = \left(\frac{Size_{required}}{Size_{base}}\right)^{n} \tag{3.5}$$

In this equation, the base cost refers to the price assigned by Capcost to a piece of equipment with a standard reference size (e.g., length, area, volume, or shaft power) within its range of applicability. The parameter *n* is the cost exponent, a value between 0 and 1 depending on the type of equipment. Examples of cost exponents provided by Turton et al. (2018) and Peters and Timmerhaus (2003) include 0.59 for heat exchangers, 0.84 for reciprocating compressors, 0.62 for distillation columns, and 0.30 for vertical vessels. A more generalized approach is the six-tenths rule, which assumes a cost exponent of 0.6 for any equipment requiring scale-up or scale-down adjustments (Turton et al., 2018). Once the purchase costs of equipment are estimated, these values are multiplied by an installation factor to account for additional costs incurred during installation, such as piping and labor. Capcost employs various installation factors, typically ranging between 1.5 and 4, depending on specific construction characteristics, including equipment type, MOC, and wall thickness. For equipment sizes outside the applicability ranges of Capcost, Eq. 3.5 is used to determine purchase costs, which are then multiplied by the installation factors recommended by Capcost, ensuring consistency in the final installation cost estimation.

The only exceptions to this methodology are the reactors used in the simulated processes (i.e., R-101, R-201, R-202, R-301), for which the specific data and assumptions utilized to estimate both purchase and installation costs are detailed in Table 3.9.

Table 3.9: Design data and assumptions made for the estimation of purchase and installation costs of the simulated reactor systems

REACTOR ID	PURCHASE COST	INSTALLATION COST
R-101 (HTL Reactor System)	-	The installation cost of a pilot reactor working with a feed of 100 tonne/day is obtained from personal communication. Then, a scale-up to the simulated feed value, namely 5,460 tonne/day, is performed using the six-tenth rule.
R-201 (Hydrogenation Reactor System)	The design parameters from Table 3.4 are used as input data in Capcost to evaluate the purchase costs of vertical vessels and heat exchangers working at 40 bar and made of stainless steel. The overall purchase cost is then obtained summing up the costs of eight vessels, eight heat exchangers, and the inert packing.	Installation factors by Capcost for these specific pieces of equipment are 1.85 for the vessels and 2.15 for the heat exchangers. The installation factor for carbon steel reactors is 4 (Turton et al., 2018). An average installation factor of 2 is applied to the overall purchase cost.
R-202 (Dehydration/Dehydrogenation Reactor System)	The design parameters from Table 3.6 are used as input data in Capcost to evaluate the purchase costs of horizontal vessels and heat exchangers working at 40 bar and made of stainless steel. The overall purchase cost is then obtained summing up the costs of three vessels, three heat exchangers, and the inert packing.	Installation factors by Capcost for these specific pieces of equipment are 1.85 for the vessels and 2.15 for the heat exchangers. The installation factor for carbon steel reactors is 4 (Turton et al., 2018). An average installation factor of 2 is applied to the overall purchase cost.
R-301 (Alkylation Reactor System)	The design parameters from Table 3.8 are used as input data in Capcost to evaluate the purchase costs of vertical vessels working at 40 bar and made of stainless steel, and of the rotary drum filter. The overall purchase cost is then obtained summing up the costs of four vessels, one rotary drum filter, and the inert sand.	Turton et al. (2018) proposes an installation factor of 5 for carbon steel fluidized bed reactors, accounting for internal coils. An average installation factor of 2.5 is applied to the overall purchase cost.

3.1.3 Total Capital Investment (TCI)

After estimating the installation costs for all equipment, these values are used as the basis for calculating total direct and indirect costs (TDC and TIC), which are subsequently summed to determine the fixed capital investment (FCI). The FCI is then combined with land costs and working capital to evaluate the total capital investment (TCI). The approach applied in this work involves estimating the inside battery limits costs (ISBL), defined as the overall installation costs (or a fraction of them), and using these estimates to calculate additional capital costs in proportion to the ISBL, as outlined in the biorefinery report by NREL.

Initially, assumptions are made regarding the ISBL value for each process to prevent overestimating the TCI due to high-cost individual units. Portions of the installation costs for specific equipment are

allocated to the ISBL, while the remaining costs are added directly to the TDC as outside battery limits (OSBL). The key assumptions made for each process are as follows:

- Biorefinery: according to the NREL report, the ISBL does not include the installation costs for the wastewater treatment (WWT) system and the combustor.
- HTL Process: the HTL reactor system (R-101) accounts for approximately 77% of the total installation costs of the HTL process (Chapter 4). In this work, it is assumed that the installation cost of R-101 allocated to the ISBL is equivalent to that of the overall distillation system, presuming a similar impact on other direct and indirect costs.
- Transesterification process: in the absence of significantly high-cost individual units, the ISBL is set equal to the total installation costs.
- HDO and Alkylation processes: given the substantial installation costs of the three reactor systems (R-201, R-202, R-301), it is assumed that the impact on other capital costs from the three dehydration/dehydrogenation reactors (R-202) and the four alkylation reactors (R-301) is comparable to that of the distillation system for these processes (comprising five distillation columns, each with one condenser and one reboiler). The impact of the eight hydrogenation reactors (R-201) is assumed to be twice the one of the distillation system.

Once the total ISBL value is defined, the remaining capital costs are estimated according to the guidelines from the NREL report. The only exception is the land cost, which is calculated as 3.3% of the ISBL, based on the proportion between land price and ISBL found in the report, adjusted for the updated cost of industrial land in the U.S. for 2022. Table 3.10 provides a detailed breakdown of all CAPEX associated with the plant construction.

Table 3.10: CAPEX evaluation and description

CAPEX	VALUE	DESCRIPTION
ISBL (Inside Battery Limits)	Fraction of installation costs	Fraction of equipment installation costs which directly causes other capital costs.
OSBL (Outside Battery Limits)	Installation costs not allocated to the ISBL + 17.5% of ISBL	Fraction of the equipment installation costs which are not allocated to the ISBL; warehouse; site development; additional piping.
TDC (Total Direct Costs)	ISBL + OSBL	Overall direct costs for the plant construction.
TIC (Total Indirect Costs)	60% of TDC	Proretable expenses; field expenses; home office and construction fee; project contingency.
FCI (Fixed Capital Investment)	TDC + TIC	Sum of total direct and indirect costs, not accounting for land and working capital.
TCI (Total Capital Investment)	FCI + Land (3.3% of ISBL) + Working Capital (5% of FCI)	Total capital investment necessary for the complete construction and start-up of the plant.

3.2 OPEX

Operational costs are divided into variable OPEX (e.g., raw materials and utilities), which are directly related to plant production levels, and fixed OPEX (e.g., salaries and maintenance), which remain constant regardless of production activity.

Variable costs associated with raw material consumption are determined by using mass balances from process simulations, while utility costs are derived primarily from energy balances, also obtained through the Aspen simulations. Fixed OPEX is evaluated as a proportion of the CAPEX. In determining net OPEX, revenues from the sale of by-products are critical as they decrease overall costs.

Most raw materials and by-products prices are based on 2022 U.S. market data obtained from various web sources, while utility costs are retrieved from Turton et al. (2018).

3.2.1 Raw Materials

Key raw materials for the ethanol production process include corn stover, sulfuric acid, ammonia, and glucose. For both the processes with and without the integrated biolubricant production, biorefinery's raw material prices were updated from 2007 to 2022. A comparison of old and updated prices, maintaining the units of measure ($ per pound) used in the NREL report, is provided in Table 3.11. For some raw materials whose recent market data are missing, NREL's reported prices were kept due to their minimal impact on overall OPEX, given their limited use.

Table 3.11: Comparison between 2007 and 2022 prices for biorefinery's raw materials

Raw Material	2007 Price ($/lb)	2022 Price ($/lb)	Reference
Feedstock (corn stover)	0.0224	0.025	[2] [3]
Sulfuric acid 93%	0.0399	0.0274	[4]
Ammonia	0.1993	0.550	[5]
Corn steep liquor	0.0252	0.100	[6]
Diammonium phosphate	0.4385	0.3619	[7]
Sorbitol	0.5005	0.5156	[8]
Glucose	0.2579	0.2902	[9]
SO_2	0.1378	0.1378	NREL
Enzyme nutrients	0.3727	0.3727	NREL
Caustic	0.0678	0.1642	[10]
Lime	0.0904	0.0581	[11]
Boiler chemicals	2.2661	2.2661	NREL
Cooling tower chemicals	1.358	1.358	NREL
Make-up water	0.0001	0.0001	Turton et al. (2018)

The main differences in the newly evaluated biorefinery's raw materials prices regard corn stover, which is the main operational cost of the plant, and ammonia, whose price has increased by approximately 64% compared to the NREL report's value.

Raw materials for the integrated biolubricant production process include solvents, hydrogen, WCO, and catalysts. Updated wholesale prices ($/tonne) in the U.S. for these raw materials, categorized by process, are summarized in Table 3.12.

Table 3.12: Wholesale prices of raw materials in the integrated processes

Process Area	Raw Material	Price ($/tonne)	Reference
HTL	Fresh water	0.177	Turton et al. (2018)
	Phenol	1,439	[12]
	Methanol	382	[13]
	MTBE	1,146	[14]
	K_2CO_3	880	[15]
Transesterification	WCO	1,301	[16]
	KOH	747	[17]
	K_3PO_4	773	[18]
HDO	Cyclohexane	1,262	[19]
	Heptane	1,451	[20]
	Hydrogen	4,500	Salehmin et al. (2022)
	Pd	34,000,000	[21]
	Al_2O_3	10,000	[22]
Alkylation	K30 Montmorillonite	10,000	[23]

Hydrogen pricing depends on production method and conditions. For this work, hydrogen is supplied at 80 °C and 30 bar, produced through proton exchange membrane (PEM) synthesis using wind energy as the power source (Salehmin et al., 2022).

Catalyst pricing presents challenges, as accurate values are only available from specific vendors. Catalyst consumption, including make-ups, was also considered, even though they were not modeled in Aspen Plus, and thus material balances were not available for their evaluation. Further details regarding catalyst pricing and consumption assumptions are provided in the subsequent sub-section.

3.2.1.1 Catalysts

To ensure consistency, the catalysts used in laboratory-scale reactions are assumed to be employed in industrial-scale processes, with the same proportions compared to the feeds. However, scaling up necessitates additional assumptions regarding catalyst consumption and recovery.

The homogeneous catalyst of the HTL process (K_2CO_3) is assumed to be completely dissolved, and it follows the water throughout the entire process (Shah et al., 2022), leaving the process from the bottoms of T-103. Catalyst loss is therefore proportional to unrecycled water. Moreover, in the absence of studies about K_2CO_3 deactivation during HTL processes, recovery rates from pulping processes

(Tran et al., 2008) were used as an analogue, assuming that 3% of the recycled catalyst is lost, necessitating an additional make-up.

On the other hand, cost evaluations for solid catalysts such as Pd/C depend on their quality, shape, and loading in the reactors. For the hydrogenation and dehydration/dehydrogenation reactions, Pd/C loading is 0.29 wt% and 0.32 wt%, respectively. Economic evaluation assumes Pd/C (7%) is replaced annually (Azarpour et al., 2015), with costs estimated based on the consumed amount of pure Pd. Similarly, Al_2O_3 (3.2 wt% in the dehydration/dehydrogenation experiment) is replaced annually, and its cost is approximated as ten times the cost of inert packing material.

Finally, wholesale pricing for K30 montmorillonite clays is estimated at $10/kg. Based on experimental data, the catalyst deactivates after 6 hours (three times the alkylation reaction residence time), requiring frequent make-ups. The process demands 5 wt% of this catalyst, resulting in significant consumption costs.

3.2.2 Utilities and Waste Disposal

In the process, the utilities used are cooling or heating media, and electricity. Moreover, this section introduces two additional variable OPEX, related to the disposal of wastes, namely WWT and ash disposal costs.

Heating media are employed in the reboilers of distillation columns and for supplying heat during the endothermic dehydration/dehydrogenation process. The plant uses steam at different pressure levels (low, medium, and high pressure) as well as condensing DOWTHERM A vapor at 355 °C. The latter is specifically utilized in the biodiesel purification column reboiler (in the transesterification process) and in T-301 (for separating unreacted benzene from the biolubricant product). These reboilers work above 300 °C, and the constant temperature of the condensing vapor prevents overheating that could degrade FAMEs. DOWTHERM A is also selected as the heating medium for intermediate heat exchangers in R-202, which are employed to keep the temperature of the reacting system at 250 °C.

In the integrated process, DOWTHERM A is vaporized in the biorefinery combustor, with additional heating provided by burning corn stover, which is used as the primary energy source instead of natural gas or other fossil fuels. The cost of DOWTHERM A, expressed in $/GJ, is directly based on the amount of corn stover needed to generate 1 GJ of heat, assuming no heat dissipation in the loop. This calculation assumes a lower heating value (LHV) for corn stover of 16.74 MJ/kg (Rafiq et al., 2016) and a combustor efficiency of 80%, according to the NREL report.

Similarly, it is assumed that an additional amount of corn stover is directly burnt into the combustor as a substitute of the lignin that is not combusted in the integrated process, in order to obtain same amounts of steam and electricity from the biorefinery's combustor.

Prices for standard heating and cooling media (steam and cooling water) are taken from Turton et al. (2018) in $/GJ, allowing for a direct cost estimation given the heat duties of the equipment obtained by the Aspen simulations. Electricity price is the average electrical power cost in 2022 for industrial plants in the Midwest (location where the biorefinery should be built, according to NREL).
Waste disposal costs account for WWT and ash management. A secondary WWT (filtration followed by activated sludge employment) is performed on the water removed through the decanters in the HDO process, while ash disposal cost is applied to combustor's wastes.
Table 3.13 summarizes the costs of utilities and waste disposal.

Table 3.13: Costs of utilities and waste disposal

Component	Unit	Value	Reference
Cooling water (30°C)	$/GJ	0.378	Turton et al. (2018)
Refrigerated water (5°C)	$/GJ	4.77	Turton et al. (2018)
LPS (134°C, 2 barg)	$/GJ	4.54	Turton et al. (2018)
MPS (184°C, 10 barg)	$/GJ	4.77	Turton et al. (2018)
HPS (254°C, 41 barg)	$/GJ	5.66	Turton et al. (2018)
DOWTHERM A (355°C)	$/GJ	4.12	[2] [3]
Electricity	$/kWh	0.078	[24]
WWT (filtration + activated sludge)	$/m^3	0.043	Turton et al. (2018)
Ash disposal	$/tonne	31.82	NREL

3.2.3 Fixed OPEX

Fixed OPEX include salaries, labor burden, maintenance and property insurance. Their values are evaluated according to NREL guidelines. However, proper estimation of number of employees and salaries is challenging, thus a simplified approach is utilized in this work. During the updating of the biorefinery's costs, salaries are updated through comparisons of average salaries in the chemical industry between 2007 and 2021 [25]. After that, the ratio between total salaries and TCI is calculated, and it is applied also to the integrated process. All the other fixed OPEX are based on NREL report.
Table 3.14 summarizes the values of the fixed OPEX.

Table 3.14: Fixed OPEX values

Fixed OPEX	Value
Salaries	0.59% of TCI
Labor burden	90% of salaries
Maintenance	3% of ISBL
Property insurance	0.7% of FCI

3.2.4 By-Products

The objective of this economic analysis is to determine the minimum selling price of ethanol, the primary product of the biorefinery. The integrated process also produces a biolubricant improver as the main by-product, with its market price estimated based on similar commercial biolubricants. Additionally, the plant generates other by-products, including glycerol and K_3PO_4 from the transesterification process, along with a fraction of unreacted benzene which is not recycled back to the alkylation reactor. These compounds have established markets and can be sold as valuable by-products, thereby improving the economic performance of the biorefinery.

Table 3.15 summarizes by-products prices, updated to 2022 values in the U.S.

Table 3.15: By-products wholesale prices

By-Product	Price ($/tonne)	Reference
Biolubricant	3,500	Personal Communication
Benzene	1,073	[26]
Glycerol	700	[27]
K_3PO_4	857	[28]

3.3 Cash Flow Analysis

After defining FCI and TCI, variable and fixed OPEX, and revenues from by-products sales, a discounted cash flow rate of return (DCFROR) analysis is employed to calculate the MESP ($/gal). This process involves adjusting the ethanol selling price iteratively until the project's net present value (NPV) equals zero. This analysis considers factors such as expected plant lifetime, discount rate, depreciation method, federal tax rates, and construction start-up timeline. Additionally, since the plant is equity-financed, some assumptions about loan conditions must also be considered.

Parameters required to perform this cash flow analysis are sourced from the NREL report. However, some adjustments are made, such as a unique overall plant depreciation and recovery period, and a complete return of the land cost after plant dismissing. The main parameters applied to the cash flow analysis, taken from the NREL report, are detailed in Table 3.16.

Table 3.16: Discounted cash flow analysis parameters

Parameter	**Value**
Plant lifetime	30 years
Discount rate	10%
Plant depreciation method	200% declining balance (DB)
Plant recovery period	7 years
Federal tax rate	35%
Financing	40% equity
Loan conditions	10-year loan at 8% APR
Construction period	3 years
First year's costs	8%
Second year's costs	60%
Third year's costs	32%
Working capital	5% of FCI
Start-up time	3 months
Revenues during start-up	50%
Variable OPEX during start-up	75%
Fixed OPEX during start-up	100%

The cash flow analysis parameters utilized in this study are derived from the 2011 NREL report, and some financial assumptions may differ for 2022. However, the primary objective of this work is to compare the MESP between scenarios with and without the integrated biolubricant production process. Therefore, the proposed methodology is considered valid, provided it is consistently applied to both plant configurations.

Chapter 4: Results and Discussion

This chapter presents the results of the techno-economic analysis, including material and energy balances, and CAPEX and OPEX for the overall integrated process. Additionally, it includes the results of the cash flow analysis, focusing on the comparison of the MESP value both with and without the integration of the biolubricant production process. The chapter concludes with a sensitivity analysis to assess the impact of key cost variables on the MESP.

The first section summarizes simulation results, including material balances organized by process area, energy balances for heating and cooling duties, and electricity consumption.

The second section provides a comprehensive summary of capital and operational costs, comparing the biorefinery's 2007 costs with those updated for 2022. It also details the CAPEX and OPEX of the integrated process.

The third section focuses on the main objective of this thesis: comparing the MESP for ethanol production processes with and without the inclusion of the biolubricant production process.

The final section presents a sensitivity analysis of the major costs affecting the biorefinery's economic performance, such as the price of WCO and of biolubricant.

4.1 Simulation Results

Simulation results include material and energy balances for the processes studied, incorporating data from the transesterification process simulation by Hussein et al. (2021) and the biorefinery simulations performed by NREL (2011).

4.1.1 Material Balances

Material balances for the overall process are illustrated in Figure 4.1. Internal recycle streams are not included, meaning that the raw material inputs correspond to the process make-up requirements. Vapor streams exiting distillation column partial condensers and potential purge streams from recycles are also neglected. All flow rates are expressed in tonnes per day (t/d). The detailed stream tables are reported in Appendix A.

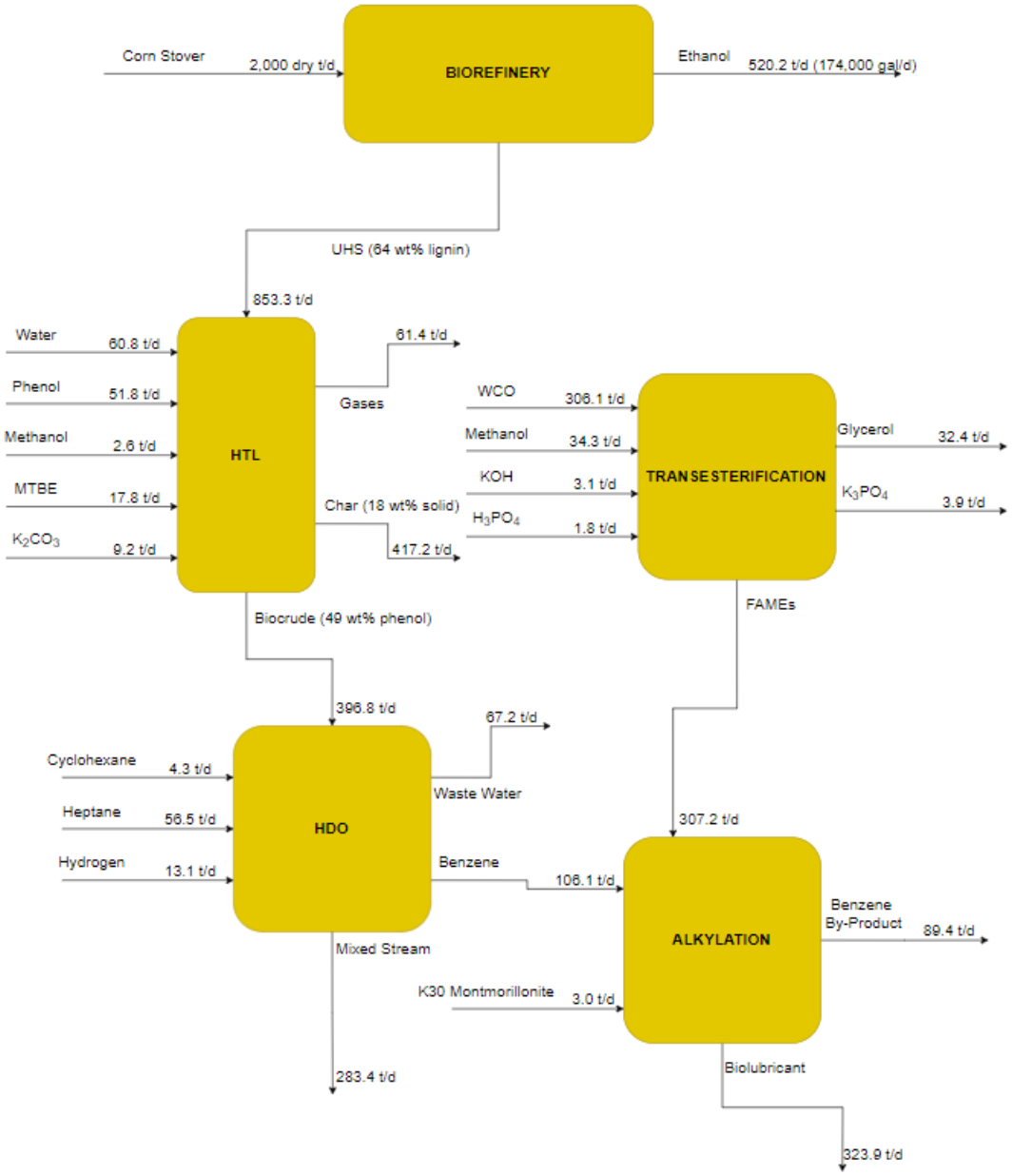

Figure 4.1: Material balances on the main streams of the overall process (flowrates are in tonne/day)

Material balances obtained from the simulations are used to determine raw material consumption and the production of main products and by-products, which serve as inputs for the economic analysis. Plant operating hours are fixed at 8,410 hours per year (96% capacity), consistent with NREL (2011) assumptions. Table 4.1 summarizes the annual consumption of raw materials and catalysts, while Table 4.2 presents the yearly production of by-products. Amount of raw materials, catalysts and products from the biorefinery are not detailed here, considering that the data from the NREL report were directly updated in terms of CAPEX and OPEX. Methanol consumption is reported separately for the HTL and transesterification processes to emphasize its distinct usage in the two plant sections.

Table 4.1: Raw materials consumption rates for the integrated processes (i.e., HTL, transesterification, HDO, alkylation)

Process Area	Raw Material	Consumption rate (tonne/yr)
HTL	Fresh water	21,294
	Phenol	18,140
	Methanol	925
	MTBE	6,223
	K_2CO_3	3,255
Transesterification	WCO	107,270
	KOH	1,076
	Methanol	12,009
	H_3PO_4	622
HDO	Cyclohexane	1,514
	Heptane	19,797
	Hydrogen	4,575
	Pd	0.05
	Al_2O_3	2.8
Alkylation	K30 Montmorillonite	1,068

Table 4.2: By-products production rates for the integrated processes

By-Product	Production rate (tonne/yr)
Biolubricant	113,510
Benzene	31,310
Glycerol	11,337
K_3PO_4	1,354

Although heptane functions as a solvent rather than a reactant, its make-up requirement is significant due to losses incurred in the "mixed stream," a liquid mixture of various organic components detailed in Section 2.3. Since the final application of this stream is not investigated in this work, it is neither evaluated as a by-product nor classified as waste. However, possible uses of this stream include recycling back some components to the HDO process to increase the benzene production rate;

separating some components (e.g., cyclohexanol) and selling them as by-products; hydrogenating the overall stream in order to obtain a fuel additive.

4.1.2 Energy Balances

In the biorefinery design proposed by NREL (2011), the combustor burns the UHS and the anaerobic biogas from the WWT system (Figure 1.4), generating all the steam and electricity required for ethanol production, while also producing additional electricity (12.8 MW) that is sold to the grid. However, the integration of the biolubricant production process removes UHS from the combustor feed, reducing its energy output.

To maintain the combustor's original energy output, additional biomass fuel is proposed, supplied by the char from the HTL process and additional corn stover, as discussed in Section 3.2. Specifically, the heat flowrate of UHS to the combustor (based on its LHV) is 113 MW. Char contributes with 38 MW, while the remaining 75 MW deficit is covered by approximately 387 tonnes/day of corn stover, an operational cost considered in the integrated biolubricant production process.

However, the integrated process presents significant heating and cooling requirements, driven by the need to bring feeds to reaction conditions and subsequent separations through atmospheric distillation columns. Although multiple heat recovery systems are implemented, as described in Chapter 2, the plant is not energetically self-sufficient. Table 4.3 summarizes the total energy duties for the integrated processes (HTL, transesterification, HDO, alkylation), along with energy recovered through intermediate heat exchangers and bfw for steam production. Negative values indicate energy recovered.

Table 4.3: Overall energy duties of the integrated process

Type of Energy Duty	Component	Unit of Measure	Value
COOLING DUTIES	Overall cooling duty	GJ/h	1034.8
	BFW	GJ/h	-43.7
	Intermediate HEX	GJ/h	-106.7
	Net cooling duty	**GJ/h**	**884.4**
HEATING DUTIES	Overall heating duty	GJ/h	801.4
	Steam produced through BFW	GJ/h	-43.7
	Intermediate HEX	GJ/h	-106.7
	Net heating duty	**GJ/h**	**651.0**
ELECTRICITY DEMAND	Overall electricity demand	MW	110.48
	Electricity from combustor	MW	-12.80
	Net electricity demand	**MW**	**97.68**

Most hot streams and exothermic reactors are cooled through bfw and intermediate heat exchangers. However, the net cooling duty primarily originates from column condensers and other coolers operating near ambient temperature. Consequently, cooling water is the main cooling medium, delivering 883 GJ/h of cooling (99.8% of the total net cooling duty). Refrigerated water provides the remaining 1.4 GJ/h.

The integrated process's electricity demand is mainly caused by the IHRS for the HTL process, requiring 109.20 MW of power (98.8% of total electricity demand), according to scale-up data provided through personal communication. Despite this significant requirement, IHRS remains a valuable option due to its high electrical efficiency (i.e., the ratio between heat duty from a simulated heat exchanger raising HTL feed temperature to 320 °C and energy duty of the IHRS), equal to 88.8%. The remaining electricity is consumed by pumps and the hydrogen compressor. Although additional electricity is supplied by the biorefinery's combustor, net electricity consumption constitutes one of the highest OPEX.

The heating media used in the plant include steam at various pressures (low, medium, and high) and DOWTHERM A. Additionally, corn stover is utilized as a substitute for UHS in the combustor. Table 4.4 summarizes the heat duties associated with each type of heating medium.

Table 4.4: Heat duties of the different heating media in the integrated process

Heating Medium	Component	Value (GJ/h)
LPS (134 °C, 2 barg)	Overall LPS consumed	29.0
	LPS produced	-14.0
	Net LPS required	15.0
MPS (184 °C, 10 barg)	Overall MPS consumed	34.7
	MPS produced	-29.7
	Net MPS required	5.0
HPS (254 °C, 41 barg)	HPS consumed	387.0
DOWTHERM A	DOWTHERM A consumed	28.0
Corn stover-to-combustor	Missing combustor heat duty	216.0

4.2 Economic Analysis Results

The economic analysis results include CAPEX and OPEX of the overall process for the two scenarios, namely with and without the integration of the biolubricant production process. This section provides a comparison of CAPEX and OPEX between 2007 (NREL, 2011) and 2022 (updated) biorefineries. After that, the main results of CAPEX and OPEX evaluation for the integrated processes are detailed, followed by a final comparison of capital and operational costs of the two scenarios.

4.2.1 Biorefinery CAPEX and OPEX Update

The results show an increase in both CAPEX and OPEX for 2022 compared to 2007. The rise in CAPEX is attributed to the higher CEPCI, which increased from 525.4 in 2007 to 813.0 in 2022 (*Chemical Engineering Magazine* [1]). Consequently, fixed OPEX, which scales proportionally with CAPEX, also increased. On the other hand, variable OPEX rose primarily due to slight increases in corn stover prices (which represent approximately 63% of the 2007 variable OPEX) and sharp increases in the costs of ammonia and caustic soda.

For electricity, the sale price to the grid is assumed to match the 2022 industrial electricity price in the Midwest ($0.078/kWh, [24]), leading to higher revenues than in 2007 when the sale price was $0.057/kWh (NREL, 2011). Table 4.5 summarizes the main CAPEX for 2007 and 2022, while Table 4.6 compares fixed and variable OPEX.

Table 4.5: Comparison of biorefinery base case CAPEX between 2007 and 2022

CAPEX	2007 Costs (MM$)	2022 Costs (MM$)
Installation Costs	232.1	359.1
ISBL	104.7	162.0
TDC	250.4	387.5
TIC	150.2	232.5
FCI	400.6	619.9
TCI	**422.5**	**656.3**

Table 4.6: Comparison of biorefinery's OPEX and revenues from by-products between 2007 and 2022

OPEX	Component	2007 Costs (MM$/yr)	2022 Costs (MM$/yr)
Variable OPEX	Feedstock (Corn Stover)	45.2	50.45
	Sulfuric acid 93%	1.49	1.02
	Ammonia	4.40	12.14
	Corn steep liquor	0.63	2.50
	Diammonium phosphate	1.18	0.97
	Sorbitol	0.42	0.43
	Glucose	11.8	13.28
	SO_2	0.04	0.04
	Enzyme nutrients	0.47	0.47
	Caustic	2.83	6.85
	Lime	1.50	0.96
	Boiler chemicals	0.01	0.01
	Cooling tower chemicals	0.06	0.06
	Fresh water	0.32	0.32
	Disposal of ash	1.53	1.53
	Total Variable OPEX	**71.88**	**91.04**
Fixed OPEX	Total salaries	2.48	3.47
	Labor burden	2.23	3.12
	Maintenance	3.14	4.86
	Property insurance	2.80	4.34
	Total Fixed OPEX	**10.65**	**15.79**
By-Products	Electricity to the grid	6.56	9.17

Corn stover remains a major cost driver, accounting for more than 50% of the overall variable OPEX. This dependence makes it a primary source of ethanol price fluctuations. A breakdown of the variable OPEX for the updated 2022 biorefinery base case (i.e., without the biolubricant production integration) is illustrated in the pie chart in Figure 4.2.

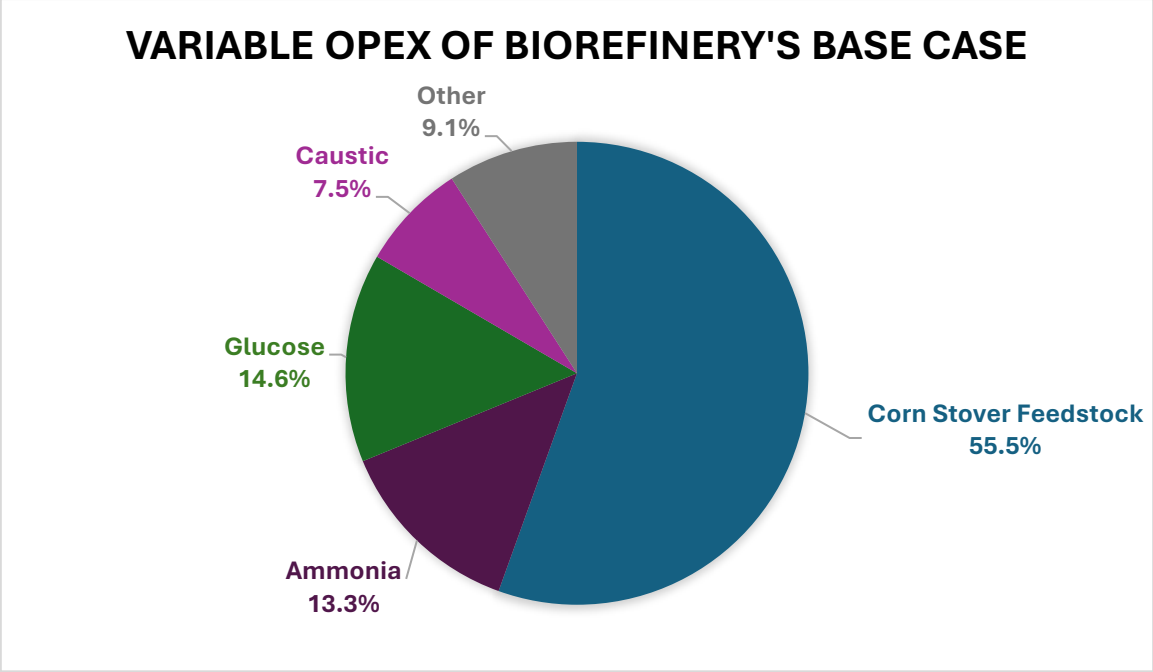

Figure 4.2: Pie chart of the main variable OPEX in the updated biorefinery's base case

4.2.2 Installation Costs of Biolubricant Production Process Equipment

Estimating the purchase and installation costs of equipment for the integrated processes is critical for evaluating the additional CAPEX incurred. The analysis, conducted using the methods described in Section 3.1, highlights that reactors constitute approximately 80% of the overall installation costs, significantly influencing total CAPEX. However, reactor sizing and cost estimation are subject to uncertainties, and more precise data should be retrieved from vendors.

Table 4.7 details installation costs for the integrated processes (HTL, transesterification, HDO, alkylation), categorized by equipment type. Reactor installation costs include associated intermediate heat exchangers, inert packing materials, and auxiliary components, as described in Section 3.1.1. The pie chart in Figure 4.3 illustrates the contribution of different equipment types to the overall installation costs. A comprehensive list of purchase and installation costs is provided in Appendix B.

Table 4.7: Installation costs of integrated processes equipment

Type of Equipment	Installation Cost (MM$)
Centrifuges (2 units)	0.161
Shell-and-tube Heat Exchangers (38 units)	9.461
Kettle Reboilers (13 units)	18.254
Towers (13 units)	11.930
Centrifugal Pumps (7 units)	1.234
Reciprocating Compressors (1 unit)	1.248
Vertical and Horizontal Vessels (9 units)	2.457
Filters (1 unit)	0.234
Jacketed Agitated Reactors (2 units)	0.529
IHRS (R-101)	77.550
Multistage TBR (R-201)	52.662
Multistage FBR (R-202)	29.106
Multistage FzBR (R-301)	19.045
Overall Installation Costs	**223.871**

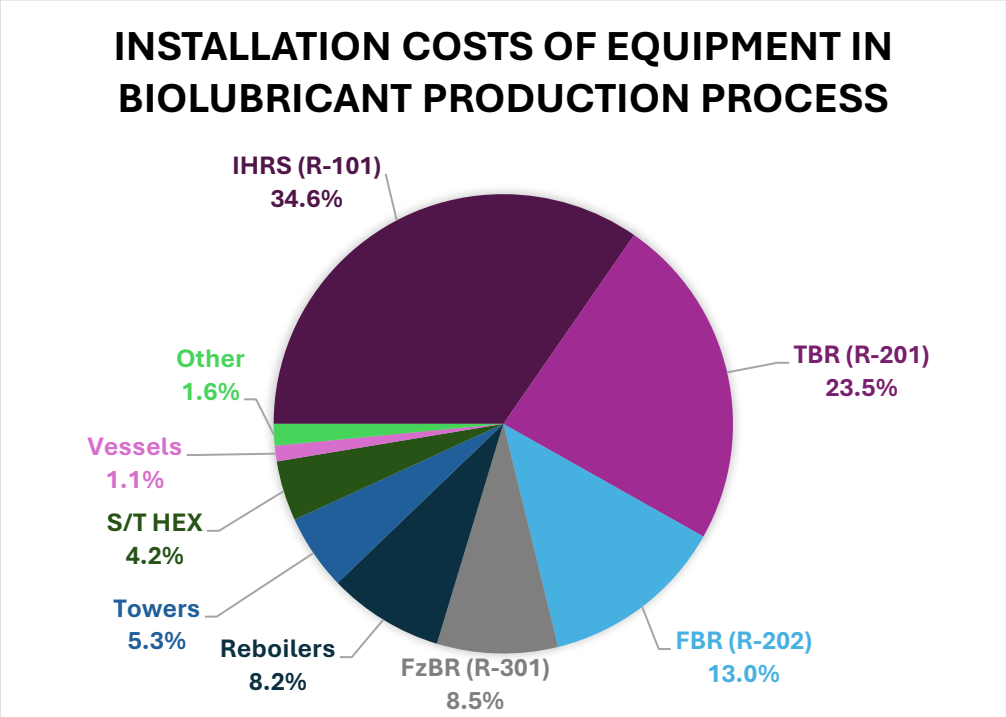

Figure 4.3: Pie chart of the main equipment installation costs in the integrated processes

4.2.3 Variable OPEX of Biolubricant Production Process

The biolubricant production process presents substantial variable OPEX, driven mainly by the cost of WCO, which constitutes approximately 40% of total variable OPEX due to its significant feedstock requirement (over 107,000 tonnes/year) and high price in 2022 ($1,301/tonne). Other critical raw materials include heptane, phenol, and hydrogen, while major utility costs come from electricity and hps consumptions.

Table 4.8 summarizes the variable OPEX for the integrated processes, while the pie chart in Figure 4.4 illustrates the contributions of key raw materials and utilities to the operational costs of the biolubricant production process.

Table 4.8: Variable OPEX of the biolubricant production process

Variable OPEX	Component	Cost (MM$/yr)
Raw Materials	Fresh water	0.004
	Phenol	26.104
	Methanol	0.353
	MTBE	7.132
	K_2CO_3	2.864
	WCO	139.558
	KOH	0.804
	Methanol	4.588
	H_3PO_4	0.481
	Cyclohexane	1.910
	Heptane	28.726
	Hydrogen	20.588
	Pd/C	1.700
	Al_2O_3	0.028
	K30 Montmorillonite	10.681
	Total Raw Materials Costs	**245.520**
Utilities	Cooling water	2.807
	Refrigerated water	0.056
	LPS (134 °C, 2 barg)	0.573
	MPS (184 °C, 10 barg)	0.201
	HPS (254 °C, 41 barg)	18.421
	DOWTHERM A (355 °C)	0.970
	Corn stover-to-combustor	7.484
	Electricity	64.075
	WWT	0.001
	Total Utilities Costs	**94.588**
	TOTAL VARIABLE OPEX	**340.108**

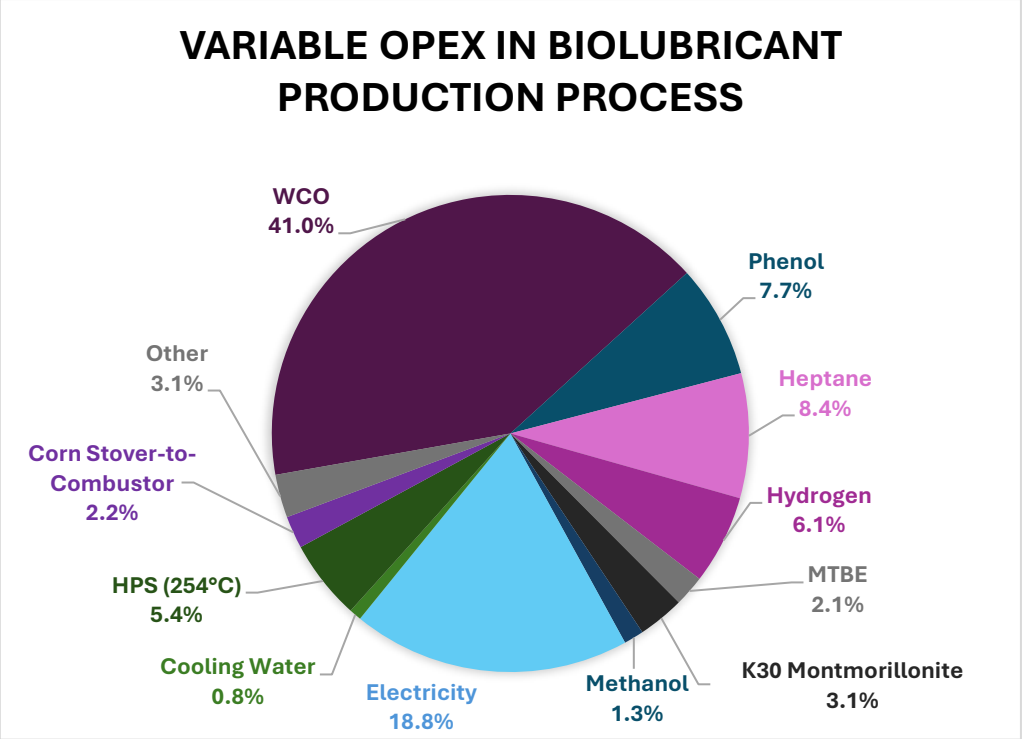

Figure 4.4: Pie chart of main variable OPEX of the biolubricant production process

The variable OPEX for the biolubricant production process are approximately four times higher than those for ethanol production. However, the revenues generated from by-products, mainly the biolubricant, offset these increased operational costs. The detailed revenues evaluation from by-products sales is presented in Table 4.9.

Table 4.9: Revenues from by-products sales in the integrated processes

By-Product	Revenues (MM$/yr)
Biolubricant	397.284
Benzene	33.596
Glycerol	7.936
K_3PO_4	1.160
Total By-Products Sales	**439.976**

4.2.4 Overall Process Economics

The economic evaluation of the updated biorefinery, incorporating the biolubricant production process, includes both CAPEX and OPEX. All assumptions and calculations outlined in Chapter 3 are employed to determine the total capital and operational costs. A comparative analysis of the economic

performance of the updated biorefinery, with and without the integrated biolubricant production process, is summarized in Table 4.10.

Table 4.10: Overall economics of the updated biorefinery with and without biolubricant production integration

CAPEX	**Biorefinery Base Case (MM$)**	**Biorefinery + Biolubricant Production (MM$)**
Installation Costs	359.1	583.0
ISBL	162.0	268.5
TDC	387.5	631.7
TIC	232.5	379.0
FCI	619.9	1,010.8
TCI	**656.3**	**1,070.2**
OPEX	**Biorefinery Base Case (MM$/yr)**	**Biorefinery + Biolubricant Production (MM$/yr)**
Variable OPEX	91.0	431.2
Fixed OPEX	15.8	27.2
Overall OPEX	**106.8**	**458.4**
By-Products	**Biorefinery Base Case (MM$/yr)**	**Biorefinery + Biolubricant Production (MM$/yr)**
By-Products Sales	**9.2**	**440.0**

The integration of the biolubricant production process leads to a significant economic impact. The total capital investment (TCI) for plant construction increases by approximately 63% compared to the base case (ethanol production only). Similarly, overall OPEX rises by nearly 330%, attributed to the additional operational costs associated with the biolubricant production. Despite these increases, the higher revenues generated from by-products justify the added costs. In the base case, electricity sold to the grid is the only by-product revenue source. With the biolubricant integration, by-product revenues exceed 400 MM$/yr, improving the plant's economic performances.

The integration also modifies the composition of OPEX. Corn stover, which dominates OPEX in the base case, is surpassed by WCO, the primary raw material for biolubricant production, and electricity consumption, driven by the high power requirements of the IHRS of the HTL process. The overall OPEX breakdown is illustrated in Figure 4.5.

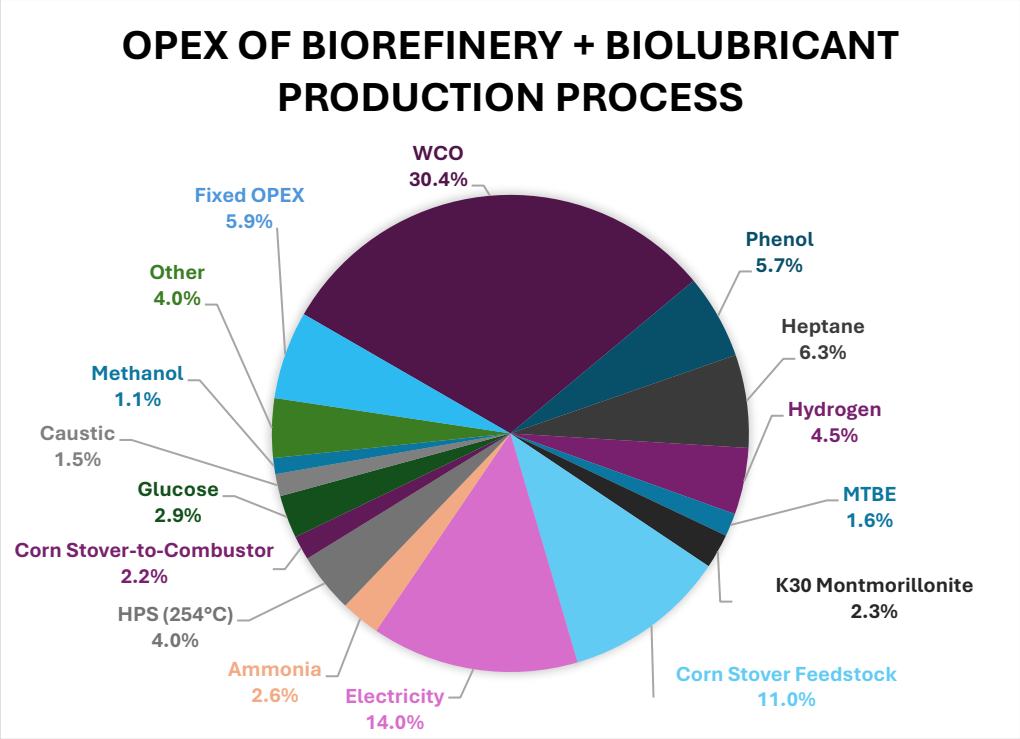

Figure 4.5: Pie chart of main variable OPEX of the overall integrated process

4.3 Minimum Ethanol Selling Price (MESP)

The economic results for the two plant scenarios (with and without the integration of the biolubricant production process) are used to perform a discounted cash flow analysis in order to evaluate the minimum ethanol selling price to obtain an NPV equal to zero at the end of the plant lifetime (30 years).

According to the techno-economic analysis performed by NREL (2011), a biorefinery producing approximately 61 million gallons per year (MMgal/yr) of ethanol had a MESP of $2.15/gal in 2007. Adjusting for 2022 costs, this increases to $3.02/gal, a 40% rise due to higher CAPEX and OPEX. Incorporating the biolubricant production process, the MESP decreases to $2.64/gal, resulting in a 13% reduction compared to the base case. This improvement is driven by increased by-product revenues, offsetting the higher CAPEX and OPEX. Table 4.11 details the MESP values for the two scenarios. The detailed cash flow analysis worksheet is presented in Appendix C.

Table 4.11: MESP values for the two scenarios (with and without the integration of the biolubricant production process)

	Biorefinery Base Case	Biorefinery + Integrated Biolubricant Production
MESP	$3.02/gal	$2.64/gal

4.4 Sensitivity Analysis

To further examine the economic performance of the overall integrated process, a sensitivity analysis evaluates the impact of fluctuations in the prices of key components: WCO (main cost) and biolubricant (main revenue).

4.4.1 WCO Price

Yellow grease, a processed form of WCO with low free fatty acid (FFA) content suitable for biodiesel production, is used as the baseline raw material. In 2022, the average WCO price in Minnesota, a potential biorefinery location according to NREL, was $1,301/tonne, according to the United States Department of Agriculture (USDA) [16].

Considering price variability between 2022 and 2024, the analysis results indicate that by taking the minimum WCO price registered in the last two years ($700/tonne), MESP decreases by 40% compared to the integrated process base value and by 48% relative to the base case, reaching $1.58/gal. On the other hand, by taking the maximum WCO price ($1,411/tonne), the corresponding MESP ($2.84/gal) increases by 8% relative to the overall integrated process and decreases by 6% compared to the base case.

Table 4.12 details the WCO prices used in the sensitivity analysis (retrieved by the USDA, [16]), with Figure 4.6 illustrating the MESP trend as a function of WCO price.

Table 4.12: Yellow grease (WCO) price in Minnesota (2nd column) and corresponding MESP (3rd column)

Reference Period	WCO Price ($/tonne)	MESP ($/gal)
Minimum (January 2024)	700	1.58
Maximum (September 2022)	1,411	2.84
Average (2022-2024)	1,056	2.21
Base Value (average 2022)	1,301	2.64

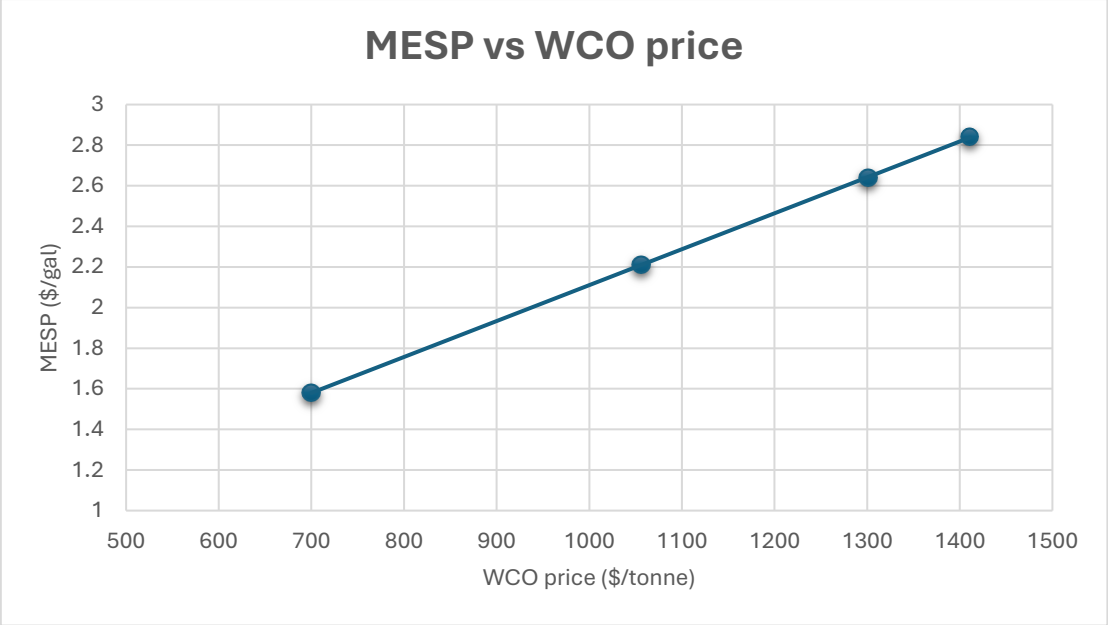

Figure 4.6: MESP as a function of WCO price

4.4.2 Biolubricant Price

In the absence of detailed pricing data for the specific biolubricant improver made of FAMEs and PBFAMEs, its price is varied within a ±20% range relative to the assumed base price of $3,500/tonne. This range spans from $2,800 to $4,200/tonne.

The analysis reveals a strong dependence of the MESP on the biolubricant selling price. This correlation is expected, as biolubricant sales at the baseline price of $3,500/tonne account for approximately 90% of total by-product revenues and 66% of the plant's overall annual sales (including ethanol revenues).

For a decrease of 20% in biolubricant selling price ($2,800/tonne), MESP increases by approximately 49%. On the other hand, with an increase in biolubricant selling price of 20% ($4,200/tonne), MESP value is reduced by 49%. This indicates a linear relationship between biolubricant selling price and MESP, which was expected by considering that the sum of the revenues of biolubricant and ethanol sales (93% of total annual revenues) must be constant to get an NPV value of zero.

Table 4.13 details the biolubricant prices used in the sensitivity analysis and the corresponding MESP values, while Figure 4.7 illustrates the MESP trend as a function of biolubricant selling price.

Table 4.13: Values of MESP related to biolubricant selling price

Reference Value	Biolubricant Price ($/tonne)	MESP ($/gal)
-20%	2,800	3.94
-10%	3,150	3.29
Base Value	3,500	2.64
+10%	3,850	1.99
+20%	4,200	1.34

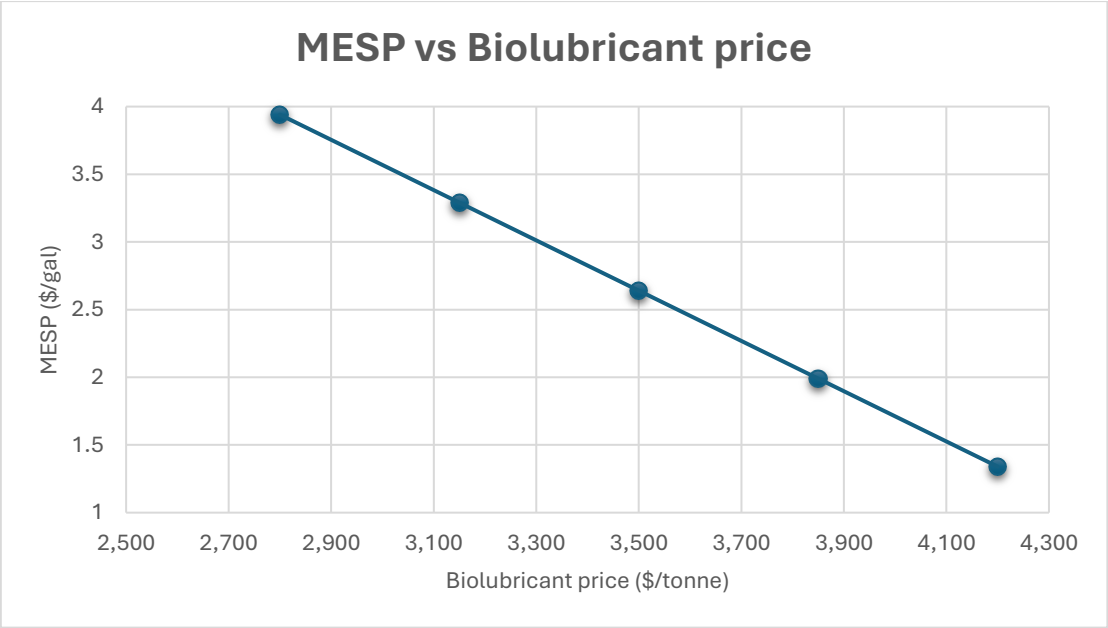

Figure 4.7: MESP as a function of biolubricant price

According to the graph, the integration of the biolubricant production process becomes economically favorable (i.e., it lowers the MESP compared to the base case) for a biolubricant price of approximately $3,300/tonne, at which the MESP value is near $3.00/gal.

The objective of this work is to perform a techno-economic analysis of integrating the biolubricant production process into the biorefinery, focusing on the comparison of MESP between the two scenarios rather than determining the absolute MESP value. Nevertheless, it is worth noting that the average ethanol selling price in 2022 was slightly lower, at $2.48/gal [29]. This highlights the need for further optimization of the overall integrated process to achieve greater economic competitiveness.

Conclusions

This thesis focused on the techno-economic analysis of the integration of a biolubricant production process into a conventional biorefinery that produces ethanol from corn stover. The proposed biolubricant, a mixture of fatty acid methyl esters (FAMEs) and phenyl-branched FAMEs (PBFAMEs), is synthesized using waste cooking oil (WCO) and lignin, with the latter sourced as unhydrolyzed solids (UHS), a by-product typically burnt in the base biorefinery configuration. The integration of this process not only aims to improve the economic performance of the biorefinery, but also represents a step toward sustainable waste valorization.

The production approach includes several steps. Lignin is processed through hydrothermal liquefaction (HTL) to produce liquid biocrude, rich in phenolic compounds such as phenol, which is subsequently hydrodeoxygenated (HDO) to aromatic compounds like benzene. Meanwhile, WCO is converted into FAMEs through transesterification, generating by-products such as glycerol and potassium phosphate (K_3PO_4), which can be sold to offset operational costs. The final step involves the alkylation of benzene with the unsaturated fraction of FAMEs to produce the biolubricant, a product with improved lubricity and oxidation stability compared to standard FAMEs. This integration demonstrates the potential for utilizing lignin and WCO, two abundant waste components, to create a value-added product while improving the economic performance of the biorefinery.

The material and energy balances of the integrated processes were derived from rigorous process simulations using Aspen Plus, with yield distributions based on experimental data and adapted to industrial-scale conditions. Key results show that processing 546 tonne/day of lignin through HTL generates 397 tonne/day of biocrude (49 wt% phenol). After partial recovery and recycling, the phenol-rich biocrude undergoes hydrogenation in a multistage trickle bed reactor (TBR), consuming 13 tonne/day of hydrogen, followed by dehydration/dehydrogenation in a multistage fixed bed reactor (FBR), yielding 106 tonne/day of benzene. The transesterification of WCO produces 307 tonne/day of FAMEs, which, along with purified benzene, undergo alkylation in a multistage fluidized bed reactor (FzBR) to yield 324 tonne/day of the biolubricant product.

Economic evaluations revealed a 63% increase in the total capital investment (TCI) of the integrated plant compared to the base biorefinery, rising from 656 MM$ to 1,070 MM$. This increase is primarily attributed to the high costs of the reactors, such as the induction-heating reactor systems (IHRS) used for HTL (77.550 MM$) and the multistage HDO reactors (which sum up to approximately 82 MM$). The operational expenses (OPEX) of the integrated system also increase significantly, from 107

MM$/yr in the ethanol-only scenario to 458 MM$/yr with the biolubricant production integration. This increase was driven by the costs of raw materials, particularly WCO, which emerged as the largest contributor to operational costs at 140 MM$/yr, and utilities, such as electricity consumption, which accounted for 64 MM$/yr.

Despite these cost increases, the integration of the biolubricant process proved economically advantageous due to the high revenues generated by the sale of the biolubricant and other by-products. The annual revenue from biolubricant sales alone was estimated at 397 MM$/yr, with additional contributions from the sale of surplus benzene, glycerol, and potassium phosphate, amounting to a total increase in by-product revenues of more than 400 MM$/yr compared to the base case. This improved revenue stream enabled a reduction in the minimum ethanol selling price (MESP) from $3.02/gal in the base case to $2.64/gal in the integrated scenario, representing a 13% decrease and demonstrating an overall improvement in plant economic performance.

Sensitivity analyses further supported the robustness of the integration, highlighting the influence of key variables such as WCO price and biolubricant selling price on economic performances. Results showed that the process remained profitable even taking the maximum WCO price in the last two years ($1,411/tonne), with a resulting MESP of $2.84/tonne. On the other hand, the sensitivity analysis on the biolubricant selling price showed that the integration would no longer offer economic advantages compared to the base case when the price is below $3,300/tonne (resulting in a MESP above $3.00/gal), underlining the critical importance of market conditions for by-product sales.

The results of this study demonstrated the potential of integrating biolubricant production into existing biorefineries as a pathway for both economic and environmental improvements. However, several aspects deserve further investigation. Reducing the electricity demand of the IHRS, minimizing the consumption of phenol in the HTL process and heptane in the HDO process, and addressing catalyst deactivation in the alkylation reactor are critical areas for future research. Additionally, the valorization of the compounds exiting the HDO process which are not used in the alkylation process (e.g., anisole, cyclohexanol, methoxycyclohexane, dicyclohexyl ether, etc.) could further improve the economic and environmental sustainability of the integrated system.

In conclusion, the integration of biolubricant production into a lignocellulosic ethanol biorefinery demonstrates significant promise as a strategy for waste valorization and economic improvement. Future work should focus on enhancing process efficiencies and expanding product utilization to maximize the benefits of this innovative integration.

Appendix A

STREAM TABLES: HTL PROCESS

(from Aspen Plus)

Stream Name	UHS	WATER	PHENOL	METHANOL	MTBE	1	2	3	4	5
Temperature (°C)	55.000	25.000	25.000	25.000	25.000	26.880	30.385	320.000	319.879	262.019
Pressure (bar)	6.991	1.013	1.013	1.013	1.013	1.013	115.000	116.524	116.524	116.524
Mass Vapor Fraction	0.000	0.000	0.000	0.000	0.000	0.000	0.000	0.472	0.449	0.011
Mass Liquid Fraction	0.360	1.000	1.000	1.000	1.000	0.900	0.900	0.501	0.525	0.962
Mass Solid Fraction	0.640	0.000	0.000	0.000	0.000	0.100	0.100	0.027	0.027	0.027
Mass Density (kg/cum)	1174.2	994.0	1079.7	792.9	736.1	1026.5	1023.3	93.7	98.1	670.0
Mass Flows (kg/h)	35554	182896	9102	110	740	227552	227552	227552	227552	227552
Mass Fractions										
WATER	0.360	1.000	0.000	0.000	0.000	0.860	0.860	0.845	0.845	0.845
PHENOL	0.000	0.000	1.000	0.000	0.000	0.040	0.040	0.067	0.067	0.067
CH4	0.000	0.000	0.000	0.000	0.000	0.000	0.000	0.000	0.000	0.000
CO	0.000	0.000	0.000	0.000	0.000	0.000	0.000	0.002	0.002	0.002
CO2	0.000	0.000	0.000	0.000	0.000	0.000	0.000	0.009	0.009	0.009
LACTIC ACID	0.000	0.000	0.000	0.000	0.000	0.000	0.000	0.002	0.002	0.002
ACETIC ACID	0.000	0.000	0.000	0.000	0.000	0.000	0.000	0.001	0.001	0.001
GLYCOLIC ACID	0.000	0.000	0.000	0.000	0.000	0.000	0.000	0.003	0.003	0.003
METHANOL	0.000	0.000	0.000	1.000	0.000	0.000	0.000	0.010	0.010	0.010
ANISOLE	0.000	0.000	0.000	0.000	0.000	0.000	0.000	0.015	0.015	0.015
CATECHOL	0.000	0.000	0.000	0.000	0.000	0.000	0.000	0.009	0.009	0.009
GUAIACOL	0.000	0.000	0.000	0.000	0.000	0.000	0.000	0.006	0.006	0.006
XANTHENE	0.000	0.000	0.000	0.000	0.000	0.000	0.000	0.003	0.003	0.003
MTBE	0.000	0.000	0.000	0.000	1.000	0.000	0.000	0.000	0.000	0.000
LIGNIN	0.640	0.000	0.000	0.000	0.000	0.100	0.100	0.000	0.000	0.000
CHAR	0.000	0.000	0.000	0.000	0.000	0.000	0.000	0.027	0.027	0.027

Stream Name	5	6	7	8	9	10	11	12	13	14	15
Temperature (°C)	262.019	220.978	32.000	32.000	32.193	32.193	63.682	111.159	114.327	66.271	66.271
Pressure (bar)	116.524	116.524	1.013	1.013	6.900	6.900	1.000	1.000	40.000	1.000	1.000
Mass Vapor Fraction	0.011	0.004	0.011	0.000	0.000	0.000	0.000	0.000	0.000	1.000	0.000
Mass Liquid Fraction	0.962	0.969	0.962	0.973	0.973	0.821	1.000	1.000	1.000	0.000	1.000
Mass Solid Fraction	0.027	0.027	0.027	0.027	0.027	0.179	0.000	0.000	0.000	0.000	0.000
Mass Density (kg/cum)	670.0	764.7	119.0	1011.3	1011.1	1131.8	790.8	1015.2	1012.0	1.1	773.2
Mass Flows (kg/h)	227552	227552	227552	224994	224994	33825	320120	16535	16535	15	303569
Mass Fractions											
WATER	0.845	0.845	0.845	0.855	0.855	0.352	0.082	0.039	0.039	0.034	0.085
PHENOL	0.067	0.067	0.067	0.068	0.068	0.241	0.026	0.494	0.494	0.000	0.000
CH4	0.000	0.000	0.000	0.000	0.000	0.000	0.000	0.000	0.000	0.000	0.000
CO	0.002	0.002	0.002	0.000	0.000	0.000	0.000	0.000	0.000	0.001	0.000
CO2	0.009	0.009	0.009	0.001	0.001	0.000	0.000	0.000	0.000	0.039	0.000
LACTIC ACID	0.002	0.002	0.002	0.002	0.002	0.001	0.000	0.001	0.001	0.000	0.000
ACETIC ACID	0.001	0.001	0.001	0.001	0.001	0.001	0.000	0.001	0.001	0.000	0.000
GLYCOLIC ACID	0.003	0.003	0.003	0.003	0.003	0.001	0.000	0.002	0.002	0.000	0.000
METHANOL	0.010	0.010	0.010	0.010	0.010	0.004	0.790	0.014	0.014	0.898	0.832
ANISOLE	0.015	0.015	0.015	0.015	0.015	0.100	0.089	0.204	0.204	0.026	0.083
CATECHOL	0.009	0.009	0.009	0.009	0.009	0.062	0.007	0.127	0.127	0.000	0.000
GUAIACOL	0.006	0.006	0.006	0.006	0.006	0.038	0.004	0.077	0.077	0.000	0.000
XANTHENE	0.003	0.003	0.003	0.003	0.003	0.020	0.002	0.041	0.041	0.000	0.000
MTBE	0.000	0.000	0.000	0.000	0.000	0.000	0.000	0.000	0.000	0.000	0.000
LIGNIN	0.000	0.000	0.000	0.000	0.000	0.000	0.000	0.000	0.000	0.000	0.000
CHAR	0.027	0.027	0.027	0.027	0.027	0.179	0.000	0.000	0.000	0.000	0.000

Stream Name	15	16	17	18	19	20	21	22	23	24
Temperature (°C)	66.271	66.258	32.193	30.263	25.000	25.000	24.998	27.548	25.000	25.000
Pressure (bar)	1.000	1.000	6.900	1.000	1.000	1.000	1.000	1.000	1.000	1.000
Mass Vapor Fraction	0.000	0.000	0.000	0.000	1.000	0.000	0.000	0.000	1.000	0.000
Mass Liquid Fraction	1.000	1.000	1.000	1.000	0.000	1.000	1.000	1.000	0.000	1.000
Mass Solid Fraction	0.000	0.000	0.000	0.000	0.000	0.000	0.000	0.000	0.000	0.000
Mass Density (kg/cum)	773.2	773.2	992.4	753.5	2.3	752.4	747.1	978.2	2.3	747.8
Mass Flows (kg/h)	303569	303679	191169	248024	154	240925	250408	193553	258	8742
Mass Fractions										
WATER	0.085	0.085	0.944	0.016	0.011	0.016	0.017	0.933	0.014	0.021
PHENOL	0.000	0.000	0.037	0.052	0.000	0.026	0.025	0.003	0.000	0.000
CH4	0.000	0.000	0.000	0.000	0.003	0.000	0.000	0.000	0.000	0.000
CO	0.000	0.000	0.000	0.000	0.003	0.000	0.000	0.000	0.003	0.000
CO2	0.000	0.000	0.001	0.001	0.497	0.001	0.001	0.001	0.495	0.000
LACTIC ACID	0.000	0.000	0.003	0.001	0.000	0.000	0.000	0.001	0.000	0.000
ACETIC ACID	0.000	0.000	0.002	0.001	0.000	0.001	0.001	0.002	0.000	0.000
GLYCOLIC ACID	0.000	0.000	0.003	0.001	0.000	0.000	0.000	0.003	0.000	0.000
METHANOL	0.832	0.833	0.011	0.002	0.001	0.002	0.002	0.011	0.001	0.002
ANISOLE	0.083	0.083	0.000	0.000	0.000	0.000	0.000	0.000	0.000	0.000
CATECHOL	0.000	0.000	0.000	0.000	0.000	0.000	0.000	0.000	0.000	0.000
GUAIACOL	0.000	0.000	0.000	0.000	0.000	0.000	0.000	0.000	0.000	0.000
XANTHENE	0.000	0.000	0.000	0.000	0.000	0.000	0.000	0.000	0.000	0.000
MTBE	0.000	0.000	0.000	0.926	0.484	0.953	0.954	0.048	0.487	0.977
LIGNIN	0.000	0.000	0.000	0.000	0.000	0.000	0.000	0.000	0.000	0.000
CHAR	0.000	0.000	0.000	0.000	0.000	0.000	0.000	0.000	0.000	0.000

Stream Name	BIOCRUDE	CHAR	GASES	LBO-RECYCLE	WATER-RECYCLE
Temperature (°C)	250.000	63.682	32.000	182.793	95.372
Pressure (bar)	40.000	1.000	1.013	1.000	1.000
Mass Vapor Fraction	0.000	0.000	1.000	0.000	0.000
Mass Liquid Fraction	1.000	0.651	0.000	1.000	1.000
Mass Solid Fraction	0.000	0.349	0.000	0.000	0.000
Mass Density (kg/cum)	856.3	777.2	1.5	939.5	920.2
Mass Flows (kg/h)	16535	17384	2558	6945	184553
Mass Fractions					
WATER	0.039	0.649	0.022	0.000	0.977
PHENOL	0.494	0.000	0.001	0.931	0.003
CH4	0.000	0.000	0.039	0.000	0.000
CO	0.000	0.000	0.143	0.000	0.000
CO2	0.000	0.001	0.759	0.000	0.000
LACTIC ACID	0.001	0.001	0.000	0.053	0.001
ACETIC ACID	0.001	0.001	0.000	0.000	0.002
GLYCOLIC ACID	0.002	0.001	0.000	0.016	0.003
METHANOL	0.014	0.000	0.002	0.000	0.011
ANISOLE	0.204	0.000	0.035	0.000	0.000
CATECHOL	0.127	0.000	0.000	0.000	0.000
GUAIACOL	0.077	0.000	0.000	0.000	0.000
XANTHENE	0.041	0.000	0.000	0.000	0.000
MTBE	0.000	0.000	0.000	0.000	0.003
LIGNIN	0.000	0.000	0.000	0.000	0.000
CHAR	0.000	0.349	0.000	0.000	0.000

STREAM TABLES: HDO & ALKYLATION PROCESSES (from Aspen Plus)

Stream Name	BIOCRUDE	CYCLOHEXANE	HYDROGEN	HEPTANE	FAME	25	26	27	28	29
Temperature (°C)	250.0	25.0	80.0	25.0	320.0	250.4	250.0	180.2	172.6	135.0
Pressure (bar)	40	1	30	1	0.58	40	40	40	40	40
Mass Vapor Fraction	0.000	0.000	1.000	0.000	0.000	0.000	0.000	0.000	0.000	0.000
Mass Liquid Fraction	1.000	1.000	0.000	1.000	1.000	1.000	1.000	1.000	1.000	1.000
Mass Solid Fraction	0.000	0.000	0.000	0.000	0.000	0.000	0.000	0.000	0.000	0.000
Mass Density (kg/cum)	839.5	773.3	2.0	682.4	627.6	644.3	609.6	710.9	720.2	764.1
Mass Fractions										
PHENOL	0.494	0.000	0.000	0.000	0.000	0.242	0.003	0.003	0.003	0.003
WATER	0.039	0.000	0.000	0.000	0.000	0.020	0.036	0.036	0.036	0.036
LACTIC ACID	0.001	0.000	0.000	0.000	0.000	0.001	0.001	0.001	0.001	0.001
ACETIC ACID	0.001	0.000	0.000	0.000	0.000	0.000	0.000	0.000	0.000	0.000
GLYCOLIC ACID	0.002	0.000	0.000	0.000	0.000	0.001	0.001	0.001	0.001	0.001
METHANOL	0.014	0.000	0.000	0.000	0.000	0.010	0.007	0.007	0.007	0.007
ANISOLE	0.204	0.000	0.000	0.000	0.000	0.101	0.041	0.041	0.041	0.041
CATECHOL	0.127	0.000	0.000	0.000	0.000	0.062	0.000	0.000	0.000	0.000
GUAIACOL	0.077	0.000	0.000	0.000	0.000	0.038	0.029	0.029	0.029	0.029
XANTHENE	0.041	0.000	0.000	0.000	0.000	0.020	0.020	0.020	0.020	0.020
CYCLOHEXANOL	0.000	0.000	0.000	0.000	0.000	0.002	0.193	0.193	0.193	0.193
CYCLOHEXANONE	0.000	0.000	0.000	0.000	0.000	0.000	0.037	0.037	0.037	0.037
METHOXYCHEXANE	0.000	0.000	0.000	0.000	0.000	0.004	0.071	0.071	0.071	0.071
CYCLOHEXANE	0.000	1.000	0.000	0.000	0.000	0.499	0.489	0.489	0.489	0.489
D.H. HETER	0.000	0.000	0.000	0.000	0.000	0.000	0.071	0.071	0.071	0.071
HEPTANE	0.000	0.000	0.000	1.000	0.000	0.000	0.000	0.000	0.000	0.000
BENZENE	0.000	0.000	0.000	0.000	0.000	0.000	0.000	0.000	0.000	0.000
HYDROGEN	0.000	0.000	1.000	0.000	0.000	0.000	0.000	0.000	0.000	0.000
M-OLEATE	0.000	0.000	0.000	0.000	0.236	0.000	0.000	0.000	0.000	0.000
M-LINOLEATE	0.000	0.000	0.000	0.000	0.358	0.000	0.000	0.000	0.000	0.000
M-LINOLENATE	0.000	0.000	0.000	0.000	0.033	0.000	0.000	0.000	0.000	0.000
M-PALMITATE	0.000	0.000	0.000	0.000	0.299	0.000	0.000	0.000	0.000	0.000
M-STEARATE	0.000	0.000	0.000	0.000	0.075	0.000	0.000	0.000	0.000	0.000
MPO	0.000	0.000	0.000	0.000	0.000	0.000	0.000	0.000	0.000	0.000

Stream Name	30	31	32	33	34	35	36	37	38	39	40	41	42	43
Temperature (°C)	50.0	53.2	50.0	152.9	156.2	210.0	250.0	250.3	250.0	223.2	157.7	135.0	35.0	25.0
Pressure (bar)	40	1	1	1	40	40	40	40	40	40	40	40	40	40
Mass Vapor Fraction	0.000	0.000	0.000	0.000	0.000	0.000	0.000	0.000	0.000	0.000	0.000	0.000	0.000	0.000
Mass Liquid Fraction	1.000	1.000	1.000	1.000	1.000	1.000	1.000	1.000	1.000	1.000	1.000	1.000	1.000	1.000
Mass Solid Fraction	0.000	0.000	0.000	0.000	0.000	0.000	0.000	0.000	0.000	0.000	0.000	0.000	0.000	0.000
Mass Density (kg/cum)	851.0	835.8	834.3	837.8	834.4	776.0	727.3	506.2	424.2	468.7	567.5	594.4	693.2	697.9
Mass Fractions														
PHENOL	0.003	0.003	0.003	0.007	0.007	0.007	0.007	0.003	0.017	0.015	0.015	0.015	0.015	0.015
WATER	0.036	0.036	0.007	0.000	0.000	0.000	0.000	0.000	0.020	0.027	0.027	0.027	0.027	0.027
LACTIC ACID	0.001	0.001	0.000	0.001	0.001	0.001	0.001	0.000	0.000	0.000	0.000	0.000	0.000	0.000
ACETIC ACID	0.000	0.000	0.000	0.001	0.001	0.001	0.001	0.000	0.000	0.000	0.000	0.000	0.000	0.000
GLYCOLIC ACID	0.001	0.001	0.000	0.000	0.000	0.000	0.000	0.000	0.000	0.000	0.000	0.000	0.000	0.000
METHANOL	0.007	0.007	0.006	0.000	0.000	0.000	0.000	0.000	0.000	0.000	0.000	0.000	0.000	0.000
ANISOLE	0.041	0.041	0.042	0.088	0.088	0.088	0.088	0.032	0.045	0.044	0.044	0.044	0.044	0.044
CATECHOL	0.000	0.000	0.000	0.000	0.000	0.000	0.000	0.000	0.000	0.000	0.000	0.000	0.000	0.000
GUAIACOL	0.029	0.029	0.030	0.063	0.063	0.063	0.063	0.024	0.010	0.009	0.009	0.009	0.009	0.009
XANTHENE	0.020	0.020	0.017	0.037	0.037	0.037	0.037	0.013	0.016	0.013	0.013	0.013	0.013	0.013
CYCLOHEXANOL	0.193	0.193	0.200	0.416	0.416	0.416	0.416	0.152	0.033	0.030	0.030	0.030	0.030	0.030
CYCLOHEXANONE	0.037	0.037	0.039	0.080	0.080	0.080	0.080	0.029	0.000	0.000	0.000	0.000	0.000	0.000
METHOXYCHEXANE	0.071	0.071	0.073	0.146	0.146	0.146	0.146	0.055	0.058	0.054	0.054	0.054	0.054	0.054
CYCLOHEXANE	0.489	0.489	0.508	0.004	0.004	0.004	0.004	0.002	0.001	0.001	0.001	0.001	0.001	0.001
D.H. HETER	0.071	0.071	0.074	0.156	0.156	0.156	0.156	0.057	0.066	0.056	0.056	0.056	0.056	0.056
HEPTANE	0.000	0.000	0.000	0.000	0.000	0.000	0.000	0.629	0.653	0.642	0.642	0.642	0.642	0.642
BENZENE	0.000	0.000	0.000	0.000	0.000	0.000	0.000	0.004	0.080	0.107	0.107	0.107	0.107	0.107
HYDROGEN	0.000	0.000	0.000	0.000	0.000	0.000	0.000	0.000	0.003	0.003	0.003	0.003	0.003	0.003
M-OLEATE	0.000	0.000	0.000	0.000	0.000	0.000	0.000	0.000	0.000	0.000	0.000	0.000	0.000	0.000
M-LINOLEATE	0.000	0.000	0.000	0.000	0.000	0.000	0.000	0.000	0.000	0.000	0.000	0.000	0.000	0.000
M-LINOLENATE	0.000	0.000	0.000	0.000	0.000	0.000	0.000	0.000	0.000	0.000	0.000	0.000	0.000	0.000
M-PALMITATE	0.000	0.000	0.000	0.000	0.000	0.000	0.000	0.000	0.000	0.000	0.000	0.000	0.000	0.000
M-STEARATE	0.000	0.000	0.000	0.000	0.000	0.000	0.000	0.000	0.000	0.000	0.000	0.000	0.000	0.000
MPO	0.000	0.000	0.000	0.000	0.000	0.000	0.000	0.000	0.000	0.000	0.000	0.000	0.000	0.000

Stream Name	44	45	46	47	48	49	50	51	52	53	54	55	56	57
Temperature (°C)	25.0	25.0	25.0	57.0	69.0	69.0	61.0	66.7	175.0	210.1	210.0	175.0	135.0	40.0
Pressure (bar)	40	40	1	1	1	1	1	40	40	40	40	40	40	40
Mass Vapor Fraction	0.000	0.000	0.000	0.000	0.000	0.000	0.000	0.000	0.000	0.000	0.000	0.000	0.000	0.000
Mass Liquid Fraction	1.000	1.000	1.000	1.000	1.000	1.000	1.000	1.000	1.000	1.000	1.000	1.000	1.000	1.000
Mass Solid Fraction	0.000	0.000	0.000	0.000	0.000	0.000	0.000	0.000	0.000	0.000	0.000	0.000	0.000	0.000
Mass Density (kg/cum)	763.0	740.2	740.2	698.9	818.1	816.2	824.1	818.0	685.4	628.8	615.8	644.6	675.3	741.5
Mass Fractions														
PHENOL	0.015	0.015	0.015	0.000	0.000	0.000	0.000	0.000	0.000	0.000	0.000	0.000	0.000	0.000
WATER	0.027	0.002	0.002	0.006	0.019	0.003	0.003	0.003	0.003	0.001	0.001	0.001	0.001	0.001
LACTIC ACID	0.000	0.000	0.000	0.000	0.000	0.000	0.000	0.000	0.000	0.000	0.000	0.000	0.000	0.000
ACETIC ACID	0.000	0.000	0.000	0.000	0.000	0.000	0.000	0.000	0.000	0.000	0.000	0.000	0.000	0.000
GLYCOLIC ACID	0.000	0.000	0.000	0.000	0.000	0.000	0.000	0.000	0.000	0.000	0.000	0.000	0.000	0.000
METHANOL	0.000	0.000	0.000	0.000	0.000	0.000	0.000	0.000	0.000	0.000	0.000	0.000	0.000	0.000
ANISOLE	0.044	0.045	0.045	0.000	0.000	0.000	0.000	0.000	0.000	0.000	0.000	0.000	0.000	0.000
CATECHOL	0.000	0.000	0.000	0.000	0.000	0.000	0.000	0.000	0.000	0.000	0.000	0.000	0.000	0.000
GUAIACOL	0.009	0.009	0.009	0.000	0.000	0.000	0.000	0.000	0.000	0.000	0.000	0.000	0.000	0.000
XANTHENE	0.013	0.013	0.013	0.000	0.000	0.000	0.000	0.000	0.000	0.000	0.000	0.000	0.000	0.000
CYCLOHEXANOL	0.030	0.031	0.031	0.001	0.000	0.000	0.000	0.000	0.000	0.000	0.000	0.000	0.000	0.000
CYCLOHEXANONE	0.000	0.000	0.000	0.000	0.000	0.000	0.000	0.000	0.000	0.000	0.000	0.000	0.000	0.000
METHOXYCHEXANE	0.054	0.055	0.055	0.003	0.000	0.000	0.000	0.000	0.000	0.000	0.000	0.000	0.000	0.000
CYCLOHEXANE	0.001	0.001	0.001	0.002	0.003	0.003	0.003	0.003	0.003	0.001	0.001	0.001	0.001	0.001
D.H. HETER	0.057	0.058	0.058	0.000	0.000	0.000	0.000	0.000	0.000	0.000	0.000	0.000	0.000	0.000
HEPTANE	0.644	0.661	0.661	0.690	0.042	0.042	0.045	0.045	0.045	0.017	0.017	0.017	0.017	0.017
BENZENE	0.107	0.110	0.110	0.298	0.937	0.952	0.949	0.949	0.949	0.365	0.332	0.332	0.332	0.332
HYDROGEN	0.000	0.000	0.000	0.000	0.000	0.000	0.000	0.000	0.000	0.000	0.000	0.000	0.000	0.000
M-OLEATE	0.000	0.000	0.000	0.000	0.000	0.000	0.000	0.000	0.000	0.145	0.090	0.090	0.090	0.090
M-LINOLEATE	0.000	0.000	0.000	0.000	0.000	0.000	0.000	0.000	0.000	0.220	0.137	0.137	0.137	0.137
M-LINOLENATE	0.000	0.000	0.000	0.000	0.000	0.000	0.000	0.000	0.000	0.020	0.020	0.020	0.020	0.020
M-PALMITATE	0.000	0.000	0.000	0.000	0.000	0.000	0.000	0.000	0.000	0.184	0.185	0.185	0.185	0.185
M-STEARATE	0.000	0.000	0.000	0.000	0.000	0.000	0.000	0.000	0.000	0.046	0.047	0.047	0.047	0.047
MPO	0.000	0.000	0.000	0.000	0.000	0.000	0.000	0.000	0.000	0.000	0.171	0.171	0.171	0.171

Stream Name	58	59	60	61	62	63	64	65	66	67	68	69	70	71
Temperature (°C)	40.0	327.3	327.3	309.2	263.8	220.0	190.0	135.0	122.1	95.8	175.0	250.0	63.0	67.5
Pressure (bar)	0.58	0.58	1	1	1	1	1	1	40	40	40	40	1	40
Mass Vapor Fraction	0.000	0.000	0.000	0.000	0.000	0.000	0.000	0.000	1.000	1.000	1.000	1.000	0.000	0.000
Mass Liquid Fraction	1.000	1.000	1.000	1.000	1.000	1.000	1.000	1.000	0.000	0.000	0.000	0.000	1.000	1.000
Mass Solid Fraction	0.000	0.000	0.000	0.000	0.000	0.000	0.000	0.000	0.000	0.000	0.000	0.000	0.000	0.000
Mass Density (kg/cum)	741.5	617.3	617.2	634.5	675.1	711.3	734.9	775.9	2.4	2.7	2.2	1.9	741.7	737.3
Mass Fractions														
PHENOL	0.000	0.000	0.000	0.000	0.000	0.000	0.000	0.000	0.000	0.000	0.000	0.000	0.000	0.000
WATER	0.001	0.000	0.000	0.000	0.000	0.000	0.000	0.000	0.000	0.002	0.002	0.002	0.001	0.001
LACTIC ACID	0.000	0.000	0.000	0.000	0.000	0.000	0.000	0.000	0.000	0.000	0.000	0.000	0.000	0.000
ACETIC ACID	0.000	0.000	0.000	0.000	0.000	0.000	0.000	0.000	0.000	0.000	0.000	0.000	0.000	0.000
GLYCOLIC ACID	0.000	0.000	0.000	0.000	0.000	0.000	0.000	0.000	0.000	0.000	0.000	0.000	0.000	0.000
METHANOL	0.000	0.000	0.000	0.000	0.000	0.000	0.000	0.000	0.000	0.000	0.000	0.000	0.007	0.007
ANISOLE	0.000	0.000	0.000	0.000	0.000	0.000	0.000	0.000	0.000	0.000	0.000	0.000	0.001	0.001
CATECHOL	0.000	0.000	0.000	0.000	0.000	0.000	0.000	0.000	0.000	0.000	0.000	0.000	0.000	0.000
GUAIACOL	0.000	0.000	0.000	0.000	0.000	0.000	0.000	0.000	0.000	0.000	0.000	0.000	0.000	0.000
XANTHENE	0.000	0.000	0.000	0.000	0.000	0.000	0.000	0.000	0.000	0.000	0.000	0.000	0.000	0.000
CYCLOHEXANOL	0.000	0.000	0.000	0.000	0.000	0.000	0.000	0.000	0.000	0.000	0.000	0.000	0.004	0.004
CYCLOHEXANONE	0.000	0.000	0.000	0.000	0.000	0.000	0.000	0.000	0.000	0.000	0.000	0.000	0.001	0.001
METHOXYCHEXANE	0.000	0.000	0.000	0.000	0.000	0.000	0.000	0.000	0.000	0.000	0.000	0.000	0.007	0.007
CYCLOHEXANE	0.001	0.000	0.000	0.000	0.000	0.000	0.000	0.000	0.000	0.000	0.000	0.000	0.979	0.979
D.H. HETER	0.000	0.000	0.000	0.000	0.000	0.000	0.000	0.000	0.000	0.000	0.000	0.000	0.000	0.000
HEPTANE	0.017	0.000	0.000	0.000	0.000	0.000	0.000	0.000	0.000	0.009	0.009	0.009	0.000	0.000
BENZENE	0.332	0.000	0.000	0.000	0.000	0.000	0.000	0.000	0.000	0.011	0.011	0.011	0.000	0.000
HYDROGEN	0.000	0.000	0.000	0.000	0.000	0.000	0.000	0.000	1.000	0.978	0.978	0.978	0.000	0.000
M-OLEATE	0.090	0.139	0.139	0.139	0.139	0.139	0.139	0.139	0.000	0.000	0.000	0.000	0.000	0.000
M-LINOLEATE	0.137	0.211	0.211	0.211	0.211	0.211	0.211	0.211	0.000	0.000	0.000	0.000	0.000	0.000
M-LINOLENATE	0.020	0.031	0.031	0.031	0.031	0.031	0.031	0.031	0.000	0.000	0.000	0.000	0.000	0.000
M-PALMITATE	0.185	0.285	0.285	0.285	0.285	0.285	0.285	0.285	0.000	0.000	0.000	0.000	0.000	0.000
M-STEARATE	0.047	0.072	0.072	0.072	0.072	0.072	0.072	0.072	0.000	0.000	0.000	0.000	0.000	0.000
MPO	0.171	0.263	0.263	0.263	0.263	0.263	0.263	0.263	0.000	0.000	0.000	0.000	0.000	0.000

Stream Name	72	73	74	75	76	77	78	79	80	81	82	83	84	85
Temperature (°C)	245.0	269.0	50.0	63.3	63.3	63.3	63.3	63.3	250.0	194.9	135.0	35.0	25.0	25.0
Pressure (bar)	40	40	1	1	1	1	1	1	40	40	40	40	40	40
Mass Vapor Fraction	0.000	0.000	0.000	0.000	0.000	0.000	0.000	0.000	1.000	0.301	0.079	0.017	0.016	0.000
Mass Liquid Fraction	1.000	1.000	1.000	1.000	1.000	1.000	1.000	1.000	0.000	0.699	0.921	0.983	0.984	1.000
Mass Solid Fraction	0.000	0.000	0.000	0.000	0.000	0.000	0.000	0.000	0.000	0.000	0.000	0.000	0.000	0.000
Mass Density (kg/cum)	496.6	422.7	971.5	743.5	741.4	892.0	741.4	741.4	38.1	64.5	99.9	155.7	161.3	666.7
Mass Fractions														
PHENOL	0.000	0.000	0.001	0.000	0.000	0.000	0.000	0.000	0.003	0.003	0.003	0.003	0.003	0.003
WATER	0.001	0.001	0.802	0.013	0.001	0.745	0.001	0.001	0.065	0.065	0.065	0.065	0.065	0.066
LACTIC ACID	0.000	0.000	0.008	0.000	0.000	0.000	0.000	0.000	0.000	0.000	0.000	0.000	0.000	0.000
ACETIC ACID	0.000	0.000	0.000	0.000	0.000	0.000	0.000	0.000	0.000	0.000	0.000	0.000	0.000	0.000
GLYCOLIC ACID	0.000	0.000	0.020	0.000	0.000	0.004	0.000	0.000	0.000	0.000	0.000	0.000	0.000	0.000
METHANOL	0.007	0.007	0.045	0.011	0.007	0.245	0.007	0.007	0.000	0.000	0.000	0.000	0.000	0.000
ANISOLE	0.001	0.001	0.001	0.001	0.001	0.000	0.001	0.001	0.034	0.034	0.034	0.034	0.034	0.035
CATECHOL	0.000	0.000	0.000	0.000	0.000	0.000	0.000	0.000	0.000	0.000	0.000	0.000	0.000	0.000
GUAIACOL	0.000	0.000	0.001	0.000	0.000	0.000	0.000	0.000	0.005	0.005	0.005	0.005	0.005	0.005
XANTHENE	0.000	0.000	0.093	0.000	0.000	0.000	0.000	0.000	0.000	0.000	0.000	0.000	0.000	0.000
CYCLOHEXANOL	0.004	0.004	0.018	0.004	0.004	0.002	0.004	0.004	0.012	0.012	0.012	0.012	0.012	0.012
CYCLOHEXANONE	0.001	0.001	0.010	0.001	0.001	0.001	0.001	0.001	0.000	0.000	0.000	0.000	0.000	0.000
METHOXYCHEXANE	0.007	0.007	0.002	0.007	0.007	0.001	0.007	0.007	0.030	0.030	0.030	0.030	0.030	0.030
CYCLOHEXANE	0.979	0.979	0.000	0.963	0.979	0.001	0.979	0.979	0.001	0.001	0.001	0.001	0.001	0.001
D.H. HETER	0.000	0.000	0.000	0.000	0.000	0.000	0.000	0.000	0.001	0.001	0.001	0.001	0.001	0.001
HEPTANE	0.000	0.000	0.000	0.000	0.000	0.000	0.000	0.000	0.569	0.569	0.569	0.569	0.569	0.579
BENZENE	0.000	0.000	0.000	0.000	0.000	0.000	0.000	0.000	0.258	0.258	0.258	0.258	0.258	0.262
HYDROGEN	0.000	0.000	0.000	0.000	0.000	0.000	0.000	0.000	0.022	0.022	0.022	0.022	0.022	0.006
M-OLEATE	0.000	0.000	0.000	0.000	0.000	0.000	0.000	0.000	0.000	0.000	0.000	0.000	0.000	0.000
M-LINOLEATE	0.000	0.000	0.000	0.000	0.000	0.000	0.000	0.000	0.000	0.000	0.000	0.000	0.000	0.000
M-LINOLENATE	0.000	0.000	0.000	0.000	0.000	0.000	0.000	0.000	0.000	0.000	0.000	0.000	0.000	0.000
M-PALMITATE	0.000	0.000	0.000	0.000	0.000	0.000	0.000	0.000	0.000	0.000	0.000	0.000	0.000	0.000
M-STEARATE	0.000	0.000	0.000	0.000	0.000	0.000	0.000	0.000	0.000	0.000	0.000	0.000	0.000	0.000
MPO	0.000	0.000	0.000	0.000	0.000	0.000	0.000	0.000	0.000	0.000	0.000	0.000	0.000	0.000

Stream Name	86	87	88	89	90	91	92	93	94	95	96	97	98	99
Temperature (°C)	25.0	25.0	25.0	106.2	95.5	96.2	96.2	96.2	90.6	94.4	215.0	252.0	97.2	69.0
Pressure (bar)	40	40	40	1	1	1	1	1	1	40	40	40	1	1
Mass Vapor Fraction	1.000	1.000	0.000	0.000	0.000	0.000	0.000	0.000	0.000	0.000	0.000	0.000	0.000	0.000
Mass Liquid Fraction	0.000	0.000	1.000	1.000	1.000	1.000	1.000	1.000	1.000	1.000	1.000	1.000	1.000	1.000
Mass Solid Fraction	0.000	0.000	0.000	0.000	0.000	0.000	0.000	0.000	0.000	0.000	0.000	0.000	0.000	0.000
Mass Density (kg/cum)	3.4	3.5	998.7	673.4	618.2	618.5	618.5	618.5	623.9	620.1	468.4	382.1	618.9	950.2
Mass Fractions														
PHENOL	0.000	0.000	0.007	0.024	0.000	0.000	0.000	0.000	0.000	0.000	0.000	0.000	0.000	0.000
WATER	0.006	0.005	0.954	0.000	0.000	0.000	0.000	0.000	0.000	0.000	0.000	0.000	0.000	0.997
LACTIC ACID	0.000	0.000	0.000	0.000	0.000	0.000	0.000	0.000	0.000	0.000	0.000	0.000	0.000	0.000
ACETIC ACID	0.000	0.000	0.000	0.000	0.000	0.000	0.000	0.000	0.000	0.000	0.000	0.000	0.000	0.000
GLYCOLIC ACID	0.000	0.000	0.000	0.000	0.000	0.000	0.000	0.000	0.000	0.000	0.000	0.000	0.000	0.000
METHANOL	0.000	0.000	0.000	0.000	0.000	0.000	0.000	0.000	0.000	0.000	0.000	0.000	0.000	0.000
ANISOLE	0.000	0.000	0.000	0.071	0.000	0.000	0.000	0.000	0.000	0.000	0.000	0.000	0.001	0.000
CATECHOL	0.000	0.000	0.000	0.000	0.000	0.000	0.000	0.000	0.000	0.000	0.000	0.000	0.000	0.000
GUAIACOL	0.000	0.000	0.001	0.015	0.001	0.001	0.001	0.001	0.001	0.001	0.001	0.001	0.001	0.000
XANTHENE	0.000	0.000	0.036	0.020	0.000	0.000	0.000	0.000	0.000	0.000	0.000	0.000	0.000	0.000
CYCLOHEXANOL	0.000	0.000	0.001	0.049	0.001	0.001	0.001	0.001	0.001	0.001	0.001	0.001	0.001	0.000
CYCLOHEXANONE	0.000	0.000	0.000	0.000	0.000	0.000	0.000	0.000	0.000	0.000	0.000	0.000	0.000	0.000
METHOXYCHEXANE	0.000	0.001	0.000	0.086	0.002	0.002	0.002	0.002	0.002	0.002	0.002	0.002	0.004	0.000
CYCLOHEXANE	0.000	0.000	0.000	0.000	0.000	0.001	0.001	0.001	0.000	0.000	0.000	0.000	0.001	0.000
D.H. HETER	0.000	0.000	0.000	0.092	0.000	0.000	0.000	0.000	0.000	0.000	0.000	0.000	0.000	0.000
HEPTANE	0.002	0.054	0.000	0.644	0.996	0.988	0.988	0.988	0.989	0.989	0.989	0.989	0.976	0.000
BENZENE	0.050	0.023	0.000	0.000	0.000	0.007	0.007	0.007	0.006	0.006	0.006	0.006	0.016	0.003
HYDROGEN	0.941	0.916	0.000	0.001	0.000	0.000	0.000	0.000	0.000	0.000	0.000	0.000	0.000	0.000
M-OLEATE	0.000	0.000	0.000	0.000	0.000	0.000	0.000	0.000	0.000	0.000	0.000	0.000	0.000	0.000
M-LINOLEATE	0.000	0.000	0.000	0.000	0.000	0.000	0.000	0.000	0.000	0.000	0.000	0.000	0.000	0.000
M-LINOLENATE	0.000	0.000	0.000	0.000	0.000	0.000	0.000	0.000	0.000	0.000	0.000	0.000	0.000	0.000
M-PALMITATE	0.000	0.000	0.000	0.000	0.000	0.000	0.000	0.000	0.000	0.000	0.000	0.000	0.000	0.000
M-STEARATE	0.000	0.000	0.000	0.000	0.000	0.000	0.000	0.000	0.000	0.000	0.000	0.000	0.000	0.000
MPO	0.000	0.000	0.000	0.000	0.000	0.000	0.000	0.000	0.000	0.000	0.000	0.000	0.000	0.000

Stream Name	100	101	102	103	104	BENZENE	BIOLUBRICANT	MIXED STREAM
Temperature (°C)	49.5	49.6	49.6	323.3	227.1	49.6	30.0	131.5
Pressure (bar)	0.58	1	1	40	40	1	1	1
Mass Vapor Fraction	0.000	0.000	0.000	0.000	0.000	0.000	0.000	0.000
Mass Liquid Fraction	1.000	1.000	1.000	1.000	1.000	1.000	1.000	1.000
Mass Solid Fraction	0.000	0.000	0.000	0.000	0.000	0.000	0.000	0.000
Mass Density (kg/cum)	835.1	835.0	835.0	624.3	710.0	835.0	848.3	749.9
Mass Fractions								
PHENOL	0.000	0.000	0.000	0.000	0.000	0.000	0.000	0.055
WATER	0.003	0.003	0.003	0.000	0.000	0.003	0.000	0.000
LACTIC ACID	0.000	0.000	0.000	0.000	0.000	0.000	0.000	0.000
ACETIC ACID	0.000	0.000	0.000	0.000	0.000	0.000	0.000	0.000
GLYCOLIC ACID	0.000	0.000	0.000	0.000	0.000	0.000	0.000	0.000
METHANOL	0.000	0.000	0.000	0.000	0.000	0.000	0.000	0.000
ANISOLE	0.000	0.000	0.000	0.000	0.000	0.000	0.000	0.159
CATECHOL	0.000	0.000	0.000	0.000	0.000	0.000	0.000	0.000
GUAIACOL	0.000	0.000	0.000	0.000	0.000	0.000	0.000	0.031
XANTHENE	0.000	0.000	0.000	0.000	0.000	0.000	0.000	0.045
CYCLOHEXANOL	0.000	0.000	0.000	0.000	0.000	0.000	0.000	0.108
CYCLOHEXANONE	0.000	0.000	0.000	0.000	0.000	0.000	0.000	0.000
METHOXYCHEXANE	0.000	0.000	0.000	0.000	0.000	0.000	0.000	0.190
CYCLOHEXANE	0.003	0.003	0.003	0.000	0.000	0.003	0.000	0.000
D.H. HETER	0.000	0.000	0.000	0.000	0.000	0.000	0.000	0.206
HEPTANE	0.050	0.050	0.050	0.000	0.000	0.050	0.000	0.203
BENZENE	0.944	0.944	0.944	0.000	0.000	0.944	0.000	0.000
HYDROGEN	0.000	0.000	0.000	0.000	0.000	0.000	0.000	0.002
M-OLEATE	0.000	0.000	0.000	0.236	0.236	0.000	0.139	0.000
M-LINOLEATE	0.000	0.000	0.000	0.358	0.358	0.000	0.211	0.000
M-LINOLENATE	0.000	0.000	0.000	0.033	0.033	0.000	0.031	0.000
M-PALMITATE	0.000	0.000	0.000	0.299	0.299	0.000	0.285	0.000
M-STEARATE	0.000	0.000	0.000	0.075	0.075	0.000	0.072	0.000
MPO	0.000	0.000	0.000	0.000	0.000	0.000	0.263	0.000

Appendix B

EQUIPMENT COSTS: HTL PROCESS

(from Capcost, 2017)

EQUIPMENT ID	EQUIPMENT TYPE	PURCHASE COST ($)	INSTALLATION COST ($)
S-102	Centrifugal Centrifuge	51,200	80,400
T-103 COND	Fixed, Sheet, or U-Tube HEX	55,200	182,000
HE-102	Floating Head HEX	370,000	1,030,000
HE-101	Fixed, Sheet, or U-Tube HEX	84,600	193,000
S-101	Leaf Filter	142,000	234,000
P-102 A/B	Centrifugal Pump	51,200	132,000
P-103 A/B	Centrifugal Pump	75,400	156,000
V-101	Vertical Vessel	49,600	202,000
S-103	Vertical Vessel	155,000	431,000
T-102 COND A/B	2 Condensers	363,350	1,195,422
T-101 COND A/B/C	3 Condensers	411,570	1,354,065
T-101 REB A/B/C	3 Kettle Reboilers	1,283,546	3,901,983
T-103 REB	Kettle Reboiler	501,222	1,248,042
T-102 REB A/B	2 Kettle reboilers	2,045,310	5,092,822
T-103	Tower	164,302	437,044
T-102 A/B	2 Parallel Towers	1,351,442	2,905,598
T-101 A/B/C	3 Parallel Towers	2,049,147	4,856,477
R-101	IHRS	-	77,550,000
CEPCI = 813			**TOTAL: $ 101,182,000**

EQUIPMENT COSTS: TRANSESTERIFICATION PROCESS

(from Capcost, 2017) (Hussein et al., 2021)

EQUIPMENT ID	EQUIPMENT TYPE	PURCHASE COST ($)	INSTALLATION COST ($)
V-200	Centrifugal Centrifuge	51,200	80,400
E-100	Floating Head HEX	65,900	217,000
COND of T-100	Fixed, Sheet, or U-Tube HEX	40,100	132,000
COND of T-200	Fixed, Sheet, or U-Tube HEX	31,400	103,000
R-100	Jacketed Agitated Reactor	121,000	485,000
R-200	Jacketed Agitated Reactor	11,100	44,300
T-100	Tower	76,600	173,000
T-200	Tower	507,000	856,000
V-100	Vertical Vessel	18,100	73,500
REB of T-100	Kettle Reboiler	283,900	934,000
REB of T-200	Kettle Reboiler	414,300	1,060,600
CEPCI = 813			**TOTAL: $ 4,159,000**

EQUIPMENT COSTS: HDO & ALKYLATION PROCESSES

(from Capcost, 2017)

EQUIPMENT ID	EQUIPMENT TYPE	PURCHASE COST ($)	INSTALLATION COST ($)
HE-204	Fixed, Sheet, or U-Tube HEX	53,400	163,000
HE-210	Fixed, Sheet, or U-Tube HEX	40,800	124,000
HE-303	Floating Head HEX	137,000	298,000
HE-306	Floating Head HEX	107,000	240,000
HE-209	Fixed, Sheet, or U-Tube HEX	62,500	190,000
HE-214	Fixed, Sheet, or U-Tube HEX	106,000	230,000
HE-215	Fixed, Sheet, or U-Tube HEX	101,000	219,000
HE-203	Fixed, Sheet, or U-Tube HEX	116,000	354,000
HE-208	Fixed, Sheet, or U-Tube HEX	117,000	356,000
HE-302	Floating Head HEX	279,000	605,000
HE-305	Floating Head HEX	205,000	462,000
HE-213	Fixed, Sheet, or U-Tube HEX	200,000	433,000
HE-304	Floating Head HEX	115,000	258,000
HE-201	Fixed, Sheet, or U-Tube HEX	54,100	164,000
HE-202	Fixed, Sheet, or U-Tube HEX	101,000	219,000
HE-207	Fixed, Sheet, or U-Tube HEX	63,200	192,000
HE-211	Floating Head HEX	131,000	284,000
HE-212	Floating Head HEX	121,000	262,000
HE-216	Floating Head HEX	131,000	283,000
HE-205	Fixed, Sheet, or U-Tube HEX	38,900	118,000
HE-206	Floating Head HEX	137,000	296,000
HE-301	Floating Head HEX	131,000	284,000
T-201 COND	Fixed, Sheet, or U-Tube HEX	43,900	144,000
T-202 COND	Fixed, Sheet, or U-Tube HEX	44,800	147,000
T-203 COND	Fixed, Sheet, or U-Tube HEX	43,000	141,000
T-204 COND	Fixed, Sheet, or U-Tube HEX	42,400	140,000
T-301 COND	Fixed, Sheet, or U-Tube HEX	98,600	223,000
P-201 A/B	Centrifugal Pump	80,000	165,000
P-202 A/B	Centrifugal Pump	87,500	181,000
P-203 A/B	Centrifugal Pump	119,000	245,000
P-304 A/B	Centrifugal Pump	122,000	225,000
P-301 A/B	Centrifugal Pump	62,800	130,000
T-201	Tower	166,000	382,000
T-202	Tower	250,000	598,000
T-203	Tower	340,000	761,000
T-204	Tower	203,000	495,000
T-301	Tower	253,000	466,000
V-206	Vertical Vessel	187,000	368,000
V-202	Vertical Vessel	570,000	1,090,000
V-201	Horizontal Vessel	13,900	41,800
V-205	Horizontal Vessel	11,800	35,500
V-203	Horizontal Vessel	107,000	188,000
V-204	Horizontal Vessel	9,150	27,500
C-201 A/B	Reciprocating Compressor	368,000	1,247,600
T-201 REB	Kettle Reboiler	339,200	1,105,700
T-202 REB	Kettle Reboiler	400,800	1,318,600
T-203 REB	Kettle Reboiler	264,800	871,200
T-204 REB	Kettle Reboiler	211,500	689,600
T-301 REB	Kettle Reboiler	793,500	2,031,300
R-201	Multistage Trickle Bed Reactor	26,331,000	52,662,000
R-202	Multistage Fixed Bed Reactor	14,553,000	29,106,000
R-301	Multistage Fluidized Bed Reactor	7,618,000	19,045,000
CEPCI = 813			**TOTAL: $ 120,305,000**

Appendix C

DISCOUNTED CASH FLOW RATE OF RETURN WORKSHEET: BASE CASE

(ETHANOL PRODUCTION ONLY)

YEAR	-2	-1	0	1	2	3	4	5	6	7	8
FCI (MM$)	19.837	148.776	79.347								
Land (MM$)	5.3										
Working Capital (MM$)			30.995								
Loan Payment (MM$)				55.430	55.430	55.430	55.430	55.430	55.430	55.430	55.430
Loan Interest Payment (MM$)	2.380	20.234	29.755	29.755	27.701	25.483	23.087	20.500	17.705	14.687	11.428
Loan Principal (MM$)	29.755	252.919	371.940	346.265	318.536	288.589	256.246	221.316	183.591	142.849	98.846
Ethanol Sales (MM$)				161.266	184.305	184.305	184.305	184.305	184.305	184.305	184.305
By-Products Sales (MM$)				8.024	9.170	9.170	9.170	9.170	9.170	9.170	9.170
TOTAL ANNUAL SALES (MM$)				169.290	193.475	193.475	193.475	193.475	193.475	193.475	193.475
Var OPEX (MM$)				85.35	91.040	91.040	91.040	91.040	91.040	91.040	91.040
Fixed OPEX (MM$)				15.790	15.790	15.790	15.790	15.790	15.790	15.790	15.790
TOTAL PRODUCT COST (MM$)				101.140	106.830	106.830	106.830	106.830	106.830	106.830	106.830
Plant Writedown				0.1429	0.2449	0.1749	0.1249	0.0893	0.0893	0.0892	0.0446
Depreciation Charge (MM$)				88.584	151.814	108.421	77.426	55.357	55.357	55.295	27.648
Remaining Value (MM$)			619.900	531.316	379.503	271.082	193.657	138.300	82.943	27.648	0.000
Net Revenue (MM$)				-50.189	-92.870	-47.259	-13.868	10.788	13.582	16.662	47.569
Losses Forward (MM$)					-50.189	-143.059	-190.318	-204.186	-193.398	-179.816	-163.154
Taxable Income (MM$)				-50.189	-143.059	-190.318	-204.186	-193.398	-179.816	-163.154	-115.584
Income Tax (MM$)											
Annual Cash Income (MM$)				12.720	31.215	31.215	31.215	31.215	31.215	31.215	31.215
Discount Factor	1.21	1.1	1	0.9091	0.8264	0.7513	0.6830	0.6209	0.5645	0.5132	0.4665
Annual Present Value (MM$)				11.564	25.797	23.452	21.320	19.382	17.620	16.018	14.562
TCI+Interest (MM$)	33.296	185.910	140.097								

YEAR	9	10	11	12	13	14	15	16	17	18	19
FCI (MM$)											
Land (MM$)											
Working Capital (MM$)											
Loan Payment (MM$)	55.430	55.430									
Loan Interest Payment (MM$)	7.908	4.106									
Loan Principal (MM$)	51.324	0.000									
Ethanol Sales (MM$)	184.305	184.305	184.305	184.305	184.305	184.305	184.305	184.305	184.305	184.305	184.305
By-Products Sales (MM$)	9.170	9.170	9.170	9.170	9.170	9.170	9.170	9.170	9.170	9.170	9.170
TOTAL ANNUAL SALES (MM$)	193.475	193.475	193.475	193.475	193.475	193.475	193.475	193.475	193.475	193.475	193.475
Var OPEX (MM$)	91.040	91.040	91.040	91.040	91.040	91.040	91.040	91.040	91.040	91.040	91.040
Fixed OPEX (MM$)	15.790	15.790	15.790	15.790	15.790	15.790	15.790	15.790	15.790	15.790	15.790
TOTAL PRODUCT COST (MM$)	106.830	106.830	106.830	106.830	106.830	106.830	106.830	106.830	106.830	106.830	106.830
Plant Writedown											
Depreciation Charge (MM$)											
Remaining Value (MM$)											
Net Revenue (MM$)	78.737	82.539	86.645	86.645	86.645	86.645	86.645	86.645	86.645	86.645	86.645
Losses Forward (MM$)	-115.584	-36.848									
Taxable Income (MM$)	-36.848	45.691	86.645	86.645	86.645	86.645	86.645	86.645	86.645	86.645	86.645
Income Tax (MM$)		15.992	30.326	30.326	30.326	30.326	30.326	30.326	30.326	30.326	30.326
Annual Cash Income (MM$)	31.215	15.223	56.319	56.319	56.319	56.319	56.319	56.319	56.319	56.319	56.319
Discount Factor	0.4241	0.3855	0.3505	0.3186	0.2897	0.2633	0.2394	0.2176	0.1978	0.1799	0.1635
Annual Present Value (MM$)	13.238	5.869	19.739	17.945	16.314	14.831	13.482	12.257	11.142	10.129	9.209
TCI+Interest (MM$)											

YEAR	20	21	22	23	24	25	26	27	28	29	30
FCI (MM$)											
Land (MM$)											-5.3
Working Capital (MM$)											-30.995
Loan Payment (MM$)											
Loan Interest Payment (MM$)											
Loan Principal (MM$)											
Ethanol Sales (MM$)	184.305	184.305	184.305	184.305	184.305	184.305	184.305	184.305	184.305	184.305	184.305
By-Products Sales (MM$)	9.170	9.170	9.170	9.170	9.170	9.170	9.170	9.170	9.170	9.170	9.170
TOTAL ANNUAL SALES (MM$)	193.475	193.475	193.475	193.475	193.475	193.475	193.475	193.475	193.475	193.475	193.475
Var OPEX (MM$)	91.040	91.040	91.040	91.040	91.040	91.040	91.040	91.040	91.040	91.040	91.040
Fixed OPEX (MM$)	15.790	15.790	15.790	15.790	15.790	15.790	15.790	15.790	15.790	15.790	15.790
TOTAL PRODUCT COST (MM$)	106.830	106.830	106.830	106.830	106.830	106.830	106.830	106.830	106.830	106.830	106.830
Plant Writedown											
Depreciation Charge (MM$)											
Remaining Value (MM$)											
Net Revenue (MM$)	86.645	86.645	86.645	86.645	86.645	86.645	86.645	86.645	86.645	86.645	86.645
Losses Forward (MM$)											
Taxable Income (MM$)	86.645	86.645	86.645	86.645	86.645	86.645	86.645	86.645	86.645	86.645	86.645
Income Tax (MM$)	30.326	30.326	30.326	30.326	30.326	30.326	30.326	30.326	30.326	30.326	30.326
Annual Cash Income (MM$)	56.319	56.319	56.319	56.319	56.319	56.319	56.319	56.319	56.319	56.319	56.319
Discount Factor	0.1486	0.1351	0.1228	0.1117	0.1015	0.0923	0.0839	0.0763	0.0693	0.0630	0.0573
Annual Present Value (MM$)	8.371	7.610	6.919	6.290	5.718	5.198	4.725	4.296	3.905	3.550	3.228
TCI+Interest (MM$)											-7.076

TOTAL TCI+INTEREST = $352,227,000 // TOTAL ANNUAL PRESENT VALUE = $353,680,000

NPV = $1,452,000 // MESP = $3.02/gal

DISCOUNTED CASH FLOW RATE OF RETURN WORKSHEET: INTEGRATED CASE

(ETHANOL+BIOLUBRICANT PRODUCTIONS)

YEAR	-2	-1	0	1	2	3	4	5	6	7	8
FCI (MM$)	32.344	242.582	129.377								
Land (MM$)	8.859										
Working Capital (MM$)			50.538								
Loan Payment (MM$)				90.380	90.380	90.380	90.380	90.380	90.380	90.380	90.380
Loan Interest Payment (MM$)	3.881	32.991	48.516	48.516	45.167	41.550	37.644	33.425	28.869	23.948	18.633
Loan Principal (MM$)	48.516	412.390	606.456	564.593	519.380	470.551	417.815	360.860	299.349	232.918	161.171
Ethanol Sales (MM$)				140.975	161.114	161.114	161.114	161.114	161.114	161.114	161.114
By-Products Sales (MM$)				384.979	439.976	439.976	439.976	439.976	439.976	439.976	439.976
TOTAL ANNUAL SALES (MM$)				525.954	601.090	601.090	601.090	601.090	601.090	601.090	601.090
Var OPEX (MM$)				404.20594	431.153	431.153	431.153	431.153	431.153	431.153	431.153
Fixed OPEX (MM$)				27.166	27.166	27.166	27.166	27.166	27.166	27.166	27.166
TOTAL PRODUCT COST (MM$)				431.372	458.319	458.319	458.319	458.319	458.319	458.319	458.319
Plant Writedown				0.1429	0.2449	0.1749	0.1249	0.0893	0.0893	0.0892	0.0446
Depreciation Charge (MM$)				144.438	247.535	176.782	126.244	90.261	90.261	90.160	45.080
Remaining Value (MM$)			1010.760	866.322	618.787	442.005	315.761	225.501	135.240	45.080	0.000
Net Revenue (MM$)				-98.372	-149.932	-75.561	-21.117	19.085	23.641	28.663	79.058
Losses Forward (MM$)					-98.372	-248.304	-323.865	-344.982	-325.898	-302.256	-273.593
Taxable Income (MM$)				-98.372	-248.304	-323.865	-344.982	-325.898	-302.256	-273.593	-194.536
Income Tax (MM$)											
Annual Cash Income (MM$)				4.202	52.391	52.391	52.391	52.391	52.391	52.391	52.391
Discount Factor	1.21	1.1	1	0.9091	0.8264	0.7513	0.6830	0.6209	0.5645	0.5132	0.4665
Annual Present Value (MM$)				3.820	43.298	39.362	35.784	32.531	29.573	26.885	24.441
TCI+Interest (MM$)	54.552	303.131	228.432								

YEAR	9	10	11	12	13	14	15	16	17	18	19
FCI (MM$)											
Land (MM$)											
Working Capital (MM$)											
Loan Payment (MM$)	90.380	90.380									
Loan Interest Payment (MM$)	12.894	6.695									
Loan Principal (MM$)	83.685	0.000									
Ethanol Sales (MM$)	161.114	161.114	161.114	161.114	161.114	161.114	161.114	161.114	161.114	161.114	161.114
By-Products Sales (MM$)	439.976	439.976	439.976	439.976	439.976	439.976	439.976	439.976	439.976	439.976	439.976
TOTAL ANNUAL SALES (MM$)	601.090	601.090	601.090	601.090	601.090	601.090	601.090	601.090	601.090	601.090	601.090
Var OPEX (MM$)	431.153	431.153	431.153	431.153	431.153	431.153	431.153	431.153	431.153	431.153	431.153
Fixed OPEX (MM$)	27.166	27.166	27.166	27.166	27.166	27.166	27.166	27.166	27.166	27.166	27.166
TOTAL PRODUCT COST (MM$)	458.319	458.319	458.319	458.319	458.319	458.319	458.319	458.319	458.319	458.319	458.319
Plant Writedown											
Depreciation Charge (MM$)											
Remaining Value (MM$)											
Net Revenue (MM$)	129.877	136.076	142.771	142.771	142.771	142.771	142.771	142.771	142.771	142.771	142.771
Losses Forward (MM$)	-194.536	-64.658									
Taxable Income (MM$)	-64.658	71.418	142.771	142.771	142.771	142.771	142.771	142.771	142.771	142.771	142.771
Income Tax (MM$)		24.996	49.970	49.970	49.970	49.970	49.970	49.970	49.970	49.970	49.970
Annual Cash Income (MM$)	52.391	27.395	92.801	92.801	92.801	92.801	92.801	92.801	92.801	92.801	92.801
Discount Factor	0.4241	0.3855	0.3505	0.3186	0.2897	0.2633	0.2394	0.2176	0.1978	0.1799	0.1635
Annual Present Value (MM$)	22.219	10.562	32.526	29.569	26.881	24.437	22.216	20.196	18.360	16.691	15.174
TCI+Interest (MM$)											

YEAR	20	21	22	23	24	25	26	27	28	29	30
FCI (MM$)											
Land (MM$)											-8.859
Working Capital (MM$)											-50.538
Loan Payment (MM$)											
Loan Interest Payment (MM$)											
Loan Principal (MM$)											
Ethanol Sales (MM$)	161.114	161.114	161.114	161.114	161.114	161.114	161.114	161.114	161.114	161.114	161.114
By-Products Sales (MM$)	439.976	439.976	439.976	439.976	439.976	439.976	439.976	439.976	439.976	439.976	439.976
TOTAL ANNUAL SALES (MM$)	601.090	601.090	601.090	601.090	601.090	601.090	601.090	601.090	601.090	601.090	601.090
Var OPEX (MM$)	431.153	431.153	431.153	431.153	431.153	431.153	431.153	431.153	431.153	431.153	431.153
Fixed OPEX (MM$)	27.166	27.166	27.166	27.166	27.166	27.166	27.166	27.166	27.166	27.166	27.166
TOTAL PRODUCT COST (MM$)	458.319	458.319	458.319	458.319	458.319	458.319	458.319	458.319	458.319	458.319	458.319
Plant Writedown											
Depreciation Charge (MM$)											
Remaining Value (MM$)											
Net Revenue (MM$)	142.771	142.771	142.771	142.771	142.771	142.771	142.771	142.771	142.771	142.771	142.771
Losses Forward (MM$)											
Taxable Income (MM$)	142.771	142.771	142.771	142.771	142.771	142.771	142.771	142.771	142.771	142.771	142.771
Income Tax (MM$)	49.970	49.970	49.970	49.970	49.970	49.970	49.970	49.970	49.970	49.970	49.970
Annual Cash Income (MM$)	92.801	92.801	92.801	92.801	92.801	92.801	92.801	92.801	92.801	92.801	92.801
Discount Factor	0.1486	0.1351	0.1228	0.1117	0.1015	0.0923	0.0839	0.0763	0.0693	0.0630	0.0573
Annual Present Value (MM$)	13.794	12.540	11.400	10.364	9.422	8.565	7.787	7.079	6.435	5.850	5.318
TCI+Interest (MM$)											-11.755

TOTAL TCI+INTEREST = $574,360,000 // TOTAL ANNUAL PRESENT VALUE = $573,081,000

NPV = -$1,279,000 // MESP = $2.64/gal

Bibliography

Azarpour, A., Alwi, S. R. W., Zahedi, G., Madooli, M., & Millar, G. J. (2015). Catalytic activity evaluation of industrial Pd/C catalyst via gray-box dynamic modeling and simulation of hydropurification reactor. *Applied Catalysis A: General*, *489*, 262-271.

Bagnato, G., & Sanna, A. (2019). Process and techno-economic analysis for fuel and chemical production by hydrodeoxygenation of bio-oil. *Catalysts*, *9*(12), 1021.

Barbera, E., Hirayama, K., Maglinao, R. L., Davis, R. W., & Kumar, S. (2024). Recent developments in synthesizing biolubricants—a review. *Biomass Conversion and Biorefinery*, *14*(3), 2867-2887.

Bi, Z., Zhang, J., Zhu, Z., Liang, Y., & Wiltowski, T. (2018). Generating biocrude from partially defatted Cryptococcus curvatus yeast residues through catalytic hydrothermal liquefaction. *Applied Energy*, *209*, 435-444.

Bian, P. C., Xu, W. J., Gang, H. Z., Liu, J. F., Mu, B. Z., & Yang, S. Z. (2017). Insight into the shift and rearrangement of carbocation in Friedel-Crafts alkylation of unsaturated fatty acids revealed by GC–MS. *International Journal of Mass Spectrometry*, *415*, 85-91.

Biomass Multi-Year Program Plan (MYPP), April 2011, DOE

Biomass Multi-Year Program Plan (MYPP), April 2023, DOE

Borges, M. E., & Díaz, L. (2012). Recent developments on heterogeneous catalysts for biodiesel production by oil esterification and transesterification reactions: A review. *Renewable and Sustainable Energy Reviews*, *16*(5), 2839-2849.

Bu, Q., Lei, H., Zacher, A. H., Wang, L., Ren, S., Liang, J., ... & Ruan, R. (2012). A review of catalytic hydrodeoxygenation of lignin-derived phenols from biomass pyrolysis. *Bioresource technology*, *124*, 470-477.

Busca, G. (2007). Acid catalysts in industrial hydrocarbon chemistry. *Chemical Reviews*, *107*(11), 5366-5410.

Cai Junmeng, Yifeng He, Xi Yu, Scott W. Banks, Yang Yang, Xingguang Zhang, Yang Yu, Ronghou Liu, Anthony V. Bridgwater, Review of physicochemical properties and analytical characterization of lignocellulosic biomass, Renewable and Sustainable Energy Reviews, Volume 76, 2017, Pages 309-322, ISSN 1364-0321, https://doi.org/10.1016/j.rser.2017.03.072.

Castello, D., Pedersen, T. H., & Rosendahl, L. A. (2018). Continuous hydrothermal liquefaction of biomass: A critical review. *Energies*, *11*(11), 3165.

Cecilia, J. A., Ballesteros Plata, D., Alves Saboya, R. M., Tavares de Luna, F. M., Cavalcante Jr, C. L., & Rodríguez-Castellón, E. (2020). An overview of the biolubricant production process: Challenges and future perspectives. *Processes*, *8*(3), 257.

Chan, C. H., Tang, S. W., Mohd, N. K., Lim, W. H., Yeong, S. K., & Idris, Z. (2018). Tribological behavior of biolubricant base stocks and additives. *Renewable and Sustainable Energy Reviews*, *93*, 145-157.

Gebremariam, S. N., & Marchetti, J. M. (2018). Biodiesel production through sulfuric acid catalyzed transesterification of acidic oil: Techno economic feasibility of different process alternatives. *Energy Conversion and Management*, *174*, 639-648.

Gollakota, A. R. K., Kishore, N., & Gu, S. (2018). A review on hydrothermal liquefaction of biomass. *Renewable and Sustainable Energy Reviews*, *81*, 1378-1392.

He, J., Zhao, C., & Lercher, J. A. (2014). Impact of solvent for individual steps of phenol hydrodeoxygenation with Pd/C and HZSM-5 as catalysts. *Journal of catalysis*, *309*, 362-375.

Hirayama, K., Maglinao, R., Barbera, E., & Kumar, S. (2024). Production of phenolic monomers from lignin in hydrothermal medium: Effect of rapid heating and short residence time. *The Journal of Supercritical Fluids*, *205*, 106123.

Humbird, D., Davis, R., Tao, L., Kinchin, C., Hsu, D., Aden, A., ... & Dudgeon, D. (2011). *Process design and economics for biochemical conversion of lignocellulosic biomass to ethanol: dilute-acid pretreatment and enzymatic hydrolysis of corn stover* (No. NREL/TP-5100-47764). National Renewable Energy Lab.(NREL), Golden, CO (United States).

Hussein, R. Z., Attia, N. K., Fouad, M. K., & ElSheltawy, S. T. (2021). Experimental investigation and process simulation of biolubricant production from waste cooking oil. *Biomass and Bioenergy*, *144*, 105850.

Hussein, R. Z.; N.K.Attia; M. Fouad; Shakinaz T. ElSheltawy. (Volume. 8 Issue. 8, August - 2023) “Techno-economic Assessment of Bio-based Lubricant Production Process from Waste Frying Oil: A Case Study of Egypt." " International Journal of Innovative Science and Research Technology (IJISRT), www.ijisrt.com. ISSN - 2456-2165 , PP :- 324-337.

Karmee, S. K., Patria, R. D., & Lin, C. S. K. (2015). Techno-economic evaluation of biodiesel production from waste cooking oil—a case study of Hong Kong. *International journal of molecular sciences*, *16*(3), 4362-4371.

Kricheldorf, H. R., Weidner, S. M., & Falkenhagen, J. (2022). The role of transesterifications in reversible polycondensations and a reinvestigation of the Jacobson–Beckmann–Stockmayer experiments. *Polymer chemistry*, *13*(9), 1177-1185.

Leung, D. Y., Wu, X., & Leung, M. K. H. (2010). A review on biodiesel production using catalyzed transesterification. *Applied energy*, *87*(4), 1083-1095.

Lin, S. K., & March, J. (2001). March's advanced organic chemistry: reactions, mechanisms, and structure. *Molecules*, *6*(12), 1064-1065.

Maglinao, R. L., Resurreccion, E. P., Kumar, S., Maglinao Jr, A. L., Capareda, S., & Moser, B. R. (2019). Hydrodeoxygenation–alkylation pathway for the synthesis of a sustainable lubricant improver from plant oils and lignin-derived phenols. *Industrial & Engineering Chemistry Research*, *58*(10), 4317-4330.

Maglinao, R. L., Taiswa, A., Davison, E. T., Andriolo, J. M., Succaw, G. L., Skinner, J. L., & Kumar, S. (2024). Role of solvent in selective hydrodeoxygenation of monomeric phenols. *Biomass and Bioenergy*, *189*, 107342.

Mahmood, Z., Yameen, M., Jahangeer, M., Riaz, M., Ghaffar, A., & Javid, I. (2018). Lignin as natural antioxidant capacity. *Lignin-trends and applications*, *10*, 181-205.

Mäki-Arvela, P., & Murzin, D. Y. (2017). Hydrodeoxygenation of lignin-derived phenols: from fundamental studies towards industrial applications. *Catalysts*, *7*(9), 265.

Mandari, V., & Devarai, S. K. (2022). Biodiesel production using homogeneous, heterogeneous, and enzyme catalysts via transesterification and esterification reactions: A critical review. *BioEnergy Research*, *15*(2), 935-961.

Nanda, S., Azargohar, R., Dalai, A. K., & Kozinski, J. A. (2015). An assessment on the sustainability of lignocellulosic biomass for biorefining. *Renewable and Sustainable Energy Reviews*, *50*, 925-941.

Nelson, R. C., Baek, B., Ruiz, P., Goundie, B., Brooks, A., Wheeler, M. C., ... & Austin, R. N. (2015). Experimental and theoretical insights into the hydrogen-efficient direct hydrodeoxygenation mechanism of phenol over Ru/TiO2. *ACS catalysis*, *5*(11), 6509-6523.

Ngo, H. L., Fox, P. S., Nuñez, A., Moreau, R. A., & Haas, M. J. (2014). Catalytic synthesis and characterization of phenol-branched-chain fatty acid isomers. *European Journal of Lipid Science and Technology*, *116*(3), 344-351.

Norjannah, B., Ong, H. C., Masjuki, H. H., Juan, J. C., & Chong, W. T. (2016). Enzymatic transesterification for biodiesel production: a comprehensive review. *RSC advances*, *6*(65), 60034-60055.

Ohata, J. (2024). Friedel–Crafts reactions for biomolecular chemistry. *Organic & Biomolecular Chemistry*, *22*(18), 3544-3558.

Oliveira, F. G., Rodrigues, F. L., de Oliveira, A. V., Marçal, D. V., & Esteves, P. M. (2017). Thoughts about the electrophilic aromatic substitution mechanism: the Friedel-crafts alkylation and acylation of benzene with acetyl and t-butyl cations in the gas phase. *Structural Chemistry*, *28*, 545-553.

Perez, V. H., Silveira Junior, E. G., Cubides, D. C., David, G. F., Justo, O. R., Castro, M. P., ... & de Castro, H. F. (2014). Trends in biodiesel production: present status and future directions. *Biofuels in Brazil: fundamental aspects, recent developments, and future perspectives*, 281-302.

Perry, R. H., Green, D. W., & Maloney, J. O. (2018). *Perry's chemical engineers' handbook* (9th ed.). McGraw-Hill Education.

Peters, M. S., Timmerhaus, K. D., & West, R. E. (2003). *Plant design and economics for chemical engineers* (5th ed.). McGraw-Hill.

Phiri, R., Rangappa, S. M., & Siengchin, S. (2023). Agro-waste for renewable and sustainable green production: A review. *Journal of Cleaner Production*, 139989.

Prabhudesai, V. S., Gurrala, L., & Vinu, R. (2021). Catalytic hydrodeoxygenation of lignin-derived oxygenates: catalysis, mechanism, and effect of process conditions. *Energy & Fuels*, *36*(3), 1155-1188.

Qu, L., Jiang, X., Zhang, Z., Zhang, X. G., Song, G. Y., Wang, H. L., ... & Chang, Y. L. (2021). A review of hydrodeoxygenation of bio-oil: model compounds, catalysts, and equipment. *Green Chemistry*, *23*(23), 9348-9376.

Rafiq, M. K., Bachmann, R. T., Rafiq, M. T., Shang, Z., Joseph, S., & Long, R. (2016). Influence of pyrolysis temperature on physico-chemical properties of corn stover (Zea mays L.) biochar and feasibility for carbon capture and energy balance. *PloS one*, *11*(6), e0156894.

Rana, M., Islam, M. N., Agarwal, A., Taki, G., Park, S. J., Dong, S., ... & Park, J. H. (2018). Production of phenol-rich monomers from kraft lignin hydrothermolysates in basic-subcritical water over MoO3/SBA-15 catalyst. *Energy & Fuels*, *32*(11), 11564-11575.

Rana, M., Taki, G., Islam, M. N., Agarwal, A., Jo, Y. T., & Park, J. H. (2019). Effects of temperature and salt catalysts on depolymerization of kraft lignin to aromatic phenolic compounds. *Energy & Fuels*, *33*(7), 6390-6404.

Ranade, V. V., Chaudhari, R., & Gunjal, P. R. (2011). *Trickle bed reactors: Reactor engineering and applications*. Elsevier.

RiYang, S. R., Li RongXuan, L. R., Lin BiQin, L. B., Wang Chao, W. C., Cheng ZhengDong, C. Z., & Chen Ying, C. Y. (2020). A review on the catalytic hydrodeoxygenation of lignin-derived phenolic compounds and the conversion of raw lignin to hydrocarbon liquid fuels.

Reeves, C. J., Siddaiah, A., & Menezes, P. L. (2017). A review on the science and technology of natural and synthetic biolubricants. *Journal of Bio-and Tribo-Corrosion*, *3*, 1-27.

Rueping, M., & Nachtsheim, B. J. (2010). A review of new developments in the Friedel–Crafts alkylation–From green chemistry to asymmetric catalysis. *Beilstein Journal of Organic Chemistry*, *6*(1), 6.

Salehmin, M. N. I., Husaini, T., Goh, J., & Sulong, A. B. (2022). High-pressure PEM water electrolyser: A review on challenges and mitigation strategies towards green and low-cost hydrogen production. *Energy Conversion and Management*, *268*, 115985.

Schuler, J., Hornung, U., Kruse, A., Dahmen, N., & Sauer, J. (2017). Hydrothermal liquefaction of lignin. *Journal of Biomaterials and Nanobiotechnology*, *8*(01), 96.

Shafaghat, H., Rezaei, P. S., & Daud, W. M. A. W. (2016). Catalytic hydrodeoxygenation of simulated phenolic bio-oil to cycloalkanes and aromatic hydrocarbons over bifunctional metal/acid catalysts of Ni/HBeta, Fe/HBeta and NiFe/HBeta. *Journal of industrial and engineering chemistry*, *35*, 268-276.

Shah, A. A., Sharma, K., Haider, M. S., Toor, S. S., Rosendahl, L. A., Pedersen, T. H., & Castello, D. (2022). The role of catalysts in biomass hydrothermal liquefaction and biocrude upgrading. *Processes*, *10*(2), 207.

Singh, S. P., & Singh, D. (2010). Biodiesel production through the use of different sources and characterization of oils and their esters as the substitute of diesel: a review. *Renewable and sustainable energy reviews*, *14*(1), 200-216.

Smirniotis, P. G., & Ruckenstein, E. (1995). Alkylation of Benzene or Toluene with MeOH or C2H4 over ZSM-5 or. beta. Zeolite: Effect of the Zeolite Pore Openings and of the Hydrocarbons Involved on the Mechanism of Alkylation. *Industrial & engineering chemistry research*, *34*(5), 1517-1528.

Totten, G. E. (2006). *Handbook of lubrication and tribology: Volume I application and maintenance*. CRC Press.

Tran, H., & Vakkilainnen, E. K. (2008). The kraft chemical recovery process. *Tappi Kraft Pulping Short Course*, 1-8.

Tursi, A. (2019). 'A review on biomass: importance, chemistry, classification, and conversion', *Biofuel Research Journal*, 6(2), pp. 962-979. doi: 10.18331/BRJ2019.6.2.3

Turton, R., Bailie, R. C., Whiting, W. B., Shaeiwitz, J. A., & Bhattacharyya, D. (2018). *Analysis, synthesis, and design of chemical processes* (5th ed.). Pearson.

Xu, Y. H., & Li, M. F. (2021). Hydrothermal liquefaction of lignocellulose for value-added products: Mechanism, parameter and production application. *Bioresource Technology*, *342*, 126035.

Yiin, C. L., bin Odita, E., Lock, S. S. M., Cheah, K. W., Chan, Y. H., Wong, M. K., ... & Yusup, S. (2022). A review on potential of green solvents in hydrothermal liquefaction (HTL) of lignin. *Bioresource Technology*, *364*, 128075.

Zhang, J., Sun, J., & Wang, Y. (2020). Recent advances in the selective catalytic hydrodeoxygenation of lignin-derived oxygenates to arenes. *Green Chemistry*, *22*(4), 1072-1098.

Zhou, X. F. (2014). Conversion of kraft lignin under hydrothermal conditions. *Bioresource technology*, *170*, 583-586.

WEB SITES

[1]: https://www.chemengonline.com

[2]: https://www.extension.iastate.edu/agdm/crops/html/a1-70.html

[3]: https://www.rockvalleyhay.com/web

[4]: https://www.indexbox.io/search/sulphuric-acid-price-the-united-states/#:~:text=Mar%C3%ADn%20Orriols-,Sulphuric%20Acid%20Price%20in%20the%20United%20States%20(FOB)%20%2D%202022,14.4%25%20against%20the%20previous%20year.

[5]: https://pubs.usgs.gov/periodicals/mcs2023/mcs2023-nitrogen.pdf

[6]:https://www.researchgate.net/publication/304365287_Use_of_corn_steep_liquor_as_an_economical_nitrogen_source_for_biosuccinic_acid_production_by_Actinobacillus_succinogenes

[7]: https://www.indexbox.io/search/diammonium-phosphate-price-the-united-states/#export

[8]: https://www.indexbox.io/search/sorbitol-price-the-united-states/

[9]: https://www.selinawamucii.com/insights/prices/united-states-of-america/glucose/#:~:text=US%20Glucose%20Import%20Prices%20%2D%20Historical%2C%20Trends%20and%20Prediction&text=The%20most%20recent%20data%20shows%20that%20the%20price%20has%20risen,over%20the%20last%20five%20years.

[10]: https://www.indexbox.io/search/caustic-soda-price-the-united-states/#:~:text=the%20United%20States-,Caustic%20Soda%20Price%20in%20the%20United%20States%20(FOB)%20%2D%202022,price%20saw%20a%20perceptible%20expansion.

[11]: https://www.macrotrends.net/stocks/charts/USLM/united-states-lime-minerals/stock-price-history

[12]: https://medium.com/intratec-products-blog/phenol-prices-latest-historical-data-in-several-countries-1d2d42cf40f

[13]: https://www.indexbox.io/search/methanol-price-the-united-states/#:~:text=Book%20Your%20Meeting-,Methanol%20Price%20in%20the%20United%20States%20(FOB)%20%2D%202022,7.1%25%20against%20the%20previous%20year.

[14]: https://medium.com/intratec-products-blog/mtbe-prices-latest-historical-data-in-several-countries-e0c35fff48dd

[15]: https://www.indexbox.io/search/carbonates-potassium-carbonate-price-the-united-states/

[16]: https://mymarketnews.ams.usda.gov/viewReport/3510

[17]: https://www.indexbox.io/search/potassium-hydroxide-price-the-united-states/#:~:text=the%20United%20States-

,Potassium%20Hydroxide%20Price%20in%20the%20United%20States%20(FOB)%20%2D%202022,6.2%25%20against%20the%20previous%20year.

[18]: https://www.indexbox.io/search/phosphoric-acid-price-the-united-states/#:~:text=the%20United%20States-,Phosphoric%20Acid%20Price%20in%20the%20United%20States%20(FOB)%20%2D%202022,export%20price%20showed%20notable%20growth.

[19]: https://medium.com/intratec-products-blog/cyclohexane-prices-latest-historical-data-in-several-countries-539f4e188c7f

[20]: https://www.chemanalyst.com/Pricing-data/n-heptane-1152

[21]: https://matthey.com/products-and-markets/pgms-and-circularity/pgm-management

[22]: https://www.usalab.com/carbon-chemistry-activated-alumina-1-5kg-7kg-14kg-120kg/

[23]: https://www.chemicalbook.com/ProdSupplierGN_EN.aspx?CBNumber=CB0875619&ProvID=1001

[24]: https://www.eia.gov/electricity/annual/html/epa_02_10.html

[25]: https://www.statista.com/statistics/258906/average-hourly-wage-of-a-us-chemical-production-worker/

[26]: https://www.indexbox.io/search/benzene-price-the-united-states/

[27]: https://www.selinawamucii.com/insights/prices/united-states-of-america/glycerol/#:~:text=The%20most%20recent%20data%20shows,dollars%20per%20kg%20in%202024.

[28]: https://farmdocdaily.illinois.edu/2022/09/fertilizer-prices-rates-and-costs-for-2023.html

[29]: https://tradingeconomics.com/commodity/ethanol